12
The Feynman path integral

12.1 Quantum mechanics as a sum over paths

The strangeness of the quantum world is evident in systems as simple as ideal gases of the previous chapter, where nothing more than the spin statistics leads to remarkably complex behavior. We still have not yet included interactions in our treatment of quantum systems, and as noted in Chapter 10, the eigenvalue problem for the Hamiltonian when interactions are included can only be solved for very small systems. For large systems, we need a statistical approach, and this brings us to the formulation of quantum mechanics proposed by Feynman (Feynman, 1948; Feynman and Hibbs, 1965). Not surprisingly, quantum strangeness is no less apparent in Feynman's formulation of quantum mechanics than it is in the pictures we have studied thus far. Although mathematically equivalent to the Heisenberg and Schrödinger pictures of quantum mechanics, Feynman's view represents a qualitative departure from these formulations.

In order to introduce Feynman's picture, consider a particle prepared in a state initially localized at a point x that evolves unobserved to a point x'. Invoking the quantum wave-like nature of the particle, the wave packet representing the initial state evolves under the action of the propagator $U(t) = \exp(-i\hat{\mathcal{H}}t/\hbar)$, and the wave packet spreads in time, causing the state to become increasingly delocalized spatially until it is finally observed at the point x' through a measurement of position, where it again localizes due to the collapse of the wave function. In contrast, Feynman's view vaguely resembles a classical particle picture, in which the particle evolves unobserved from x to x'. There is a key difference, however, from the classical view. Classically, if we do not observe the particle, we will not know what path it will take, but we do know that it will follow a definite path. In quantum mechanics, by contrast, it is not our ignorance that prevents us from specifying a particle's path (which we could, but it is the very quantum nature of the particle itself that makes specifying a path impossible. Instead of following a unique path between x and x', the particle follows a myriad of paths, specifically all possible paths, simultaneously. These paths represent *interfering alternatives*, meaning that the total amplitude for the particle to be observed at x' at time t is the sum of the amplitudes associated with all possible paths between x and x'. Thus, according to the Feynman picture, we must calculate the amplitude for each of the infinitely many paths the particle follows and then sum them to obtain the complete amplitude for the process. Recall that the probability $P(x', t)$ for the particle to be observed at x' is the square modulus of the amplitude; since the latter is a sum of amplitudes for individual paths, the cross terms constitute the interference between

individual amplitudes. This picture of quantum mechanics is known as the *sum over paths* or *path integral* formulation. How we calculate the amplitude for a path will be made explicit in the next section.

Before delving into the mathematics of path integrals, let us apply the Feynman picture heuristically to a concrete example. Consider an experiment in which electrons from a source S impinge on a double-slit system and are registered on a detection screen placed at D (see Fig. 12.1). Invoking a wave-like picture, the interference of electron

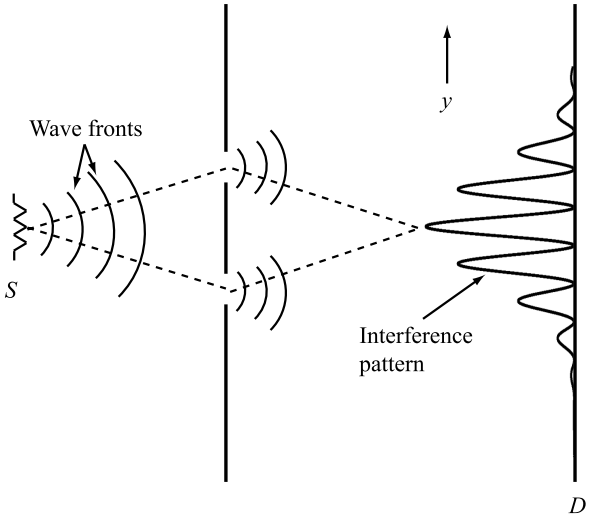

Fig. 12.1 Interference pattern observed in the electron double-slit experiment.

waves emanating from the two slits leads to the well-known interference pattern at the detector, as shown in the figure. This pattern is actually observed when the experiment is performed (Merli *et al.*, 1976). Next, consider Feynman's sum over paths formulation. If the electrons followed definite paths, as they would if they were classical particles, each path would have a separate probability and no interference pattern would be seen between the paths. We would, therefore, expect two bright spots on the screen directly opposite the slits as shown in Fig. 12.2. However, the quantum sum over paths requires that we consider all possible paths from the source S through the double-slit apparatus and finally to the detector D. Several of these paths are shown in Fig. 12.3. Let each path have a corresponding amplitude $A_i(y)$. Specifically, $A_i(y)$ is the amplitude that an electron following path i is detected at a point y on the screen at time t. The total amplitude $A(y)$ for observing an electron at y is, therefore, the sum $A(y) = A_1(y) + A_2(y) + A_3(y) + \cdots$, and the corresponding probability $P(y)$ is given by $P(y) = |A(y)|^2 = |A_1(y) + A_2(y) + A_3(y) + \cdots|^2$. Suppose there were only two such paths. Then $P(y) = |A_1(y) + A_2(y)|^2$. Since each amplitude is complex, we can write

$$A_1(y) = |A_1(y)|\mathrm{e}^{i\phi_1(y)}, \qquad A_2(y) = |A_2(y)|\mathrm{e}^{i\phi_2(y)}, \tag{12.1.1}$$

and it can be easily shown that

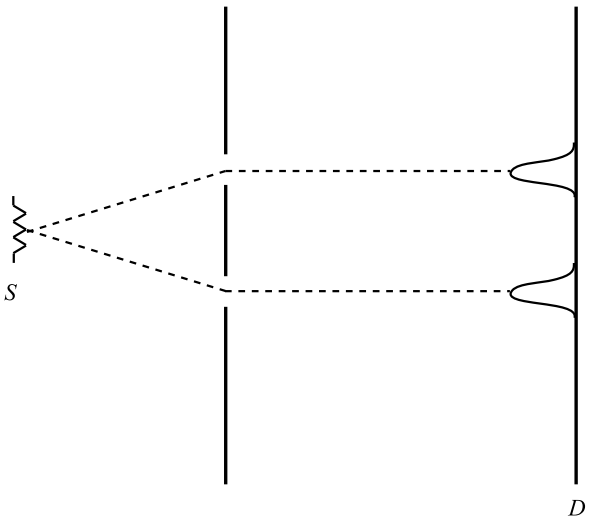

Fig. 12.2 Interference pattern expected for classical electrons impinging on the double-slit apparatus.

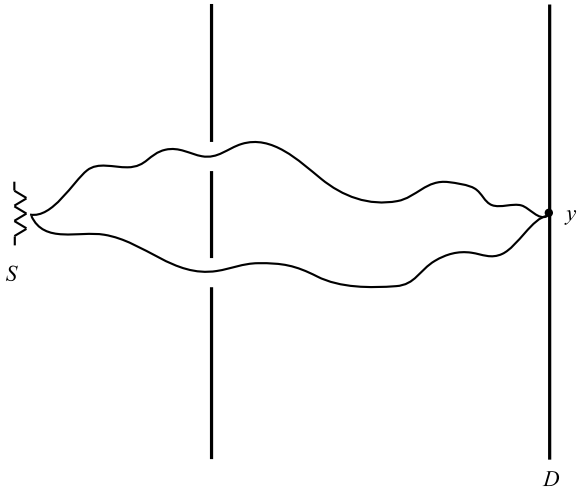

Fig. 12.3 Illustration of possible paths of quantum electrons through a double-slit apparatus.

$$P(y) = |A_1(y)|^2 + |A_2(y)|^2 + 2|A_1(y)||A_2(y)| \cos\left(\phi_1(y) - \phi_2(y)\right). \tag{12.1.2}$$

The third term in eqn. (12.1.2) is the interference term between the two paths, and the expression for $P(y)$ gives us our first clue that this term, which contains an oscillating function of the phase difference multiplied by an amplitude $|A_1(y)||A_2(y)|$, is largely responsible for the overall shape of the observed interference pattern.

Ultimately, an infinite number of amplitudes must be summed in order to obtain the overall probability, which we can express suggestively as

$$P(y) = \left| \sum_{\text{paths}} A_{\text{path}}(y) \right|^2 . \tag{12.1.3}$$

In such an expression, the number of interference terms is infinite. Nevertheless, if the sum over paths is applied to the double-slit experiment, the correct observed interference pattern, whose intensity $I(y)$ is proportional to $P(y)$, is obtained.

In their book *Quantum Mechanics and Path Integrals*, Feynman and Hibbs (1965) employ an interesting visual device to help understand the nature of the many paths. Imagine modifying the double-slit experiment by introducing a large number of intermediate gratings, each containing many slits, as shown in Fig. 12.4. The electrons

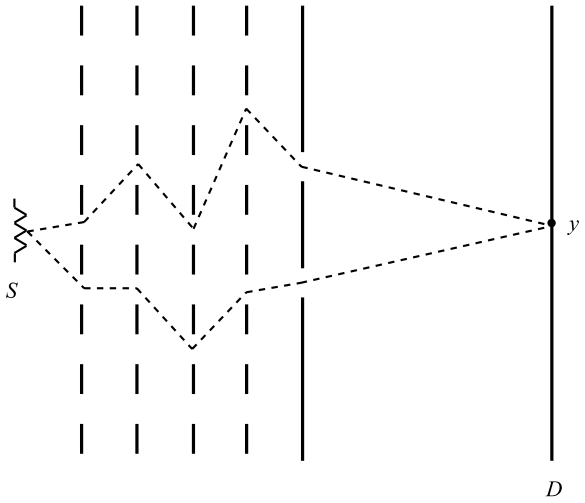

Fig. 12.4 Passage of electrons through a large number of intermediate gratings in the apparatus of the double-slit experiment.

may now pass through any sequence of slits before reaching the detector; the number of possible paths increases with both the number of intermediate gratings and the number of slits in each grating. If we now take the limit in which infinitely many gratings are placed between the source and the detector, each with an infinite number of slits, there will be an infinite number of possible paths the electrons can follow. However, when the number of slits in each intermediate grating becomes infinite, the space between the slits goes to zero, and the gratings disappear, reverting to empty space. The suggestion of this thought experiment is that empty space allows for an infinity of possible paths, and since the electrons are not observed until they reach the detector, we must sum over all of these possible paths. Indeed, this sum of path amplitudes should exactly recover or build up the amplitude pattern in a wave-like picture of the particles.

With this heuristic introduction to the sum over paths in mind, we now proceed to derive the Feynman path integral more rigorously and, in the process, learn how to determine the path amplitudes.

12.2 Derivation of path integrals for the canonical density matrix and the time evolution operator

In this and subsequent sections, the path integral concept will be given a more precise mathematical formulation and its computational advantages elucidated. For simplicity, the discussion will initially focus on a single particle moving in one spatial dimension with a Hamiltonian

$$\hat{\mathcal{H}} = \frac{\hat{p}^2}{2m} + U(\hat{x}) \equiv \hat{K} + \hat{U}. \tag{12.2.1}$$

As noted in Section 12.1, the path integral describes a process in which a particle moves unobserved between an initiation point x and a detection point x'. That is, the particle is initially prepared in an eigenstate $|x\rangle$ of the position operator, which is subsequently allowed to evolve under the action of the propagator $\exp(-i\hat{\mathcal{H}}t/\hbar)$. After a time t, we ask what the amplitude will be for detection of a particle at a point x'. This amplitude A is given by

$$A = \langle x'|\mathrm{e}^{-i\hat{\mathcal{H}}t/\hbar}|x\rangle \equiv U(x, x'; t). \tag{12.2.2}$$

Therefore, what we seek are the coordinate-space matrix elements of the quantum propagator. More generally, if a system has an initial state vector $|\Psi(0)\rangle$, then from eqn. (9.2.33), at time t, the state vector is $|\Psi(t)\rangle = \exp(-i\hat{\mathcal{H}}t/\hbar)|\Psi(0)\rangle$. Projecting this into the coordinate basis gives

$$\begin{aligned}\langle x'|\Psi(t)\rangle = \Psi(x', t) &= \langle x'|\mathrm{e}^{-i\hat{\mathcal{H}}t/\hbar}|\Psi(0)\rangle \\ &= \int \mathrm{d}x\ \langle x'|\mathrm{e}^{-i\hat{\mathcal{H}}t/\hbar}|x\rangle\langle x|\Psi(0)\rangle \\ &= \int \mathrm{d}x\ \langle x'|\mathrm{e}^{-i\hat{\mathcal{H}}t/\hbar}|x\rangle\Psi(x, 0),\end{aligned} \tag{12.2.3}$$

which also requires the coordinate-space matrix elements of the propagator. The Feynman path integral provides a technique whereby these matrix elements can be computed via a sum over all possible paths leading from x to x' in time t.

Before presenting the detailed derivation of the path integral, it is worth noting an important connection between the propagator and the canonical density matrix. If we denote the latter by $\hat{\rho}(\beta) = \exp(-\beta\hat{\mathcal{H}})$, then it is clear that

$$\hat{\rho}(\beta) = \hat{U}(-i\beta\hbar), \qquad \hat{U}(t) = \hat{\rho}(it/\hbar). \tag{12.2.4}$$

Equation (12.2.4) implies that the canonical density matrix can be obtained by evaluating the propagator at an imaginary time $t = -i\beta\hbar$. For this reason, the density matrix is often referred to as an *imaginary-time propagator*. (In Section 12.5, we will

present a way to think about imaginary-time propagation.) Similarly, the real-time propagator can be obtained by evaluating the density matrix at an imaginary inverse temperature $\beta = it/\hbar$. In fact, if we allow time and temperature to be complex components of a general complex time parameter $\theta = t + i\beta\hbar$, then the transformations $t = -i\beta\hbar$ and $\beta = it/\hbar$ can be performed by rotations in the complex θ-plane from the real axis to the imaginary axis, as shown in Fig. 12.5. These rotations are known as

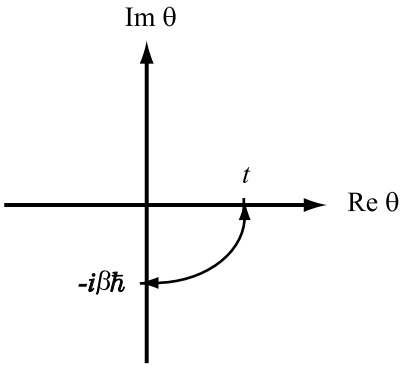

Fig. 12.5 Wick rotation in the complex time plane.

Wick rotations after the Italian physicist Giancarlo Wick (1909–1992), and they permit, in principle, the determination of the propagator given the density matrix, and vice versa. Since it is generally easier to work with a damped exponential rather than a complex one, we shall derive the Feynman path integral for the canonical density matrix and then exploit eqn. (12.2.4) to obtain a corresponding path integral expression for the quantum propagator.

Let us denote the coordinate-space matrix elements of $\hat{\rho}(\beta)$ as

$$\rho(x, x'; \beta) \equiv \langle x' | \mathrm{e}^{-\beta\hat{\mathcal{H}}} | x \rangle. \tag{12.2.5}$$

Note that $\hat{\mathcal{H}}$ is the sum of two operators $K(\hat{p})$ and $U(\hat{x})$ that do not commute with each other ($[K(\hat{p}), U(\hat{x})] \neq 0$). Consequently, the operator $\exp(-\beta\hat{\mathcal{H}})$ cannot be evaluated straightforwardly. However, as we did in Section 3.10, we can exploit the Trotter theorem (see eqn. (3.10.18) and Appendix D) to express the operator as

$$\mathrm{e}^{-\beta(\hat{K}+\hat{U})} = \lim_{P\to\infty} \left[\mathrm{e}^{-\beta\hat{U}/2P} \mathrm{e}^{-\beta\hat{K}/P} \mathrm{e}^{-\beta\hat{U}/2P} \right]^P. \tag{12.2.6}$$

Substituting eqn. (12.2.6) into eqn. (12.2.5) yields

$$\rho(x, x'; \beta) = \lim_{P\to\infty} \langle x' | \left[\mathrm{e}^{-\beta\hat{U}/2P} \mathrm{e}^{-\beta\hat{K}/P} \mathrm{e}^{-\beta\hat{U}/2P} \right]^P | x \rangle. \tag{12.2.7}$$

Let us now define an operator $\hat{\Omega}$ by

$$\hat{\Omega} = \mathrm{e}^{-\beta\hat{U}/2P} \mathrm{e}^{-\beta\hat{K}/P} \mathrm{e}^{-\beta\hat{U}/2P}. \tag{12.2.8}$$

Substituting $\hat{\Omega}$ into eqn. (12.2.7) gives

$$\rho(x, x'; \beta) = \lim_{P\to\infty} \langle x'|\hat{\Omega}^P|x\rangle = \lim_{P\to\infty} \langle x'|\hat{\Omega}\hat{\Omega}\hat{\Omega}\cdots\hat{\Omega}|x\rangle. \tag{12.2.9}$$

In order to simplify the evaluation of eqn. (12.2.9), we introduce an identity operator in the form of

$$\hat{I} = \int \mathrm{d}x\ |x\rangle\langle x| \tag{12.2.10}$$

(see also eqn. (9.2.38)) between each factor of $\hat{\Omega}$. Since there are P factors of $\hat{\Omega}$, $P-1$ insertions of the identity operator are needed. This will introduce $P-1$ integrations over coordinate labels giving the following expression for the density matrix:

$$\begin{aligned}\rho(x, x'; \beta) = \lim_{P\to\infty} \int \mathrm{d}x_2 \cdots \mathrm{d}x_P \\ \times \langle x'|\hat{\Omega}|x_P\rangle\langle x_P|\hat{\Omega}|x_{P-1}\rangle\langle x_{P-1}|\cdots|x_2\rangle\langle x_2|\hat{\Omega}|x\rangle.\end{aligned} \tag{12.2.11}$$

Inserting the identity operator $P-1$ times is analogous to inserting $P-1$ gratings with many holes in Fig. 12.4. The integration over each x_i is analogous to summing over all possible ways a particle can pass through the infinitely many holes in each grating.

The advantage of employing the Trotter theorem is that the matrix elements in eqn. (12.2.11) can be evaluated in closed form. Consider the general matrix element

$$\langle x_{k+1}|\hat{\Omega}|x_k\rangle = \langle x_{k+1}|\mathrm{e}^{-\beta\hat{U}/2P}\mathrm{e}^{-\beta\hat{K}/P}\mathrm{e}^{-\beta\hat{U}/2P}|x_k\rangle. \tag{12.2.12}$$

Note that $\hat{U} = U(\hat{x})$ is a function of the coordinate operator. Thus, $|x_k\rangle$ and $|x_{k+1}\rangle$, being coordinate eigenvectors, are eigenvectors of $\exp(-\beta U(\hat{x})/2P)$ with eigenvalues $\exp(-\beta U(x_k)/2P)$ and $\exp(-\beta U(x_{k+1})/2P)$, respectively. Hence, eqn. (12.2.12) simplifies to

$$\langle x_{k+1}|\hat{\Omega}|x_k\rangle = \mathrm{e}^{-\beta U(x_{k+1})/2P}\langle x_{k+1}|\mathrm{e}^{-\beta\hat{K}/P}|x_k\rangle\mathrm{e}^{-\beta U(x_k)/2P}. \tag{12.2.13}$$

Since $\hat{K}$ is a function of the momentum operator, the matrix element of $\exp(-\beta\hat{K}/P)$ is less trivial to evaluate. However, if we insert another identity operator, this time expressed in terms of momentum eigenvectors as

$$\hat{I} = \int \mathrm{d}p\ |p\rangle\langle p|, \tag{12.2.14}$$

into eqn. (12.2.13), we obtain

$$\langle x_{k+1}|\mathrm{e}^{-\beta\hat{K}/P}|x_k\rangle = \int \mathrm{d}p\ \langle x_{k+1}|\mathrm{e}^{-\beta\hat{K}/P}|p\rangle\langle p|x_k\rangle. \tag{12.2.15}$$

Now the operator $\exp(-\beta\hat{K}/P)$ acts on one of its eigenvectors $|p\rangle$ to yield

$$\langle x_{k+1}|\mathrm{e}^{-\beta\hat{K}/P}|x_k\rangle = \int \mathrm{d}p\, \langle x_{k+1}|p\rangle\langle p|x_k\rangle \mathrm{e}^{-\beta p^2/2mP}. \tag{12.2.16}$$

Finally, using eqn. (9.2.43), eqn. (12.2.16) becomes

$$\langle x_{k+1}|\mathrm{e}^{-\beta\hat{K}/P}|x_k\rangle = \frac{1}{2\pi\hbar}\int \mathrm{d}p\, \mathrm{e}^{-\beta p^2/2mP}\mathrm{e}^{ip(x_{k+1}-x_k)/\hbar}. \tag{12.2.17}$$

Since the range of the momentum integration is $p \in (-\infty, \infty)$, the above integral is a typical Gaussian integral that can be evaluated by completing the square. Thus, we write

$$\begin{aligned}
&\frac{\beta p^2}{2mP} - \frac{ip(x_{k+1}-x_k)}{\hbar} \\
&\quad = \frac{\beta}{2mP}\left[p^2 - \frac{2imPp(x_{k+1}-x_k)}{\beta\hbar}\right] \\
&\quad = \frac{\beta}{2mP}\left\{\left[p - \frac{imP(x_{k+1}-x_k)}{\beta\hbar}\right]^2 + \frac{m^2P^2(x_{k+1}-x_k)^2}{\beta^2\hbar^2}\right\} \\
&\quad = \frac{\beta}{2mP}\left[p - \frac{imP(x_{k+1}-x_k)}{\beta\hbar}\right]^2 + \frac{mP}{2\beta\hbar^2}(x_{k+1}-x_k)^2.
\end{aligned} \tag{12.2.18}$$

When the two last lines of eqn. (12.2.18) are substituted back into eqn. (12.2.17), and a change of variables

$$\tilde{p} = p - \frac{imP(x_{k+1}-x_k)}{\beta\hbar} \tag{12.2.19}$$

is made, we find

$$\begin{aligned}
\langle x_{k+1}|\mathrm{e}^{-\beta\hat{K}/P}|x_k\rangle &= \frac{1}{2\pi\hbar}\exp\left[-\frac{mP}{2\beta\hbar^2}(x_{k+1}-x_k)^2\right]\int_{-\infty}^{\infty}\mathrm{d}\tilde{p}\, \mathrm{e}^{-\beta\tilde{p}^2/2mP} \\
&= \left(\frac{mP}{2\pi\beta\hbar^2}\right)^{1/2}\exp\left[-\frac{mP}{2\beta\hbar^2}(x_{k+1}-x_k)^2\right].
\end{aligned} \tag{12.2.20}$$

Now, eqn. (12.2.20) is combined with eqn. (12.2.13) to yield

$$\begin{aligned}
\langle x_{k+1}|\hat{\Omega}|x_k\rangle = \left(\frac{mP}{2\pi\beta\hbar^2}\right)^{1/2}&\exp\left[-\frac{\beta}{2P}\left(U(x_{k+1})+U(x_k)\right)\right] \\
&\times\exp\left[-\frac{mP}{2\beta\hbar^2}(x_{k+1}-x_k)^2\right].
\end{aligned} \tag{12.2.21}$$

Finally, multiplying all P matrix elements together and integrating over the $P-1$ coordinate variables, we obtain for the density matrix:

$$\rho(x,x';\beta) = \lim_{P\to\infty}\left(\frac{mP}{2\pi\beta\hbar^2}\right)^{P/2}\int \mathrm{d}x_2\cdots\mathrm{d}x_P$$

$$\times\exp\left\{-\frac{1}{\hbar}\sum_{k=1}^{P}\left[\frac{mP}{2\beta\hbar}(x_{k+1}-x_k)^2+\frac{\beta\hbar}{2P}\left(U(x_{k+1})+U(x_k)\right)\right]\right\}\Bigg|_{x_1=x}^{x_{P+1}=x'} . \quad (12.2.22)$$

In eqn. (12.2.22), the quantum kinetic energy is present in the form of a harmonic nearest-neighbor coupling term that acts between points along the path. The spring constant for this interaction is $mP/\beta^2\hbar^2$.

Equation (12.2.22) is the limit $P\to\infty$ of a *discretized path integral* representation for the density matrix. As eqn. (12.2.22) indicates, the endpoints of the paths at points x_1 and x_{P+1} are fixed at the "initiation" and "detection" points, x and x', respectively. The intermediate integrations over $x_2, ..., x_P$ constitute the sum over all possible paths from x to x' in imaginary time $-i\beta\hbar$. For finite P, because the potential U only acts at the discrete points x_k, the paths are lines between successive imaginary-time points, as suggested by Fig. 12.4. Note that if the particle is confined to an interval $x\in[0,L]$, then all of the coordinate integrations must be restricted to this interval as well. The weight or amplitude assigned to each path is the value of the integrand in eqn. (12.2.22) evaluated along the discrete path.

A path integral representation for the real-time propagator can now be derived from eqn. (12.2.22) by applying eqn. (12.2.4) and setting $\beta = it/\hbar$. This yields a path integral expression for the coordinate-space matrix elements of the propagator, $\hat{U}(t)$:

$$U(x,x';t) = \lim_{P\to\infty}\left(\frac{mP}{2\pi it\hbar}\right)^{P/2}\int \mathrm{d}x_2\cdots\mathrm{d}x_P$$

$$\times\exp\left\{\frac{i}{\hbar}\sum_{k=1}^{P}\left[\frac{mP}{2t}(x_{k+1}-x_k)^2-\frac{t}{2P}\left(U(x_{k+1})+U(x_k)\right)\right]\right\}\Bigg|_{x_1=x}^{x_{P+1}=x'} . \quad (12.2.23)$$

Notice the change in relative sign between the kinetic and potential energy terms between eqns. (12.2.22) and (12.2.23) in the path integral expressions for the density matrix and the propagator. The path sums in eqns. (12.2.22) and (12.2.23) are represented pictorially in Fig. 12.6.

From eqn. (12.2.22), a path integral expression for the canonical partition function $Q(L,T)$ for a system confined to $x\in[0,L]$ can be derived. Recall that $Q(L,T) = \mathrm{Tr}[\exp(-\beta\hat{\mathcal{H}})]$. Evaluating the trace in the coordinate basis gives

$$Q(L,T) = \int_0^L \mathrm{d}x\ \langle x|\mathrm{e}^{-\beta\hat{\mathcal{H}}}|x\rangle = \int_0^L \mathrm{d}x\ \rho(x,x;\beta). \quad (12.2.24)$$

In order to evaluate eqn. (12.2.24), the diagonal elements of the density matrix in the coordinate basis are needed; these can be obtained by setting $x_1 = x_{P+1} = x$ in eqn. (12.2.22). Finally, an integration over the diagonal elements must be performed. Since

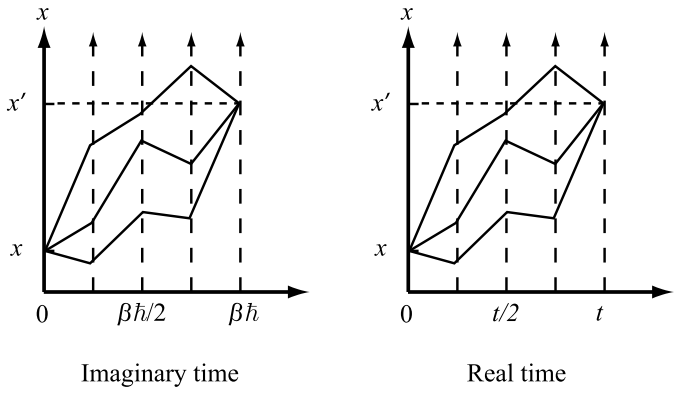

Fig. 12.6 Representative paths in the path sums of eqns. (12.2.22) and (12.2.23).

$x_1 = x$, we may rename the integration variable in eqn. (12.2.24) x_1 and perform a P-dimensional integration

$$Q(L,T) = \lim_{P\to\infty}\left(\frac{mP}{2\pi\beta\hbar^2}\right)^{P/2}\int \mathrm{d}x_1\cdots\mathrm{d}x_P \times \exp\left\{-\frac{1}{\hbar}\sum_{k=1}^{P}\left[\frac{mP}{2\beta\hbar}(x_{k+1}-x_k)^2+\frac{\beta\hbar}{2P}\left(U(x_{k+1})+U(x_k)\right)\right]\right\}\Bigg|_{x_{P+1}=x_1}, \quad (12.2.25)$$

which is subject to the condition $x_{P+1} = x_1$. This condition restricts the integration to paths that begin and end at the same point. All of the coordinate integrations in eqn. (12.2.25), must be restricted to the spatial domain $x \in [0, L]$, which we will denote as $D(L)$. Finally, note that $\sum_{k=1}^{P}(1/2)[U(x_k)+U(x_{k+1})] = (1/2)[U(x_1)+U(x_2)+U(x_2)+U(x_3)+\cdots+U(x_{P-1})+U(x_P)+U(x_P)+U(x_1)] = \sum_{k=1}^{P}U(x_k)$, where the condition $x_1 = x_{P+1}$ has been used. Thus, eqn. (12.2.25) simplifies to

$$Q(L,T) = \lim_{P\to\infty}\left(\frac{mP}{2\pi\beta\hbar^2}\right)^{P/2}\int_{D(L)} \mathrm{d}x_1\cdots\mathrm{d}x_P \times \exp\left\{-\frac{1}{\hbar}\sum_{k=1}^{P}\left[\frac{mP}{2\beta\hbar}(x_{k+1}-x_k)^2+\frac{\beta\hbar}{P}U(x_k)\right]\right\}\Bigg|_{x_{P+1}=x_1}. \quad (12.2.26)$$

The integration over cyclic paths implied by eqn. (12.2.26) is illustrated in Fig. 12.7. Interestingly, as the temperature $T \to \infty$ and $\beta \to 0$, the harmonic spring constant connecting neighboring points along the paths becomes infinite, which causes the cyclic paths in the partition function to collapse onto a single point corresponding to a classical point particle. Thus, the path integral formalism shows that the high-temperature limit is equivalent to the classical limit. Finally, note that the partition function can be expressed compactly as the limit of an expression that resembles a classical configurational partition function

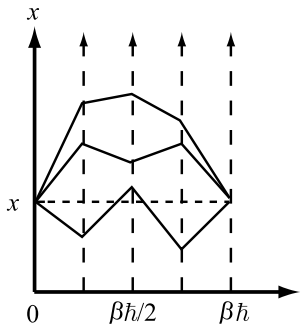

Fig. 12.7 Representative paths in the discrete path sum for the canonical partition function.

$$Q(L,T) = \lim_{P\to\infty}\left(\frac{mP}{2\pi\beta\hbar^2}\right)^{P/2}\int_{D(L)} \mathrm{d}x_1\cdots\mathrm{d}x_P\ \mathrm{e}^{-\beta\phi(x_1,\ldots,x_P)}, \tag{12.2.27}$$

an analogy we will revisit when we discuss numerical methods for evaluating path integrals in Section 12.8. Here,

$$\phi(x_1,\ldots,x_P) = \sum_{k=1}^{P}\left[\frac{1}{2}m\omega_P^2(x_k - x_{k+1})^2 + \frac{1}{P}U(x_k)\right], \tag{12.2.28}$$

where $\omega_P = \sqrt{P}/\beta\hbar$ and $x_{P+1} = x_1$. The function $\phi(x_1,\ldots,x_P)$, with the condition $x_{P+1} = x_1$, resembles a potential energy for a cyclic chain of classical-like pseudoparticles with harmonic springs of frequency ω_P connecting nearest neighbors on the chain (see Fig. 12.12 for an illustration of a cyclic polymer, or "ring polymer", snapshot described by eqn. (12.2.28) with $P = 8$). We will have more to say about this classical-like potential and how it can be effectively sampled in Section 12.8.

An analytical calculation of the density matrix, partition function, or propagator via path integration proceeds first by carrying out the P-dimensional integration and then taking the limit of the result as $P \to \infty$. As a simple example, consider the density matrix for a free particle ($U(x) = 0$). Assume $x \in (-\infty, \infty)$. The density matrix in this case is given by

$$\rho(x,x';\beta) = \lim_{P\to\infty}\left(\frac{mP}{2\pi\beta\hbar^2}\right)^{P/2} \times \int \mathrm{d}x_2\cdots\mathrm{d}x_P\ \exp\left\{-\sum_{k=1}^{P}\left[\frac{mP}{2\beta\hbar^2}(x_{k+1}-x_k)^2\right]\right\}\Bigg|_{x_1=x}^{x_{P+1}=x'}. \tag{12.2.29}$$

In fact, we previously solved this problem in Section 4.6. Equation (4.6.33) is the partition function for a classical polymer with harmonic nearest-neighbor particle couplings and fixed endpoints. Applying the result of eqn. (4.6.33) to eqn. (12.2.29), recognizing

the extra factor of P in the force constant and the fact that eqn. (12.2.29) has $P-1$ integrations in one spatial dimension, we obtain

$$\rho(x,x';\beta) = \left(\frac{m}{2\pi\beta\hbar^2}\right)^{1/2} \exp\left[-\frac{m}{2\beta\hbar^2}(x-x')^2\right]. \tag{12.2.30}$$

Interestingly, the P dependence completely disappears so that the limit can be taken trivially. Moreover, by substituting $\beta = it/\hbar$, the quantum propagator for a free particle can also be deduced from eqn. (12.2.30):

$$U(x,x';t) = \left(\frac{m}{2\pi i\hbar t}\right)^{1/2} \exp\left[\frac{im}{2\hbar t}(x-x')^2\right]. \tag{12.2.31}$$

Analytical evaluation of the path integral is only possible for general quadratic potentials. Nevertheless, the path integral formalism renders quantum statistical mechanical calculations tenable with modern computers, even for large systems for which determination of the eigenvalues of $\hat{\mathcal{H}}$ is intractable. Of course, such computations can only be performed numerically for finite P, which leads to discrete path integral representations of the density matrix and partition function. P should be large enough that the difference between the discrete path integral and the formal limit $P \to \infty$ is negligible. Methodology for performing path integral calculations in imaginary time will be discussed in Sections 12.8.1 and 12.8.2. We will see that such calculations are a little more complicated than analogous calculations in the classical canonical ensemble (see Section 4.9) but straightforward, in principle. Moreover, they converge on time scales similar to those of classical calculations. Unfortunately, the same is not true for the quantum propagator in eqn. (12.2.23) due to the complex exponential in the integrand. The latter causes numerical calculations to oscillate wildly as different paths are sampled, leading to a severe convergence problem known as the *dynamical sign problem*. Thus, while computing quantum equilibrium properties via path integrals has become routine, the calculation of dynamical properties from path integrals remains one of the most challenging problems in computational physics and chemistry. As of the writing of this book, no truly satisfactory solution has been achieved.

12.3 Thermodynamics and expectation values from path integrals

Path integral expressions for expectation values of Hermitian operators follow from the basic relation

$$\langle \hat{A} \rangle = \frac{1}{Q(L,T)} \mathrm{Tr}\left[\hat{A}\mathrm{e}^{-\beta\hat{\mathcal{H}}}\right]. \tag{12.3.1}$$

Performing the trace in the coordinate basis gives

$$\langle \hat{A} \rangle = \frac{1}{Q(L,T)} \int \mathrm{d}x\, \langle x|\hat{A}\mathrm{e}^{-\beta\hat{\mathcal{H}}}|x\rangle. \tag{12.3.2}$$

(We will not continue to include the spatial domain $D(L)$ in the expressions, but it must be remembered that the spatial integrals carry this restriction implicitly.) A

common case for which we need to evaluate eqn. (12.3.2) is ultimately the simplest. If $\hat{A}$ is purely a function of $\hat{x}$, then $|x\rangle$ is an eigenvector of $\hat{A}(\hat{x})$ satisfying

$$\hat{A}(\hat{x})|x\rangle = a(x)|x\rangle, \tag{12.3.3}$$

where $a(x)$ is the corresponding eigenvalue, and eqn. (12.3.2) reduces to

$$\langle \hat{A} \rangle = \frac{1}{Q(L,T)} \int \mathrm{d}x \; a(x) \langle x | \mathrm{e}^{-\beta \hat{\mathcal{H}}} | x \rangle. \tag{12.3.4}$$

Thus, for operators that are functions only of position, eqn. (12.3.4) indicates that only the diagonal elements of the density matrix are needed. Substituting eqn. (12.2.22) for $x = x'$ into eqn. (12.3.4) leads to a path integral expression for the expectation value of $\hat{A}(\hat{x})$:

$$\langle \hat{A} \rangle = \frac{1}{Q(L,T)} \lim_{P \to \infty} \left(\frac{mP}{2\pi\beta\hbar^2} \right)^{P/2} \int \mathrm{d}x_1 \cdots \mathrm{d}x_P \; a(x_1) \times \exp \left\{ -\frac{1}{\hbar} \sum_{k=1}^{P} \left[\frac{mP}{2\beta\hbar} (x_{k+1} - x_k)^2 + \frac{\beta\hbar}{P} U(x_k) \right] \right\} \Bigg|_{x_{P+1} = x_1} . \tag{12.3.5}$$

Although eqn. (12.3.5) is perfectly correct, it appears to favor one particular position variable (x_1) over the others, since $a(x)$ is evaluated only at this point. Equation (12.3.5) will consequently converge slowly and is not particularly useful for actual computations. Because the paths are cyclic, however, all points $x_1, ..., x_P$ of a path are equivalent. The equivalence can be proved by noting that the argument of the exponential is invariant under a cyclic relabeling of the coordinate variables

$$x'_2 = x_1, \quad x'_3 = x_2, \quad \cdots \quad x'_P = x_{P-1}, \quad x'_1 = x_P. \tag{12.3.6}$$

If such a relabeling is introduced into eqn. (12.3.5), a completely equivalent expression for the expectation value results:

$$\langle \hat{A} \rangle = \frac{1}{Q(L,T)} \lim_{P \to \infty} \left(\frac{mP}{2\pi\beta\hbar^2} \right)^{P/2} \int \mathrm{d}x'_1 \cdots \mathrm{d}x'_P \; a(x'_2) \times \exp \left\{ -\frac{1}{\hbar} \sum_{k=1}^{P} \left[\frac{mP}{2\beta\hbar} (x'_{k+1} - x'_k)^2 + \frac{\beta\hbar}{P} U(x'_k) \right] \right\} \Bigg|_{x'_{P+1} = x'_1} . \tag{12.3.7}$$

A second relabeling, $x''_3 = x'_2$, $x''_4 = x'_3$,....,$x''_P = x'_{P-1}$, $x''_1 = x'_P$, $x''_2 = x'_1$, would yield a similar expression with $a(x)$ evaluated at x''_3. Since P such relabelings are possible, we can derive P equivalent expressions for the expectation value, each involving the evaluation of the $a(x)$ at the different coordinates $x_1, ..., x_P$. If these expressions are added together and divided by P, we find

$$\langle \hat{A} \rangle = \frac{1}{Q(L,T)} \lim_{P\to\infty} \left(\frac{mP}{2\pi\beta\hbar^2}\right)^{P/2} \int \mathrm{d}x_1 \cdots \mathrm{d}x_P \left[\frac{1}{P}\sum_{k=1}^{P} a(x_k)\right]$$
$$\times \exp\left\{-\frac{1}{\hbar}\sum_{k=1}^{P}\left[\frac{mP}{2\beta\hbar}(x_{k+1}-x_k)^2 + \frac{\beta\hbar}{P}U(x_k)\right]\right\}\Bigg|_{x_{P+1}=x_1}, \tag{12.3.8}$$

which treats the P coordinates $x_1, ..., x_P$ on an equal footing.

Equation (12.3.8) can be put into a compact form as follows: First, we define a probability distribution function $f(x_1, ..., x_P)$ by

$$f(x_1, ..., x_P) = \frac{1}{Q_P(L,T)} \left(\frac{mP}{2\pi\beta\hbar^2}\right)^{P/2}$$
$$\times \exp\left\{-\frac{1}{\hbar}\sum_{k=1}^{P}\left[\frac{mP}{2\beta\hbar}(x_{k+1}-x_k)^2 + \frac{\beta\hbar}{P}U(x_k)\right]\right\}\Bigg|_{x_{P+1}=x_1}, \tag{12.3.9}$$

where $Q_P(L,T)$ is the partition function for finite P, which is obtained by removing the limit as $P \to \infty$ from eqn. (12.2.26):

$$Q_P(L,T) = \left(\frac{mP}{2\pi\beta\hbar^2}\right)^{P/2} \int \mathrm{d}x_1 \cdots \mathrm{d}x_P$$
$$\times \exp\left\{-\frac{1}{\hbar}\sum_{k=1}^{P}\left[\frac{mP}{2\beta\hbar}(x_{k+1}-x_k)^2 + \frac{\beta\hbar}{P}U(x_k)\right]\right\}\Bigg|_{x_{P+1}=x_1}. \tag{12.3.10}$$

Clearly, $Q(L,T) = \lim_{P\to\infty} Q_P(L,T)$. The function $f(x_1, ..., x_P)$ satisfies the conditions of a probability distribution: $f(x_1, ..., x_P) \geq 0$ for all $x_1, ..., x_P$ and

$$\int \mathrm{d}x_1 \cdots \mathrm{d}x_P \; f(x_1, ..., x_P) = 1. \tag{12.3.11}$$

In Section 7.2, we introduced the concept of an *estimator* for a multi-dimensional integral. In path integral calculations, equilibrium expectation values can be approximated using estimator functions that depend on the P coordinates $x_1, ..., x_P$. Thus, for eqn. (12.3.8), an appropriate estimator for $\langle \hat{A} \rangle$ is the function $a_P(x_1, ..., x_P)$ defined to be

$$a_P(x_1, ..., x_P) = \frac{1}{P}\sum_{k=1}^{P} a(x_k). \tag{12.3.12}$$

The expectation value $\langle \hat{A} \rangle$ can be approximated for finite P as an average of the estimator in eqn. (12.3.12) with respect to the probability distribution function $f(x_1, ..., x_P)$. We write this approximation as

$$\langle \hat{A} \rangle_P = \langle a_P(x_1, ..., x_P) \rangle_f, \tag{12.3.13}$$

where $\langle \cdots \rangle_f$ indicates an average over the probability distribution function $f(x_1, ..., x_P)$. It follows that $\langle \hat{A} \rangle = \lim_{P\to\infty} \langle \hat{A} \rangle_P$.

Suppose, next, that $\hat{A}$ is a function of just the momentum operator: $\hat{A} = \hat{A}(\hat{p})$. In this case, it is no longer possible to express $\hat{A}$ in terms of the diagonal elements of the density matrix. Hence, starting with eqn. (12.3.2), $|x\rangle$ is no longer an eigenvector of $\hat{A}(\hat{p})$ and cannot be brought outside the matrix element $\langle x|\hat{A}(\hat{p})\exp(-\beta\hat{\mathcal{H}})|x\rangle$. However, if we insert an identity operator in the form of eqn. (12.2.10) between $\hat{A}$ and $\exp(-\beta\hat{\mathcal{H}})$, then we have a product of two matrix elements:

$$\langle\hat{A}\rangle = \frac{1}{Q(L,T)}\int \mathrm{d}x\ \mathrm{d}x'\ \langle x|\hat{A}|x'\rangle\langle x'|\mathrm{e}^{-\beta\hat{\mathcal{H}}}|x\rangle. \tag{12.3.14}$$

Equation (12.3.14) requires diagonal and off-diagonal elements of the density matrix. Substituting eqn. (12.2.22) into eqn. (12.3.14) gives a path integral expression for $\langle\hat{A}\rangle$:

$$\langle\hat{A}\rangle = \frac{1}{Q(L,T)}\lim_{P\to\infty}\left(\frac{mP}{2\pi\beta\hbar^2}\right)^{P/2}\int \mathrm{d}x_1\cdots\mathrm{d}x_{P+1}\langle x_1|\hat{A}|x_{P+1}\rangle$$
$$\times\exp\left\{-\frac{1}{\hbar}\sum_{k=1}^{P}\left[\frac{mP}{2\beta\hbar}(x_{k+1}-x_k)^2+\frac{\beta\hbar}{2P}\left(U(x_{k+1})+U(x_k)\right)\right]\right\}. \tag{12.3.15}$$

Note that the paths in eqn. (12.3.15) are no longer cyclic, and $x_1 \neq x_{P+1}$. In general, a sum over open paths is more difficult to evaluate than a sum over closed, cyclic paths because of the large fluctuations in the endpoints and quantities such as $\langle x_1|\hat{A}(\hat{p})|x_{P+1}\rangle$ that depend on them. According to eqn. (4.6.33), the distribution of the end-to-end distance for a free particle is a Gaussian whose width grows as $T \to 0$. An interesting example of a quantity that requires such off-diagonal elements is the momentum distribution $n(p)$, which is obtained by taking $\hat{A}(\hat{p}) = \delta(\hat{p} - p'\hat{I})$, where p' is a pure number, so that

$$n(p') = \langle\delta(\hat{p}-p'\hat{I})\rangle = \frac{1}{2\pi\hbar}\int \mathrm{d}x\ \mathrm{d}x'\mathrm{e}^{ip'(x-x')}\langle x'|\mathrm{e}^{-\beta\hat{\mathcal{H}}}|x\rangle. \tag{12.3.16}$$

This distribution can be measured in neutron Compton scattering experiments and can be computed using an algorithm introduced by Morrone *et al.* (2007).

Expectation values of operator functions that depend on both position and momentum can be equally difficult to evaluate depending on how the operators $\hat{x}$ and $\hat{p}$ appear in $\hat{A}(\hat{x},\hat{p})$ (see eqn. (9.2.51)). The thermodynamic functions in the canonical ensemble are exceptional in that they can be evaluated using cyclic path integrals, as we will now demonstrate.

Consider first the evaluation of the average energy

$$E = \langle\hat{\mathcal{H}}\rangle = \left\langle\frac{\hat{p}^2}{2m}+U(\hat{x})\right\rangle. \tag{12.3.17}$$

Although the Hamiltonian is a function of both position and momentum, and it would, therefore, seem that both closed and open paths are needed to evaluate $\langle\hat{\mathcal{H}}\rangle$, we can evaluate E straightforwardly via the thermodynamic relation

$$E = -\frac{\partial}{\partial \beta} \ln Q(L,T) = -\frac{1}{Q(L,T)} \frac{\partial Q(L,T)}{\partial \beta}. \tag{12.3.18}$$

Since $Q(L,T)$ is expressible using only cyclic paths, these are all we need to calculate E. Taking the derivative of eqn. (12.2.26) with respect to β, we obtain the following expression for the energy:

$$\begin{aligned} E = & \frac{1}{Q(L,T)} \lim_{P\to\infty} \left(\frac{mP}{2\pi\beta\hbar^2}\right)^{P/2} \int \mathrm{d}x_1 \cdots \mathrm{d}x_P \, \varepsilon_P(x_1,...,x_P) \\ & \times \exp\left\{ -\frac{1}{\hbar} \sum_{k=1}^{P} \left[\frac{mP}{2\beta\hbar}(x_{k+1}-x_k)^2 + \frac{\beta\hbar}{P} U(x_k) \right] \right\} \Bigg|_{x_{P+1}=x_1} \\ = & \lim_{P\to\infty} \langle \varepsilon_P(x_1,...,x_P) \rangle_f, \end{aligned} \tag{12.3.19}$$

where

$$\varepsilon_P(x_1,...,x_P) = \frac{P}{2\beta} - \sum_{k=1}^{P} \frac{mP}{2\beta^2\hbar^2}(x_{k+1}-x_k)^2 + \frac{1}{P}\sum_{k=1}^{P} U(x_k). \tag{12.3.20}$$

Therefore, $\varepsilon_P(x_1,...,x_P)$ is an estimator for the energy, and the average $\langle \hat{\mathcal{H}} \rangle_P = \langle \varepsilon_P(x_1,...,x_P) \rangle_f$ converges to the true thermodynamic energy E in the limit $P \to \infty$.

Similarly, we can obtain an estimator for the one-dimensional "pressure," which we will denote Π, from the thermodynamic relation

$$\Pi = kT \frac{\partial \ln Q}{\partial L} = \frac{kT}{Q} \frac{\partial Q}{\partial L}. \tag{12.3.21}$$

As was done in Section 4.7.3, the one-dimensional "volume" L is made explicit by introducing scaled variables $s_k = x_k/L$ into the path integral for the partition function, which yields

$$\begin{aligned} Q(L,T) = & \lim_{P\to\infty} \left(\frac{mP}{2\pi\beta\hbar^2}\right)^{P/2} L^P \int \mathrm{d}s_1 \cdots \mathrm{d}s_P \\ & \times \exp\left[-\frac{1}{\hbar} \sum_{k=1}^{P} \left(\frac{mP}{2\beta\hbar} L^2 (s_{i+1}-s_i)^2 + \frac{\beta\hbar}{P} U(Ls_i) \right) \right] \Bigg|_{s_{P+1}=s_1}. \end{aligned} \tag{12.3.22}$$

Equation (12.3.22) can now be differentiated with respect to L and transformed back to the original path variables $x_1, ..., x_P$ to yield

$$\Pi = \frac{1}{Q(L,T)} \lim_{P\to\infty} \left(\frac{mP}{2\pi\beta\hbar^2}\right)^{P/2} \int \mathrm{d}x_1 \cdots \mathrm{d}x_P \; \mathcal{P}_P(x_1, ..., x_P)$$
$$\times \exp\left\{ -\frac{1}{\hbar} \sum_{k=1}^{P} \left[\frac{mP}{2\beta\hbar}(x_{k+1} - x_k)^2 + \frac{\beta\hbar}{P} U(x_k) \right] \right\} \Bigg|_{x_{P+1}=x_1}$$
$$= \lim_{P\to\infty} \langle \mathcal{P}_P(\mathbf{x}_1, ..., \mathbf{x}_P) \rangle_f, \tag{12.3.23}$$

where

$$\mathcal{P}_P(x_1, ..., x_P) = \frac{P}{\beta L} - \frac{1}{L} \sum_{k=1}^{P} \left[\frac{mP}{\beta^2\hbar^2} (x_{k+1} - x_k)^2 + \frac{1}{P} x_k \frac{\partial U}{\partial x_k} \right]. \tag{12.3.24}$$

Thus, $\mathcal{P}_P(x_1, ..., x_P)$ is an estimator for the pressure (Martyna *et al.*, 1999) so that we can calculate the average pressure from $P = \lim_{P\to\infty} \langle \mathcal{P}_P(x_1, ..., x_P) \rangle_f$. As we discussed in Section 4.7.3, if the potential U has an explicit length (volume) dependence, then the estimator becomes

$$\mathcal{P}_P(x_1, ..., x_P) =$$
$$\frac{P}{\beta L} - \frac{1}{L} \sum_{k=1}^{P} \left[\frac{mP}{\beta^2\hbar^2} (x_{k+1} - x_k)^2 + \frac{1}{P} x_k \frac{\partial U}{\partial x_k} - \frac{L}{P} \frac{\partial U(x_k, L)}{\partial L} \right]. \tag{12.3.25}$$

The basic thermodynamic relations of the canonical ensemble can be used to derive estimators for other thermodynamic quantities such as the constant-volume heat capacity (Glaesemann and Fried, 2002) (see Problem 12.3). We will explore the utility of expressions like eqns. (12.3.20) and (12.3.24) in practical calculations in Section 12.8.1.

12.4 The continuous limit: Functional integrals

Before we discuss the numerical implementation of path integrals, let us examine the physical content of the path integral in greater detail by formally analyzing the $P \to \infty$ limit. This limit gives rise to a mathematical construct known as a *functional integral*. Because the physical picture associated with the functional integral is clearer for real-time quantum mechanics, we will begin the discussion by analyzing the propagator of eqn. (12.2.23) and then perform the Wick rotation to imaginary time to obtain the canonical density matrix and partition function. For this analysis, it is convenient to introduce a parameter $\epsilon = t/P$, so that $P \to \infty$ implies $\epsilon \to 0$. In terms of ϵ, eqn. (12.2.23) can be written as

$$U(x,x';t) = \lim_{\substack{P\to\infty \\ \epsilon\to 0}} \left(\frac{m}{2\pi i\epsilon\hbar}\right)^{P/2} \int \mathrm{d}x_2 \cdots \mathrm{d}x_P$$

$$\times \exp\left\{\frac{i\epsilon}{\hbar}\sum_{k=1}^{P}\left[\frac{m}{2}\left(\frac{x_{k+1}-x_k}{\epsilon}\right)^2 - \frac{1}{2}\left(U(x_{k+1})+U(x_k)\right)\right]\right\}\Bigg|_{x_1=x}^{x_{P+1}=x'} . \quad (12.4.1)$$

In the limit $P\to\infty$ and $\epsilon\to 0$, the time interval between the points $x_1, x_2, ..., x_P, x_{P+1}$ become infinitely small, while the number of points becomes infinite. Thus, in this limit, $x_1, ..., x_{P+1}$ becomes the complete set of points needed to specify a continuous function $x(s)$ satisfying $x(0)=x$, $x(t)=x'$, with the identification

$$x_k = x(s=(k-1)\epsilon). \quad (12.4.2)$$

Moreover, in the limit $\epsilon\to 0$, the quantity $(x_{k+1}-x_k)/\epsilon$ becomes

$$\lim_{\epsilon\to 0}\left(\frac{x_{k+1}-x_k}{\epsilon}\right) = \frac{dx}{ds}. \quad (12.4.3)$$

Finally, in the limit $\epsilon\to 0$, the argument of the exponential

$$\epsilon\sum_{k=1}^{P}\left[\frac{m}{2}\left(\frac{x_{k+1}-x_k}{\epsilon}\right)^2 - \frac{1}{2}\left(U(x_{k+1})+U(x_k)\right)\right]$$

is just a Riemann sum representation of an integral. Thus, we can write

$$\lim_{\epsilon\to 0}\epsilon\sum_{k=1}^{P}\left[\frac{m}{2}\left(\frac{x_{k+1}-x_k}{\epsilon}\right)^2 - \left(\frac{U(x_{k+1})+U(x_k)}{2}\right)\right]$$

$$= \int_0^t \mathrm{d}s\ \left[\frac{1}{2}m\dot{x}^2(s) - U(x(s))\right], \quad (12.4.4)$$

where $\dot{x}(s) = \mathrm{d}x/\mathrm{d}s$. Interestingly, we see that the integrand of eqn. (12.4.4) is the classical Lagrangian $\mathcal{L}(x,\dot{x}) = (m/2)\dot{x}^2 - U(x)$ for the system (see Section 1.4). In eqn. (12.4.4), the integral of the Lagrangian is taken along the path $x(s)$, and this integral is just the action integral of action functional from Section 1.8:

$$A[x] = \int_0^t \mathrm{d}s\ \left[\frac{1}{2}m\dot{x}^2(s) - U(x(s))\right]. \quad (12.4.5)$$

Thus, the weight factor for a given path $x(s)$ that begins at x and ends at x' in time t is just the complex exponential $\exp(iA[x]/\hbar)$.

We turn next to the integration measure $\mathrm{d}x_2\cdots\mathrm{d}x_P$. As noted previously, the points $x_1, ..., x_{P+1}$ comprise all of the points of the function $x(s)$ in the limit $P\to\infty$, with $x_1 = x$ and $x_{P+1} = x'$. Thus, the integration over $x_2, ..., x_P$ constitutes an

integration over all possible functions $x(s)$ that satisfy the endpoint conditions $x(0) = x$, $x(t) = x'$. In other words, as $P \to \infty$, integrating over $x_2, ..., x_P$ varies all points of the function $x(s)$, which is equivalent to varying the function, itself keeping $x(0)$ and $x(t)$ fixed at x and x', respectively. This type of integration is referred to as *functional integration*. Symbolically, it is written as follows:

$$\lim_{P\to\infty,\epsilon\to 0} \left(\frac{m}{2\pi i\epsilon\hbar}\right)^{P/2} \mathrm{d}x_2 \cdots \mathrm{d}x_P \equiv \mathcal{D}x(s). \tag{12.4.6}$$

Thus, the functional integral representation of the real-time propagator is

$$\begin{aligned} U(x,x';t) &= \int_{x(0)=x}^{x(t)=x'} \mathcal{D}x(s)\ \exp\left\{\frac{i}{\hbar}\int_0^t \mathrm{d}s\ \left[\frac{1}{2}m\dot{x}^2(s) - U(x(s))\right]\right\} \\ &= \int_{x(0)=x}^{x(t)=x'} \mathcal{D}x(s)\ \exp\left\{\frac{i}{\hbar}\int_0^t \mathrm{d}s\ \mathcal{L}(x(s),\dot{x}(s))\right\} \\ &= \int_x^{x'} \mathcal{D}x\ \mathrm{e}^{iA[x]/\hbar}. \end{aligned} \tag{12.4.7}$$

At this point, several comments are in order. Equation (12.4.7) reveals that the functional integral is truly an integral over all paths $x(s)$ that begin at x at $s = 0$ and end at x' at $s = t$ with a weight $\exp(iA[x]/\hbar)$ assigned to each path. The integral over paths is illustrated in Fig. 12.8. The last line in eqn. (12.4.7) implies that the time

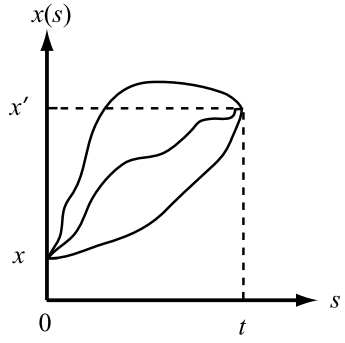

Fig. 12.8 Representative continuous paths in the path integral for the quantum propagator in eqn. (12.4.7).

label s is irrelevant, since the propagator $U(x,x';t)$ only depends on the endpoints of the paths and the time t associated with paths. Similarly, the action $A[x]$ is a function only of x, x', and t, $A(x,x';t)$. Consequently, the path integral sometimes appears in the literature as

$$U(x,x';t) = \int_{x(0)=x}^{x(t)=x'} \mathcal{D}x(\cdot)\ \mathrm{e}^{iA[x(\cdot)]/\hbar} \tag{12.4.8}$$

to indicate that the symbol used as the integration variable in the action integral is irrelevant. Finally, we point out that eqn. (12.4.7) is exactly equivalent to eqn.

(12.2.23); the former is only a symbolic representation of the latter. The functional integral notation provides a convenient and compact way of representing the more complicated discrete path integral expressions such as eqn. (12.2.23). Nevertheless, as we will see shortly, functional integrals can be directly manipulated and used for analytical calculations involving path integrals. Hence, the functional integral notation serves both a notational and a practical purpose.

Equation (12.4.7) contains some fascinating physical content. First, the weight factor $\exp(iA[x]/\hbar)$ implies that in the space of all possible paths $x(s)$, $x(0) = x$, $x(t) = x'$, the most important regions of the "path space" are those for which the action changes very little upon moving from one path to another. Indeed, when the variation in A is small, then the complex exponential oscillates very slowly in moving from path to path. Without frequent sign changes in $\exp(iA[x]/\hbar)$, the paths in this region of path space contribute significantly to the integral. On the other hand, there are other regions of path space for which A varies significantly in moving from one path to another. In this case, the exponential oscillates wildly, and the paths contribute negligibly to the path integral because contributions from closely spaced paths tend to cancel each other. More concretely, if we consider a path $x(s)$ and a slightly different path $\tilde{x}(s) = x(s)+\delta x(s)$, where $\delta x(s)$ is a small variation in $x(s)$, then these two paths will contribute significantly to the path integral if $\delta A \equiv A[x+\delta x] - A[x]$ is small. This condition is satisfied in a region where $A[x]$ is flat, that is where $\delta A/\delta x(s) \approx 0$. Note that since $x(0) = x$ and $x(t) = x'$, it follows that $\delta x(0) = \delta x(t) = 0$. Indeed, the most significant contribution occurs when $\delta A = 0$. However, recall from Section 1.8 that the condition $\delta A = 0$ is precisely the condition that leads to the Euler-Lagrange equation for the classical path:

$$\delta A = 0 \quad \Rightarrow \quad \frac{\mathrm{d}}{\mathrm{d}s}\left(\frac{\partial L}{\partial \dot{x}(s)}\right) - \frac{\partial L}{\partial x(s)} = 0. \tag{12.4.9}$$

For $L = (m/2)\dot{x}^2(s) - U(x(s))$, the equation of motion is the usual Newtonian form

$$m\frac{\mathrm{d}^2 x}{\mathrm{d}s^2} = -\frac{\partial U}{\partial x}. \tag{12.4.10}$$

We see, therefore, that the action integral and the principle of action extremization emerge naturally from the path integral formulation of quantum mechanics. This remarkable fact tells us that the most important contribution to the path integral is the region of path space around a classical path. The importance of paths that deviate from classical paths depends on the extent to which quantum effects dominate in a given system. For example, when a process occurs via quantum tunneling, paths that deviate considerably from classical paths have a significant contribution to the path integral since tunneling is a classically forbidden phenomenon. In other cases, where quantum effects are less important but not negligible, it may be possible to compute a path integral to a reasonable level of accuracy by performing an expansion about a classical path and working to a low order in the "quantum corrections." This popular approach is the basis of *semiclassical methods* for quantum dynamics. Finally, we note that the solution to the Euler-Lagrange equation with endpoint conditions $x(0) = x$ and $x(t) = x'$ may not be unique. We noted in Section 1.8 that the solution of the

Euler-Lagrange equation subject to initial values for x and $\dot{x}$ is unique; but as the path integral requires that the paths satisfy endpoint conditions, there are contribution from regions in path space around *each* classical path satisfying the endpoint conditions.

Equation (12.4.7) represents an integral over continuous real-time paths for the quantum mechanical propagator. However, due to eqn. (12.2.4), we may perform a Wick rotation and obtain functional integral expressions for the quantum mechanical density matrix and partition function in the canonical ensemble. This Wick rotation is performed by substituting $t = -i\beta\hbar$ into eqn. (12.4.7). Let the paths now be parameterized by a variable τ related to s by $\tau = is$. When $s = t = -i\beta\hbar$, $\tau = \beta\hbar$, and the action integral becomes

$$\begin{aligned}\int_0^t \mathrm{d}s \ \left[\frac{m}{2}\left(\frac{\mathrm{d}x}{\mathrm{d}s}\right)^2 - U(x(s))\right] &= \int_0^{-i\beta\hbar} \mathrm{d}(-i\tau) \ \left[\frac{m}{2}\left(\frac{\mathrm{d}x}{\mathrm{d}(-i\tau)}\right)^2 - U(x(-i\tau))\right] \\ &= i\int_0^{\beta\hbar} \mathrm{d}\tau \ \left[\frac{m}{2}\left(\frac{\mathrm{d}x}{\mathrm{d}\tau}\right)^2 + U(x(\tau))\right] \\ &\equiv iS[x]. \end{aligned} \tag{12.4.11}$$

Note that the action $S[x]$ is now the action for paths in *imaginary time* τ that start at $x(0) = x$ and end at $x(\tau) = x'$ in imaginary time $\tau = \beta\hbar$. The imaginary-time action $S[x]$ differs from the real-time action $A[x]$ by the sign of the potential. The action $S[x]$ is often called the *Euclidean action*. In terms of imaginary-time paths, we may write the density matrix elements as

$$\begin{aligned}\rho(x, x'; \beta) &= \int_{x(0)=x}^{x(\beta\hbar)=x'} \mathcal{D}x(\tau) \ \exp\left\{-\frac{1}{\hbar}\int_0^{\beta\hbar} \mathrm{d}\tau \ \left[\frac{1}{2}m\dot{x}^2(\tau) + U(x(\tau))\right]\right\} \\ &= \int_{x(0)=x}^{x(\beta\hbar)=x'} \mathcal{D}x(\tau) \ \exp\left\{-\frac{1}{\hbar}\int_0^{\beta\hbar} \mathrm{d}\tau \ \Lambda(x(\tau), \dot{x}(\tau))\right\} \\ &= \int_x^{x'} \mathcal{D}x \ \mathrm{e}^{-S[x]/\hbar}. \end{aligned} \tag{12.4.12}$$

The quantity $\Lambda(x, \dot{x}) = (m/2)\dot{x}^2 + U(x)$ is called the *imaginary-time Lagrangian* or *Euclidean Lagrangian*. The density matrix is constructed by integrating over all paths $x(\tau)$ that satisfy $x(0) = x$, $x(\beta\hbar) = x'$ weighted by $\exp(-S[x]/\hbar)$. Since this weight factor is positive definite, we can find the most important contributions to the functional integral in eqn. (12.4.12) by minimizing the Euclidean action with respect to the path $x(\tau)$. As we did for the propagator, we consider a path $x(\tau)$ and a nearby path $\tilde{x}(\tau) = x(\tau) + \delta x(\tau)$. If $x(0) = x$ and $x(\beta\hbar) = x'$, then $\delta x(0) = \delta x(\beta\hbar) = 0$. We require that the variation $\delta S = S[x + \delta x] - S[x]$ vanish to first order in the path variation δx. Following the procedure in Section 1.8, the resulting equation of motion will be exactly the form of the Euler-Lagrange equation applied to Λ:

$$\frac{\mathrm{d}}{\mathrm{d}\tau}\left(\frac{\partial\Lambda}{\partial\dot{x}(\tau)}\right)-\frac{\partial\Lambda}{\partial x(\tau)}=0. \tag{12.4.13}$$

However, when we apply the Euler-Lagrange equation to the Euclidean Lagrangian, we obtain an equation of motion of the form

$$m\frac{\mathrm{d}^2x}{\mathrm{d}\tau^2}=\frac{\partial U}{\partial x}. \tag{12.4.14}$$

Equation (12.4.14) resembles Newton's second law except that the force is calculated using not the potential $U(x)$ but an inverted potential surface $-U(x)$. This result is not unexpected: If we transform Newton's second law in real time $m\mathrm{d}^2x/\mathrm{d}s^2 = -\partial U/\partial x$ to imaginary time using $s=-i\tau$, then the equation of motion becomes $m\mathrm{d}^2x/\mathrm{d}s^2 \longrightarrow m\mathrm{d}^2x/\mathrm{d}(-i\tau)^2 = -m\mathrm{d}^2x/\mathrm{d}\tau^2 = -\partial U/\partial x$, which is just eqn. (12.4.14). Thus, dominant paths are solutions to eqn. (12.4.14) subject to the endpoint conditions $x(0)=x$ and $x(\beta\hbar)=x'$.

We can now use eqn. (12.4.12) to construct a functional integral expression for the partition function $Q(\beta)$. Since

$$Q(\beta)=\int \mathrm{d}x\ \rho(x,x;\beta), \tag{12.4.15}$$

we begin by taking the diagonal element of $\hat{\rho}$ in eqn. (12.4.12):

$$\begin{aligned}\rho(x,x;\beta)&=\int_{x(0)=x}^{x(\beta\hbar)=x}\mathcal{D}x(\tau)\ \exp\left\{-\frac{1}{\hbar}\int_0^{\beta\hbar}\mathrm{d}\tau\ \left[\frac{1}{2}m\dot{x}^2(\tau)+U(x(\tau))\right]\right\}\\&=\int_{x(0)=x}^{x(\beta\hbar)=x}\mathcal{D}x(\tau)\ \exp\left\{-\frac{1}{\hbar}\int_0^{\beta\hbar}\mathrm{d}\tau\ \Lambda(x(\tau),\dot{x}(\tau))\right\}\\&=\int_x^x\mathcal{D}x\ \mathrm{e}^{-S[x]/\hbar}.\end{aligned} \tag{12.4.16}$$

Note that although the upper and lower limits of integration on the functional measure $\mathcal{D}x$ are the same, the integral does not vanish as would be the case for an ordinary integral. Rather, eqn. (12.4.16) denotes an integral over all paths that begin and end at the same point x ($x(0)=x(\beta\hbar)=x$). In order to construct the partition function, we must integrate over all x, which gives

$$\begin{aligned}Q(\beta)&=\int\mathrm{d}x\int_{x(0)=x}^{x(\beta\hbar)=x}\mathcal{D}x(\tau)\ \exp\left\{-\frac{1}{\hbar}\int_0^{\beta\hbar}\mathrm{d}\tau\ \left[\frac{1}{2}m\dot{x}^2(\tau)+U(x(\tau))\right]\right\}\\&=\int\mathrm{d}x\int_{x(0)=x}^{x(\beta\hbar)=x}\mathcal{D}x(\tau)\ \exp\left\{-\frac{1}{\hbar}\int_0^{\beta\hbar}\mathrm{d}\tau\Lambda(x(\tau),\dot{x}(\tau))\right\}\\&=\int\mathrm{d}x\ \int_x^x\mathcal{D}x\ \mathrm{e}^{-S[x]/\hbar}\end{aligned}$$

$$\equiv \oint \mathcal{D}x \, \mathrm{e}^{-S[x]/\hbar}. \tag{12.4.17}$$

The $\oint$ symbol in last line of eqn. (12.4.17) indicates that the functional integral is to be taken over all paths that satisfy the condition $x(0) = x(\beta\hbar)$. These paths are periodic in imaginary time with period $\beta\hbar$. Consequently, the dominant contribution to the path integral for the partition function are paths near the solutions to eqn. (12.4.14) that satisfy $x(0) = x(\beta\hbar)$.

12.4.1 Example: The harmonic oscillator

In order to illustrate the use of the functional integral formalism, consider a simple harmonic oscillator of mass m and frequency ω described by the Hamiltonian of eqn. (9.3.18). The functional integral for the full density matrix is

$$\rho(x, x'; \beta) = \int_{x(0)=x}^{x(\beta\hbar)=x'} \mathcal{D}x(\tau) \exp\left[-\frac{1}{\hbar}\int_0^{\beta\hbar} \mathrm{d}\tau \left(\frac{1}{2}m\dot{x}^2 + \frac{1}{2}m\omega^2 x^2\right)\right]. \tag{12.4.18}$$

As we have already seen, paths in the vicinity of the classical path on the inverted potential dominate the functional integral. Thus, in order to perform the functional integral, we utilize a technique known as *expansion about the classical path*. Suppose we are able to solve eqn. (12.4.14) for a classical path $x_{\mathrm{cl}}(\tau)$ satisfying $x_{\mathrm{cl}}(0) = x$ and $x_{\mathrm{cl}}(\beta\hbar) = x'$. Given this path, we perform a "change of variables" in the functional integral; that is, we change the function of integration $x(\tau)$ to a new function $y(\tau)$ via the transformation $x(\tau) = x_{\mathrm{cl}}(\tau) + y(\tau)$. This transformation is similar to a change of variables of the form $x = a + y$ in an ordinary integral $\int f(x)\mathrm{d}x$, where a is a constant, so that $\mathrm{d}x = \mathrm{d}y$. Here, since $x_{\mathrm{cl}}(\tau)$ is a single function, it is analogous to the constant a, and $\mathcal{D}x(\tau) = \mathcal{D}y(\tau)$. For the harmonic oscillator, $x_{\mathrm{cl}}(\tau)$ satisfies the classical equation of motion $\ddot{x}_{\mathrm{cl}} = \omega^2 x_{\mathrm{cl}}$ on the inverted potential surface $-U(x) = -m\omega^2 x^2/2$, with $x_{\mathrm{cl}}(0) = x$ and $x_{\mathrm{cl}}(\beta\hbar) = x'$. Consequently, $y(0) = y(\beta\hbar) = 0$.

Substitution of this change of variables into the action integral yields

$$\begin{aligned}
S &= \int_0^{\beta\hbar} \mathrm{d}\tau \left[\frac{1}{2}m\dot{x}^2 + \frac{1}{2}m\omega^2 x^2\right] \\
&= \int_0^{\beta\hbar} \mathrm{d}\tau \left[\frac{1}{2}m(\dot{x}_{\mathrm{cl}} + \dot{y})^2 + \frac{1}{2}m\omega^2(x_{\mathrm{cl}} + y)^2\right] \\
&= \int_0^{\beta\hbar} \mathrm{d}\tau \left[\frac{1}{2}m\dot{x}_{\mathrm{cl}}^2 + \frac{1}{2}m\omega^2 x_{\mathrm{cl}}^2\right] + \int_0^{\beta\hbar} \mathrm{d}\tau \left[\frac{1}{2}m\dot{y}^2 + \frac{1}{2}m\omega^2 y^2\right] \\
&\quad + \int_0^{\beta\hbar} \mathrm{d}\tau \left[m\dot{x}_{\mathrm{cl}}\dot{y} + m\omega^2 x_{\mathrm{cl}} y\right].
\end{aligned} \tag{12.4.19}$$

The last line of eqn. (12.4.19) contains cross terms between $x_{\mathrm{cl}}(\tau)$ and $y(\tau)$, but these terms can be shown to vanish using an integration by parts:

$$\int_0^{\beta\hbar} \mathrm{d}\tau \left[m\dot{x}_{\mathrm{cl}}\dot{y} + m\omega^2 x_{\mathrm{cl}} y\right] = m\dot{x}_{\mathrm{cl}} y\Big|_0^{\beta\hbar} + \int_0^{\beta\hbar} \mathrm{d}\tau \left[-m\ddot{x}_{\mathrm{cl}} + m\omega^2 x_{\mathrm{cl}}\right] y$$

$$= 0. \tag{12.4.20}$$

The boundary term vanishes because $y(0) = y(\beta\hbar) = 0$, and the second term vanishes because $x_{\rm cl}(\tau)$ satisfies $\ddot{x}_{\rm cl} = \omega^2 x_{\rm cl}$.

The first term in the penultimate line of eqn. (12.4.19) is the classical Euclidean action integral. The solution of $\ddot{x}_{\rm cl} = \omega^2 x_{\rm cl}$ that satisfies the endpoint conditions is

$$x_{\rm cl}(\tau) = \frac{x\left(\mathrm{e}^{-\omega(\tau-\beta\hbar)} - \mathrm{e}^{\omega(\tau-\beta\hbar)}\right) + x'\left(\mathrm{e}^{\omega\tau} - \mathrm{e}^{-\omega\tau}\right)}{\mathrm{e}^{\beta\hbar\omega} - \mathrm{e}^{-\beta\hbar\omega}}, \tag{12.4.21}$$

which we derive by assuming a solution of the form $x_{\rm cl}(\tau) = A\exp(\omega\tau) + B\exp(-\omega\tau)$ and using the endpoint conditions to solve for the constants A and B. When this solution is substituted into the classical action integral, we obtain

$$\int_0^{\beta\hbar} \mathrm{d}\tau \left[\frac{1}{2}m\dot{x}_{\rm cl}^2(\tau) + \frac{1}{2}m\omega^2 x_{\rm cl}^2(\tau)\right] = \frac{m\omega}{2\sinh(\beta\hbar\omega)}\left[\left(x^2 + (x')^2\right)\cosh(\beta\hbar\omega) - 2xx'\right]. \tag{12.4.22}$$

Inserting eqn. (12.4.22) into eqn. (12.4.18), we obtain the density matrix for the harmonic oscillator as

$$\rho(x, x'; \beta) = I_0 \exp\left\{-\frac{m\omega}{2\hbar\sinh(\beta\hbar\omega)}\left[\left(x^2 + (x')^2\right)\cosh(\beta\hbar\omega) - 2xx'\right]\right\}, \tag{12.4.23}$$

where I_0 is the path integral

$$I_0 = \int_{y(0)=0}^{y(\beta\hbar)=0} \mathcal{D}y(\tau) \exp\left[-\frac{1}{\hbar}\int_0^{\beta\hbar} \mathrm{d}\tau \left(\frac{m}{2}\dot{y}^2 + \frac{m\omega^2}{2}y^2\right)\right]. \tag{12.4.24}$$

Note that the remaining functional integral I_0 does not depend on the points x and x' and therefore can only contribute an overall (temperature-dependent) constant to the density matrix. This affects the thermodynamics but not any averages of physical observables.[1] Nevertheless, it is instructive to see how such a functional integral is performed.

We first note that I_0 is a functional integral over functions $y(\tau)$ satisfying $y(0) = y(\beta\hbar) = 0$. Because of these endpoint conditions, the paths $y(\tau)$ can be expanded in a Fourier sine series:

$$y(\tau) = \sum_{n=1}^{\infty} c_n \sin(\omega_n \tau), \tag{12.4.25}$$

where

$$\omega_n = \frac{n\pi}{\beta\hbar}. \tag{12.4.26}$$

Since a given $y(\tau)$ is uniquely determined by its expansion coefficients c_n, integrating over the functions $y(\tau)$ is equivalent to integrating over all possible values of the

[1] This is only the case for the harmonic oscillator. For anharmonic potentials, a stationary-phase approximation to the path integral, which also employs an expansion about classical paths, allows the dependence of I_0 on x and x' to be approximated.

expansion coefficients. Thus, we seek to change from an integral over the functions $y(\tau)$ to an integral over the coefficients c_n. Using eqn. (12.4.25), let us first determine the argument of the exponential. We first note that

$$\dot{y}(\tau) = \sum_{n=1}^{\infty} \omega_n c_n \cos(\omega_n \tau). \tag{12.4.27}$$

Thus, the terms in the action are:

$$\int_0^{\beta\hbar} \mathrm{d}\tau \frac{m}{2}\dot{y}^2 = \frac{m}{2} \sum_{n=1}^{\infty} \sum_{n'=1}^{\infty} c_n c_{n'} \omega_n \omega_{n'} \int_0^{\beta\hbar} \mathrm{d}\tau \cos(\omega_n \tau) \cos(\omega_{n'} \tau). \tag{12.4.28}$$

Since the cosines are orthogonal on the interval $\tau \in [0, \beta\hbar]$, the integral simplifies to

$$\begin{aligned} \int_0^{\beta\hbar} \mathrm{d}\tau \frac{m}{2}\dot{y}^2 &= \frac{m}{2} \sum_{n=1}^{\infty} c_n^2 \omega_n^2 \int_0^{\beta\hbar} \mathrm{d}\tau \cos^2(\omega_n \tau) \\ &= \frac{m}{2} \sum_{n=1}^{\infty} c_n^2 \omega_n^2 \int_0^{\beta\hbar} \mathrm{d}\tau \left[\frac{1}{2} + \frac{1}{2}\cos(2\omega_n \tau)\right] \\ &= \frac{m\beta\hbar}{4} \sum_{n=1}^{\infty} c_n^2 \omega_n^2. \end{aligned} \tag{12.4.29}$$

In a similar manner, we can show that

$$\int_0^{\beta\hbar} \mathrm{d}\tau \frac{1}{2} m\omega^2 y^2 = \frac{m\beta\hbar}{4} \omega^2 \sum_{n=1}^{\infty} c_n^2. \tag{12.4.30}$$

Next, we need to change the integration measure from $\mathcal{D}y(\tau)$ to an integration over the coefficients c_n. This is rather subtle since we are transforming from a continuous functional measure to a discrete one, and it is not immediately clear how the Jacobian is computed. The simplest way to transform the measure is to assume that

$$\mathcal{D}y(\tau) = g_0 \prod_{n=1}^{\infty} g_n \mathrm{d}c_n, \tag{12.4.31}$$

where the g_0 and g_n are constants, and then adjust these parameters so that the final result yields the correct free particle limit $\omega = 0$. With this change of variables, I_0 becomes

$$I_0 = g_0 \prod_{n=1}^{\infty} \int_{-\infty}^{\infty} g_n \mathrm{d}c_n \exp\left[-\frac{m\beta}{4}(\omega^2 + \omega_n^2) c_n^2\right]$$

$$= g_0 \prod_{n=1}^{\infty} g_n \left[\frac{4\pi}{m\beta(\omega^2 + \omega_n^2)} \right]^{1/2} . \tag{12.4.32}$$

From eqn. (12.4.32), we see that the free particle limit can be recovered by choosing

$$g_0 = \left[\frac{m}{2\pi\beta\hbar^2} \right]^{1/2} , \qquad g_n = \left[\frac{m\beta\omega_n^2}{2\pi} \right]^{1/2} . \tag{12.4.33}$$

When $\omega = 0$, the product is exactly 1 for this choice of g_0 and g_n, which leaves the overall free particle prefactor in eqn. (12.2.30).

For $\omega \neq 0$, the infinite product is

$$\begin{aligned} \prod_{n=1}^{\infty} \left[\frac{\omega_n^2}{\omega^2 + \omega_n^2} \right]^{1/2} &= \prod_{n=1}^{\infty} \left[\frac{\pi^2 n^2/\beta^2\hbar^2}{\omega^2 + \pi^2 n^2/\beta^2\hbar^2} \right]^{1/2} \\ &= \left[\prod_{n=1}^{\infty} \left(1 + \frac{\beta^2\hbar^2\omega^2}{\pi^2 n^2} \right) \right]^{-1/2} . \end{aligned} \tag{12.4.34}$$

The product in the square brackets is one of many infinite product formulas for simple functions.[2] In this case, the product formula of interest is

$$\frac{\sinh(x)}{x} = \prod_{n=1}^{\infty} \left[1 + \frac{x^2}{\pi^2 n^2} \right] . \tag{12.4.35}$$

Using this formula, eqn. (12.4.34) becomes

$$I_0 = g_0 \left[\frac{\beta\hbar\omega}{\sinh(\beta\hbar\omega)} \right]^{1/2} = \left[\frac{m\omega}{2\pi\hbar\sinh(\beta\hbar\omega)} \right]^{1/2} . \tag{12.4.36}$$

Thus, the density matrix for a harmonic oscillator is finally given by

$$\begin{aligned} \rho(x, x'; \beta) = &\left[\frac{m\omega}{2\pi\hbar\sinh(\beta\hbar\omega)} \right]^{1/2} \\ &\times \exp\left\{ -\frac{m\omega}{2\hbar\sinh(\beta\hbar\omega)} \left[\left(x^2 + (x')^2\right)\cosh(\beta\hbar\omega) - 2xx' \right] \right\} . \end{aligned} \tag{12.4.37}$$

Note that in the free-particle limit, we take the limit $\omega \to 0$, set $\sinh(\beta\hbar\omega) \approx \beta\hbar\omega$ and $\cosh(\beta\hbar\omega) \approx 1$, so that eqn. (12.4.37) reduces to eqn. (12.2.30).

12.5 How to think about imaginary time propagation

In the previous sections, we introduced the concept of imaginary time, suggesting that the quantum canonical density matrix $\hat{\rho}(\beta)$ is a quantum propagator in imaginary time

[2] See, for example, Weber and Arfken's *Methods of Mathematical Physics* (2005).

$-i\hbar$. We now introduce an imaginary-time parameter $\tau \in [0, \beta\hbar]$ and an imaginary time propagator $u(x, x'; \tau) = \langle x'| \exp(-\tau\hat{\mathcal{H}}/\hbar)|x\rangle$, such that $\rho(x, x'; \beta) = u(x, x'; \beta\hbar)$. The interpretation of $u(x, x'; \tau)$ is that a system is initiated in the state $|x\rangle$, the state is then propagated in imaginary time from 0 to $\beta\hbar$, and the inner product with $\langle x'|$ is taken in order to obtain an imaginary-time "amplitude" to find the system in the state $|x'\rangle$ at $\tau = \beta\hbar$. Since $\beta = 1/kT$, it is useful to introduce a variable temperature ϑ, such that $\tau = 1/k\vartheta$, with $\vartheta = (\infty, T]$. Thus, when $\tau = 0$, $\vartheta = \infty$, *i.e.*, at $\tau = 0$, the system is at infinite temperature. At $\tau = 0$ ($\vartheta = \infty$), $\exp(-\tau\hat{\mathcal{H}}/\hbar) = \hat{I}$ becomes the identity operator, and $u(x, x'; 0) \to \langle x'|x\rangle = \delta(x - x')$, which provides another way to view the classical (high-temperature) limit. Additionally, if we cast $u(x, x'; \tau)$ in an energy basis, where

$$u(x, x'; \tau) = \sum_n \langle x'|E_n\rangle\langle E_n|x\rangle e^{-\tau E_n}, \tag{12.5.1}$$

then when $\tau \to 0$, this becomes

$$u(x, x'; 0) = \sum_n \langle x'|E_n\rangle\langle E_n|x\rangle = \delta\left(x - x'\right), \tag{12.5.2}$$

which follows from the completeness of the energy eigenstates. Thus, we see that at infinite temperature, all energy states are occupied with equal probability (recall the discussion of equal *a priori* probabilities in Section 3.2). In addition, we see that the density matrix is diagonal and describes a localized particle with zero thermal de Broglie wavelength.

Now suppose we propagate a coordinate eigenstate $|x\rangle$ in imaginary time starting from $\tau = 0$ up to an imaginary time $\tau = \beta\hbar$. If we do this in small steps $\delta\tau$, then these correspond to small steps in temperature $\delta\vartheta$ related by $\delta\tau = -(1/k\vartheta^2)\delta\vartheta$. We see that uniform steps in τ are not uniform in temperature. At $\tau = 0$, the temperature is infinite, and since $\delta\tau > 0$ and $\delta\vartheta < 0$, initial steps in τ are steps *down* in temperature ϑ. If $\delta\tau$ is fixed, the prefactor $1/k\vartheta^2$, which is small at large ϑ, causes the initial steps $\delta\vartheta$ to be large so that the temperature decreases rapidly at first, ultimately slowing until the physical temperature T is reached. That is, propagation in imaginary time can be interpreted as cooling a system from infinite temperature down to physical temperature T. As the system cools, the probabilities of occupying different energy states decrease from 1 to a set of nonuniform weights $\exp(-\tau E_n)$, such that the highest energy states depopulate relative to lower energy states. As the system becomes increasingly localized in a few low-lying energy states, it becomes increasingly delocalized spatially, consistent with the uncertainty principle, causing off-diagonal elements in $u(x, x'; \tau) = \langle x'| \exp(-\tau\hat{\mathcal{H}}/\hbar)|x\rangle$ to appear. Changes in the diagonal elements $u(x, x; \tau)$ of the imaginary-time propagator correspond to the growth of the ring polymer as the temperature decreases.

The interpretation of imaginary-time propagation as a cooling down of a system from infinite temperature to physical temperature T is not meant to be entirely rigorous, but it does provide a perspective for thinking about imaginary-time paths. At $\tau = 0$, a matrix element such as $u(x, x'; 0) = \langle x'|\hat{I}|x\rangle = \delta(x' - x)$ tells us that at infinite temperature, the system is completely delocalized in energy space and, therefore, fully localized spatially. If we now divide the interval $[0, \beta\hbar]$ into P discrete steps of length

ϵ, then a single step in imaginary time is equivalent to a cooling step that slightly localizes the system in energy space and slightly delocalizes the system spatially. Thus, a matrix element of the form $u(x, x'; \epsilon) = \langle x'| \exp(-\epsilon\hat{\mathcal{H}}/\hbar)|x\rangle$ provides a measure of how far x' is from x as a result of this slight delocalization caused by cooling. If we now take another step in imaginary time, *i.e.*, another cooling step, which further localizes the system in energy space, then the sequence of matrix elements that occurs in the construction of an imaginary-time path, $\langle x'| \exp(-\epsilon\hat{\mathcal{H}}/\hbar)|x_1\rangle\langle x_1| \exp(-\epsilon\hat{\mathcal{H}}/\hbar)|x\rangle$, measures how far x is from an intermediate point x_1 as a result of the first cooling step and then how far x' is from x_1 as a result of the second cooling step. Of course, in order to construct $u(x, x'; 2\epsilon)$, we need to integrate over all x_1 and consider all possible intermediate points, but each individual x_1 is part of a single cooling or imaginary-time path. It now becomes clear that the sequence of P matrix elements occurring in the integrand of eqn. (12.2.11)

$$\langle x'| \exp(-\epsilon\hat{\mathcal{H}}/\hbar)|x_{P-1}\rangle\langle x_{P-1}| \cdots |x_2\rangle\langle x_2| \exp(-\epsilon\hat{\mathcal{H}}/\hbar)|x_1\rangle\langle x_1| \exp(-\epsilon\hat{\mathcal{H}}/\hbar)|x\rangle,$$

which represents a single imaginary time or cooling path, measures the accessibility of each coordinate eigenstate $|x_i\rangle$ from the previous state $|x_{i-1}\rangle$ after each individual cooling step. Thus, the set of states $x, x_1, x_2, ..., x_{P-1}, x'$ provides one realization of how a system sequentially delocalizes as it steps down (nonuniformly) in temperature and will tell us about the accessibility of the state $|x'\rangle$ when the system passes through this particular sequence of states as it cools. Taking the $\epsilon \to 0$ limit then gives us a continuous path $x(\tau)$ or a continuous set of states between x and x' through which the system can pass as it cools continuously and delocalizes spatially. Of course, it must be kept in mind that the operator $\exp(-\tau\hat{\mathcal{H}}/\hbar)$ is not unitary and, therefore, is neither norm-preserving nor "imaginary-time" reversible, which tells us that the "cooling" a system undergoes along an imaginary-time path is neither unitary nor reversible. However, we would not expect it to be either of these since the very process of cooling causes a simultaneous localization in energy space and delocalization in coordinate space. It might be helpful to keep this picture of imaginary-time propagation as a putative cooling process in mind as we now proceed to ramp up the complexity and extend the concepts developed thus far to many-body systems.

12.6 Many-body path integrals

Construction of a path integral for a system of N indistinguishable particles is nontrivial because we must take into account the symmetry of the physical states. Consider, for example, the case of two identical particles described by a Hamiltonian $\hat{\mathcal{H}}$. If we wish to compute the partition function $Q = \mathrm{Tr}[\exp(-\beta\hat{\mathcal{H}})]$ by performing the trace in the coordinate basis, how we write down the proper coordinate eigenvectors depends on whether the overall state is symmetric or antisymmetric. If the coordinate labels are x_1 and x_2, then, as we saw in Section 9.4, the coordinate eigenvectors for bosons and fermions take the form

$$|\{x_1\ x_2\}_{\mathrm{B}}\rangle = \frac{1}{\sqrt{2}}\left[\ |x_1\ x_2\rangle + |x_2\ x_1\rangle\right] \qquad \text{(bosons)}$$

$$|\{x_1\ x_2\}_{\rm F}\rangle = \frac{1}{\sqrt{2}}\left[\ |x_1\ x_2\rangle - |x_2\ x_1\rangle\right] \qquad \text{(fermions)},$$

respectively. The completeness relations for these coordinate eigenstates take the form

$$\int {\rm d}x_1\ {\rm d}x_2\ |\{x_1\ x_2\}_{\rm B}\rangle\langle\{x_1\ x_2\}_{\rm B}| = \hat{I}$$

$$\int {\rm d}x_1\ {\rm d}x_2\ |\{x_1\ x_2\}_{\rm F}\rangle\langle\{x_1\ x_2\}_{\rm F}| = \hat{I}. \tag{12.6.1}$$

Thus, for bosons, the partition function is given by

$$\begin{aligned} Q &= \frac{1}{2}\int {\rm d}x_1\ {\rm d}x_2\ \left[\langle x_1\ x_2| + \langle x_2\ x_1|\ \right] {\rm e}^{-\beta\hat{\mathcal{H}}}\left[\ |x_1\ x_2\rangle + |x_2\ x_1\rangle\right] \\ &= \int {\rm d}x_1\ {\rm d}x_2\ \left[\langle x_1\ x_2|{\rm e}^{-\beta\hat{\mathcal{H}}}|x_1\ x_2\rangle + \langle x_1\ x_2|{\rm e}^{-\beta\hat{\mathcal{H}}}|x_2\ x_1\rangle\right], \end{aligned} \tag{12.6.2}$$

while for fermions, it is

$$Q = \int {\rm d}x_1\ {\rm d}x_2\ \left[\langle x_1\ x_2|{\rm e}^{-\beta\hat{\mathcal{H}}}|x_1\ x_2\rangle - \langle x_1\ x_2|{\rm e}^{-\beta\hat{\mathcal{H}}}|x_2\ x_1\rangle\right]. \tag{12.6.3}$$

Functional integral expressions for each of the two matrix elements appearing in eqns. (12.6.2) and (12.6.3) can be derived using the techniques already developed in Section 12.4. These expressions are

$$\begin{aligned} \langle x_1\ x_2|{\rm e}^{-\beta\hat{\mathcal{H}}}|x_1\ x_2\rangle &= \int_{x_1(0)=x_1,x_2(0)=x_2}^{x_1(\beta\hbar)=x_1,x_2(\beta\hbar)=x_2} \mathcal{D}x_1\ \mathcal{D}x_2\ {\rm e}^{-S[x_1,x_2]/\hbar} \\ \langle x_1\ x_2|{\rm e}^{-\beta\hat{\mathcal{H}}}|x_2\ x_1\rangle &= \int_{x_1(0)=x_1,x_2(0)=x_2}^{x_1(\beta\hbar)=x_2,x_2(\beta\hbar)=x_1} \mathcal{D}x_1\ \mathcal{D}x_2\ {\rm e}^{-S[x_1,x_2]/\hbar}. \end{aligned} \tag{12.6.4}$$

These two terms are illustrated in Fig. 12.9. In particular, note that the first term involves two independent closed paths for particles 1 and 2, respectively, in which the paths $x_1(\tau)$ and $x_2(\tau)$ satisfy $x_1(0) = x_1(\beta\hbar) = x_1$ and $x_2(0) = x_2(\beta\hbar) = x_2$. This is exactly the term that would result if the physical state of the system had no particular symmetry and could be simply described as $|x_1\ x_2\rangle$ or $|x_2\ x_1\rangle$. The second term, which results from the symmetry conditions placed on the state vector, "ties" the paths together at the endpoints because of the endpoint conditions $x_1(0) = x_2(\beta\hbar) = x_1$ and $x_2(0) = x_1(\beta\hbar) = x_2$. This second term, called an *exchange term*, is a purely quantum mechanical effect arising from the symmetry of the state vector. Exchange effects involve long-range correlations of delocalized wave functions and can often be neglected for particles such as protons unless the system is at a very low temperature. For electrons, however, such effects are nearly always important and need to be included.

In order to underscore the difficulties associated with exchange effects, consider writing eqns. (12.6.2) and (12.6.3) as limits of discrete path integrals. For compactness, we use the notation of eqn. (12.2.28), with the discretized paths denoted as $x_1^{(1)}, ..., x_1^{(P)}$

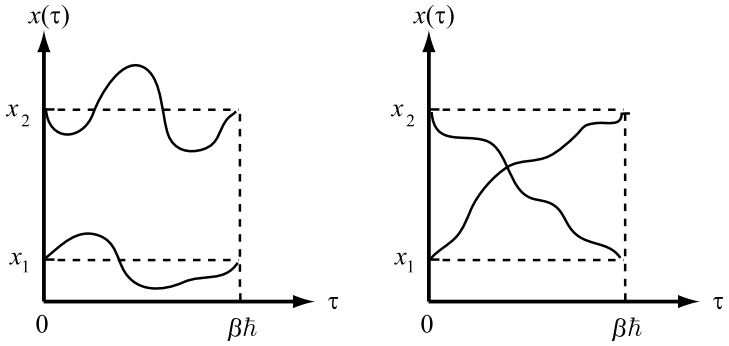

Fig. 12.9 Representative paths in the direct (*left*) and exchange (*right*) terms in the path integral of eqn. (12.6.4).

and $x_2^{(1)}, ..., x_2^{(P)}$ for particles 1 and 2, respectively. Note that the path index is now a superscript. The partition functions can be written as

$$Q(L,T) = \lim_{P\to\infty} \left(\frac{mP}{2\pi\beta\hbar^2}\right)^P \int \mathrm{d}x_1^{(1)} \cdots \mathrm{d}x_1^{(P)} \mathrm{d}x_2^{(1)} \cdots \mathrm{d}x_2^{(P)} \times \left[\mathrm{e}^{-\beta\phi\left(x_1^{(1)},\ldots,x_1^{(P)},x_2^{(1)},\ldots,x_2^{(P)}\right)} \pm \mathrm{e}^{-\beta\tilde{\phi}\left(x_1^{(1)},\ldots,x_1^{(P)},x_2^{(1)},\ldots,x_2^{(P)}\right)} \right], \tag{12.6.5}$$

where + and − are used for bosons and fermions, respectively, and

$$\phi\left(x_1^{(1)}, ..., x_1^{(P)}, x_2^{(1)}, ..., x_2^{(P)}\right) = \sum_{k=1}^{P} \left\{ \frac{1}{2} m\omega_P^2 \left[\left(x_1^{(k)} - x_1^{(k+1)}\right)^2 + \left(x_2^{(k)} - x_2^{(k+1)}\right)^2 \right] + \frac{1}{P} U(x_1^{(k)}, x_2^{(k)}) \right\}, \tag{12.6.6}$$

with $x_1^{(P+1)} = x_1^{(1)}$ and $x_2^{(P+1)} = x_2^{(1)}$. The definition of the function $\tilde{\phi}$ has the same mathematical form as eqn. (12.6.6) but with the endpoint conditions $x_1^{(P+1)} = x_2^{(1)}$ and $x_2^{(P+1)} = x_1^{(1)}$. If the term $\exp(-\beta\phi)$ is factored out of the brackets in eqn. (12.6.5), then the partition functions for fermions and bosons can be shown to be

$$Q(L,T) = \lim_{P\to\infty} \left(\frac{mP}{2\pi\beta\hbar^2}\right)^P \int \mathrm{d}x_1^{(1)} \cdots \mathrm{d}x_1^{(P)} \mathrm{d}x_2^{(1)} \cdots \mathrm{d}x_2^{(P)} \times \mathrm{e}^{-\beta\phi\left(x_1^{(1)},\ldots,x_1^{(P)},x_2^{(1)},\ldots,x_2^{(P)}\right)} \left[\det\left(\tilde{\mathrm{A}}\right)\right] \tag{12.6.7}$$

for fermions and

$$Q(L,T) = \lim_{P\to\infty} \left(\frac{mP}{2\pi\beta\hbar^2}\right)^P \int \mathrm{d}x_1^{(1)} \cdots \mathrm{d}x_1^{(P)} \mathrm{d}x_2^{(1)} \cdots \mathrm{d}x_2^{(P)}$$

$$\times \, \mathrm{e}^{-\beta\phi\left(x_1^{(1)},\ldots,x_1^{(P)},x_2^{(1)},\ldots,x_2^{(P)}\right)} \left[\mathrm{perm}\left(\tilde{\mathrm{A}}\right)\right] \tag{12.6.8}$$

for bosons. The matrix $\tilde{\mathrm{A}}$ is defined to be $\tilde{A}_{ij} = A_{ij}/A_{ii}$ with

$$A_{ij} = \exp\left[-\frac{1}{2}\beta m\omega_P^2\left(x_i^{(P)} - x_j^{(1)}\right)^2\right], \tag{12.6.9}$$

and det and perm denote the determinant and permanent of the matrix $\tilde{A}$, respectively. In this two-particle example, A and $\tilde{\mathrm{A}}$ are 2×2 matrices. For N-particle systems, they are $N \times N$ matrices, giving rise to $N!$ terms from the determinant or permanent.

The presence of the permanent or determinant in eqns. (12.6.7) and (12.6.8), respectively, can be treated as objects to be averaged over direct paths; alternatively, they can be added as additional terms in ϕ in the form $-(1/\beta)\ln\det(\tilde{\mathrm{A}})$ or $-(1/\beta)\ln\mathrm{perm}(\tilde{\mathrm{A}})$. When exchange effects are important, the fermion case becomes particularly problematic, as the determinant is composed of the difference of two terms that are large and similar in magnitude. Hence, the determinant becomes a small difference of two large numbers, which is very difficult to converge. This problem is known as the *Fermi sign problem*, which is only exacerbated in a system of N fermions where $\det(\tilde{\mathrm{A}})$ is the difference of two sums each containing $N!/2$ terms. Consequently, when $\det(\tilde{\mathrm{A}})$ is absorbed into ϕ, it exhibits large fluctuations, which are numerically problematic. The sign problem does not exist for bosons, since $\tilde{\mathrm{A}}$ and its permanent are positive definite, which means that numerical calculations for bosonic systems are tractable. Techniques for treating bosonic systems are discussed in detail, for example, in the review by Ceperley (1995), and a novel Monte Carlo scheme was suggested by Booth *et al.* (2009) for approaching the many-fermion problem, which involves sampling the space of fermion determinants. A decade later, Hirshberg *et al.* (2019, 2020) discovered a recursion relation satisfied by the permanents and determinants that show up in the treatment of N-body systems of bosons and fermions, respectively. This recursion formula yields a practical path integral molecular dynamics framework for treating bosons and fermions. This approach is an elegant one, which we will describe after the proceeding discussion of the N-body Boltzmann statistics problem.

Let us now suppose that exchange terms can be safely ignored, which is the case of Boltzmann statistics discussed in Section 11.3. In this limit, the path integral reduces to a sum over independent particle paths. Consider the Hamiltonian of an N-particle system in d dimensions of the standard form

$$\hat{\mathcal{H}} = \sum_{i=1}^{N} \frac{\hat{\mathbf{p}}_i^2}{2m_i} + U(\hat{\mathbf{r}}_1, ..., \hat{\mathbf{r}}_N). \tag{12.6.10}$$

As the limit of a discrete path integral, each particle will be characterized by a path in d dimensions specified by points $\mathbf{r}_i^{(1)}, ..., \mathbf{r}_i^{(P)}$, and the path integral for the partition function takes the form

$$Q(N,V,T) = \lim_{P\to\infty} \prod_{i=1}^{N} \left(\frac{m_i P}{2\pi\beta\hbar^2}\right)^{dP/2} \int \prod_{i=1}^{N} \mathrm{d}\mathbf{r}_i^{(1)} \cdots \mathrm{d}\mathbf{r}_i^{(P)}$$

$$\times \exp\left\{-\sum_{k=1}^{P}\left[\sum_{i=1}^{N}\frac{m_i P}{2\beta\hbar^2}\left(\mathbf{r}_i^{(k+1)}-\mathbf{r}_i^{(k)}\right)^2+\frac{\beta}{P}U\left(\mathbf{r}_1^{(k)},...,\mathbf{r}_N^{(k)}\right)\right]\right\}_{\mathbf{r}_i^{(P+1)}=\mathbf{r}_i^{(1)}} \tag{12.6.11}$$

where we now let i index the particles and k index the imaginary-time intervals. Eqn. (12.6.11) can also be written as a dN-dimensional functional integral:

$$Q(N,V,T)=\oint \mathcal{D}\mathbf{r}_1(\tau)\cdots\mathcal{D}\mathbf{r}_N(\tau)$$
$$\times\exp\left\{-\frac{1}{\hbar}\int_0^{\beta\hbar}\mathrm{d}\tau\ \sum_{i=1}^{N}\frac{1}{2}m_i\dot{\mathbf{r}}_i^2(\tau)+U(\mathbf{r}_1(\tau),...,\mathbf{r}_N(\tau))\right\}. \tag{12.6.12}$$

Using the techniques from Section 12.3, eqn. (12.6.11) yields the following estimators for the energy and pressure:

$$\epsilon_P\left(\{\mathbf{r}^{(1)},...,\mathbf{r}^{(P)}\}\right)=\frac{dNP}{2\beta}-\sum_{k=1}^{P}\sum_{i=1}^{N}\frac{1}{2}m_i\omega_P^2\left(\mathbf{r}_i^{(k)}-\mathbf{r}_i^{(k+1)}\right)^2+\frac{1}{P}\sum_{k=1}^{P}U(\mathbf{r}_1^{(k)},...,\mathbf{r}_N^{(k)})$$
$$\mathcal{P}_P\left(\{\mathbf{r}^{(1)},...,\mathbf{r}^{(P)}\}\right)=\frac{NP}{\beta V}-\frac{1}{dV}\sum_{k=1}^{P}\sum_{i=1}^{N}\left[m_i\omega_P^2\left(\mathbf{r}_i^{(k)}-\mathbf{r}_i^{(k+1)}\right)^2+\frac{1}{P}\mathbf{r}_i^{(k)}\cdot\nabla_{\mathbf{r}_i^{(k)}}U\right], \tag{12.6.13}$$

where $\{\mathbf{r}^{(1)},...,\mathbf{r}^{(P)}\}$ represents the full set of N particle paths. If U has an explicit volume dependence, then an additional term

$$-\frac{1}{P}\sum_{k=1}^{P}\frac{\partial}{\partial V}U(\mathbf{r}_1^{(k)},...,\mathbf{r}_N^{(k)},V)$$

must be added to eqn. (12.6.13) (Martyna *et al.*, 1999).

Unless one is interested in studying matter under extreme conditions or using path integrals to solve electronic structure problems, the approximation of Boltzmann statistics is generally sufficiently accurate to account for quantum effects in a calculation. However, when bosonic or fermionic statistics cannot be neglected, then the problem of including the requisite permanents or determinants must be faced. Although bosonic problems are a bit easier, as they do not involve a sign problem, the fluctuations in the permanent are still extremely large and difficult to converge, and taming these fluctuations is quite challenging. By contrast, fluctuations in fermion determinants arising from the sign problem are substantially more severe, making fermionic calculations significantly more difficult. Here, we will derive recursion relations based on the work of Hirshberg *et al.* for bosons and fermions that helps tame the violent fluctuations associated with bosonic permanents or fermionic determinants, rendering calculations involving identical bosons or fermions accessible to the numerical methods to be discussed in the remaining sections of this chapter.

In order to keep the notation simple, we introduce the following shorthand. Let $\mathbf{R}_i = (\mathbf{r}_i^{(1)}, ..., \mathbf{r}_i^{(P)})$ denote the set of beads on the ring polymer of particle i. Let

$$\mathcal{V}(\mathbf{R}_1, ..., \mathbf{R}_N) = \frac{1}{P}\sum_{k=1}^{P} U(\mathbf{r}_1^{(k)}, ..., \mathbf{r}_N^{(k)}) \tag{12.6.14}$$

denote the interaction potential between the ring polymers. Let

$$\mathcal{K}(\mathbf{R}_1, ..., \mathbf{R}_N) = \frac{1}{2} m\omega_P^2 \sum_{i=1}^{N}\sum_{k=1}^{P} \left(\mathbf{r}_i^{(k+1)} - \mathbf{r}_i^{(k)}\right)^2, \qquad \mathbf{r}_i^{(P+1)} = \mathbf{r}_i^{(1)} \tag{12.6.15}$$

denote the ring-polymer kinetic energy terms. Finally, let $\mathcal{N} = (mP/2\pi\beta\hbar^2)^{dNP/2}$ denote the overall normalization constant. Note that in these expressions, all of the masses are taken to be the same since the particles are assumed to be identical. Using the shorthand, we can write the canonical partition function of the N-particle system under the assumption of Boltzmann statistics as

$$Q(N, V, T) = \mathcal{N} \int \mathrm{d}\mathbf{R}_1 \cdots \mathrm{d}\mathbf{R}_N \; \mathrm{e}^{-\beta(\mathcal{K}(\mathbf{R}_1,...,\mathbf{R}_N)+\mathcal{V}(\mathbf{R}_1,...,\mathbf{R}_N))}. \tag{12.6.16}$$

In order to construct the partition function for an N-particle bosonic or fermionic system, we need to add in the exchange terms, the number of which grows as $N!$. However, if a simple recursion formula could be derived, then we could start with a small number of terms and build up the full N-particle partition function iteratively. In Fig. 12.10, we show ring-polymer configurations corresponding to the direct and exchange terms for $N = 2$ and $N = 3$. Terms having $\pm$ in front of them are added for bosons and subtracted for fermions. The two-particle partition functions were shown in eqns. (12.6.2) and (12.6.3). Let us start with the bosonic case. We can write the three-particle partition function as

$$Q_B(V, T) = \mathcal{N} \int \mathrm{d}\mathbf{R}_1 \, \mathrm{d}\mathbf{R}_2 \, \mathrm{d}\mathbf{R}_3 \; \mathrm{e}^{-\beta\left(\mathcal{K}_B^{(3)}(\mathbf{R}_1,\mathbf{R}_2,\mathbf{R}_3)+\mathcal{V}(\mathbf{R}_1,\mathbf{R}_2,\mathbf{R}_3)\right)}, \tag{12.6.17}$$

where

$$\mathrm{e}^{-\beta\mathcal{K}_B^{(3)}(\mathbf{R}_1,\mathbf{R}_2,\mathbf{R}_3)} = \frac{1}{6}\Big(\mathrm{e}^{-\beta\mathcal{K}_{\mathrm{ooo}}(\mathbf{R}_1,\mathbf{R}_2,\mathbf{R}_3)} + 3\mathrm{e}^{-\beta\mathcal{K}_{\mathrm{oO}}(\mathbf{R}_1,\mathbf{R}_2,\mathbf{R}_3)} + 2\mathrm{e}^{-\beta\mathcal{K}_{\bigcirc}(\mathbf{R}_1,\mathbf{R}_2,\mathbf{R}_3)}\Big). \tag{12.6.18}$$

In this expression,

$$\mathcal{K}_{\mathrm{ooo}}(\mathbf{R}_1, \mathbf{R}_2, \mathbf{R}_3) = \mathcal{K}(\mathbf{R}_1, \mathbf{R}_2, \mathbf{R}_3)$$
$$\mathcal{K}_{\mathrm{oO}}(\mathbf{R}_1, \mathbf{R}_2, \mathbf{R}_3) = \mathcal{K}(\mathbf{R}_1) + \mathcal{K}_3^{(2)}(\mathbf{R}_2, \mathbf{R}_3)$$

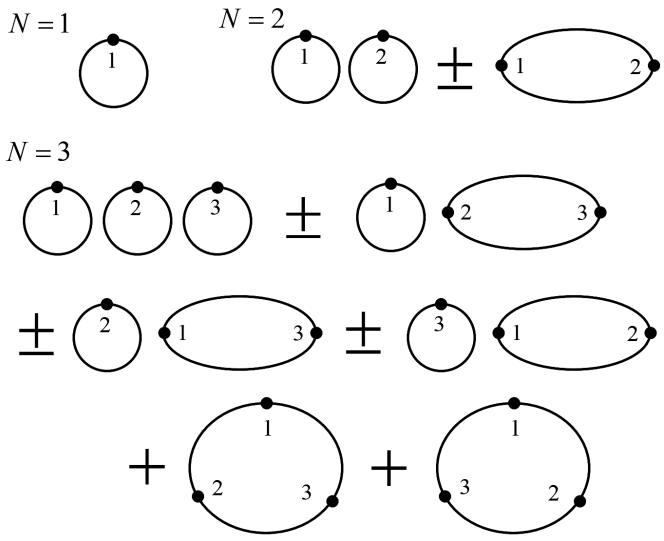

Fig. 12.10 Direct and exchange term ring-polymer configurations for $N = 1$, $N = 2$, and $N = 3$. Terms with $+/-$ are added/subtracted for bosons/fermions.

$$\mathcal{K}_{\bigcirc}(\mathbf{R}_1, \mathbf{R}_2, \mathbf{R}_3) = \mathcal{K}_3^{(3)}(\mathbf{R}_1, \mathbf{R}_2, \mathbf{R}_3) \tag{12.6.19}$$

with

$$\mathcal{K}_N^{(j)}(\mathbf{R}_{N-j+1}, ..., \mathbf{R}_N) = \frac{1}{2} m\omega_P^2 \sum_{i=N-j+1}^{N} \sum_{k=1}^{P} \left(\mathbf{r}_i^{(k+1)} - \mathbf{r}_i^{(k)} \right)^2, \tag{12.6.20}$$

subject to the endpoint conditions $\mathbf{r}_N^{(P+1)} = \mathbf{r}_{N-j+1}^{(1)}$, $\mathbf{r}_i^{(P+1)} = \mathbf{r}_{i+1}^{(1)}$. The small circle "o" indicates a one-particle ring polymer, "O" designates a two-particle ring polymer created by joining the endpoints, and "$\bigcirc$" signifies a three-particle ring polymer. The notation of "$\mathcal{K}$" for these energy terms indicates that they are all spring energies for the ring polymers in Fig. 12.10. Let us check eqn. (12.6.20) for $j = 2$ and $j = 3$ when $N = 3$. If $j = 2$ and $N = 3$, then the particle sum in eqn. (12.6.20) starts at $i = 2$ and, therefore, runs over two particles. The endpoint conditions are $\mathbf{r}_3^{(P+1)} = \mathbf{r}_2^{(1)}$ and $\mathbf{r}_2^{(P+1)} = \mathbf{r}_3^{(1)}$, which corresponds to a ring polymer composed of two individual polymers with their endpoints joined. If $j = 3$ and $N = 3$, then the particle sum in eqn. (12.6.20) starts at $i = 1$ and runs over all three particles. The endpoint conditions are $\mathbf{r}_3^{(P+1)} = \mathbf{r}_1^{(1)}$, $\mathbf{r}_1^{(P+1)} = \mathbf{r}_2^{(1)}$, and $\mathbf{r}_2^{(P+1)} = \mathbf{r}_3^{(1)}$, corresponding to a ring polymer composed of three individual polymers with polymer 1 joined to polymer 2, polymer 2 joined to polymer 3, and polymer 3 joined to polymer 1.

In order to generate a recursion relation for generating all of the distinct ring-polymer configurations, consider that eqn. (12.6.18) contains spring energies of topologically distinct terms for $N = 3$, "ooo", "oO", and "$\bigcirc$" with weights corresponding

to the number of such terms appearing in Fig. 12.10. Based on this consideration, let us now see how to generate ring-polymer configurations for $N = 2$ and $N = 3$ starting from $N = 1$. First, to generate $N = 2$, we only need to add a single ring polymer corresponding to particle 2 and a double ring polymer consisting of particles 1 and 2 joined at the endpoints. We can now take the ring-polymer configurations for $N = 1$ and $N = 2$ as a starting point to generate the ring-polymer configurations we need for $N = 3$. In order to reach $N = 3$, we would need to add to the configuration for $N = 1$ a double ring polymer consisting of particles 2 and 3 joined at the endpoints and assign the new configuration a weight of 2. We would also need to add to the configurations for $N = 2$ a single ring polymer representing particle 3 and assign the two new configurations generated a weight of 1. Finally, we need to add a triple ring polymer consisting of all three particles and assign this configuration a weight of 2. If we now generalize to N particles, the following recursion formula emerges:

$$\mathrm{e}^{-\beta\mathcal{K}_B^{(N)}(\mathbf{R}_1,\ldots,\mathbf{R}_N)} = \frac{1}{N}\sum_{j=1}^{N}\mathrm{e}^{-\beta\left(\mathcal{K}_B^{(N-j)}(\mathbf{R}_1,\ldots,\mathbf{R}_{N-j})+\mathcal{K}_N^{(j)}(\mathbf{R}_{N-j+1},\ldots,\mathbf{R}_N)\right)} \tag{12.6.21}$$

with the definition that $\exp(-\beta\mathcal{K}_B^{(0)}) = 1$. Let us now check the recursion relation for $N = 3$. According to eqn. (12.6.21), when $N = 3$,

$$\mathrm{e}^{-\beta\mathcal{K}_B^{(N)}} = \frac{1}{3}\left[\mathrm{e}^{-\beta\left(\mathcal{K}_B^{(2)}+\mathcal{K}_3^{(1)}\right)} + \mathrm{e}^{-\beta\left(\mathcal{K}_B^{(1)}+\mathcal{K}_3^{(2)}\right)} + \mathrm{e}^{-\beta\left(\mathcal{K}_B^{(0)}+\mathcal{K}_3^{(3)}\right)}\right]. \tag{12.6.22}$$

Then, since $\exp(-\beta\mathcal{K}_B^{(0)}) = 1$, $\exp(-\beta\mathcal{K}_B^{(1)}) = \exp(-\beta\mathcal{K}_\mathrm{o})$, and $\exp(-\beta\mathcal{K}_B^{(2)}) = [\exp(-\beta\mathcal{K}_\mathrm{oo}) + \exp(-\beta\mathcal{K}_\mathrm{O})]/2$, where the "o" and "O" notation has been used, we obtain

$$\begin{aligned}\mathrm{e}^{-\beta\mathcal{K}_B^{(N)}} &= \frac{1}{3}\left[\frac{1}{2}\left(\mathrm{e}^{-\beta\mathcal{K}_\mathrm{oo}} + \mathrm{e}^{-\beta\mathcal{K}_\mathrm{O}}\right)\mathrm{e}^{-\beta\mathcal{K}_\mathrm{o}} + \mathrm{e}^{-\beta\mathcal{K}_\mathrm{o}}\mathrm{e}^{-\beta\mathcal{K}_\mathrm{O}} + \mathrm{e}^{-\beta\mathcal{K}_\bigcirc}\right] \\ &= \frac{1}{6}\mathrm{e}^{-\beta\mathcal{K}_\mathrm{ooo}} + \frac{1}{2}\mathrm{e}^{-\beta\mathcal{K}_\mathrm{oO}} + \frac{1}{3}\mathrm{e}^{-\beta\mathcal{K}_\bigcirc},\end{aligned} \tag{12.6.23}$$

which matches eqn. (12.6.18). Here, we have used the additive property of the spring energies, *e.g.*, $\mathcal{K}_\mathrm{o} + \mathcal{K}_\mathrm{oo} = \mathcal{K}_\mathrm{ooo}$, $\mathcal{K}_\mathrm{oO} = \mathcal{K}_\mathrm{o} + \mathcal{K}_\mathrm{O}$, *etc.*

For fermions, a recursion relation very similar to eqn. (12.6.21) can be derived, differing only by a change of sign for certain terms. The resulting recursion formula is

$$\mathrm{e}^{-\beta\mathcal{K}_F^{(N)}(\mathbf{R}_1,\ldots,\mathbf{R}_N)} = \frac{1}{N}\sum_{j=1}^{N}(-1)^{j-1}\mathrm{e}^{-\beta\left(\mathcal{K}_F^{(N-j)}(\mathbf{R}_1,\ldots,\mathbf{R}_{N-j})+\mathcal{K}_N^{(j)}(\mathbf{R}_{N-j+1},\ldots,\mathbf{R}_N)\right)}. \tag{12.6.24}$$

In practice, we write $\exp(-\beta\mathcal{K}_{B/F}^{(N)}(\mathbf{R}_1,\ldots,\mathbf{R}_N))$ as a single Boltzmann factor by taking the logarithm of both sides of eqns. (12.6.21) or (12.6.24) to obtain

$$\mathcal{K}_{B/F}^{(N)}(\mathbf{R}_1,...,\mathbf{R}_N) =$$

$$-\frac{1}{\beta}\ln\left[\frac{1}{N}\sum_{j=1}^{N}\xi^{j-1}\mathrm{e}^{-\beta\left(\mathcal{K}_{B/F}^{(N-j)}(\mathbf{R}_1,...,\mathbf{R}_{N-j})+\mathcal{K}_N^{(j)}(\mathbf{R}_{N-j+1},...,\mathbf{R}_N)\right)}\right], \qquad (12.6.25)$$

where $\xi = 1$ for bosons and -1 for fermions. Then, the full potential energy used in path integral molecular dynamics for N-particle bosonic or fermionic systems is $\mathcal{K}_{B/F}^{(N)}(\mathbf{R}_1,...,\mathbf{R}_N) + \mathcal{V}(\mathbf{R}_1,...,\mathbf{R}_N)$. Evaluation of eqn. (12.6.25) requires evaluating $\mathcal{K}_{B/F}^{(0)},...,\mathcal{K}_{B/F}^{(N-1)}$ in order to generate all terms in the recursion relation.

Let us now discuss practical issues in the evaluation of $\mathcal{K}_{B/F}^{(N)}(\mathbf{R}_1,...,\mathbf{R}_N)$ for bosons and fermions. For bosons, $\mathcal{K}_B^{(N)}$ is positive definite, making the use of molecular dynamics or Monte Carlo to evaluate bosonic path integrals possible. However, $\mathcal{K}_N^{(j)} \geq 0$ and grows with j, so that $\exp(-\beta\mathcal{K}_N^{(j)})$ can become exponentially small. In order to stabilize the numerical calculation, we add and subtract a constant energy E_0 as

$$\mathcal{K}_B^{(N)}(\mathbf{R}_1,...,\mathbf{R}_N) = E_0$$

$$-\frac{1}{\beta}\ln\left[\frac{1}{N}\sum_{j=1}^{N}\xi^{j-1}\mathrm{e}^{-\beta\left(\mathcal{K}_F^{(N-j)}(\mathbf{R}_1,...,\mathbf{R}_{N-j})+\mathcal{K}_N^{(j)}(\mathbf{R}_{N-j+1},...,\mathbf{R}_N)-E_0\right)}\right]. \qquad (12.6.26)$$

The results are independent of the choice of E_0. As of the writing of this book, interacting bosonic systems containing $N = 32$ particles have been treated using this formulation (Hirshberg *et al.*, 2019). For fermionic systems, $\exp(-\beta(\mathcal{K}_F^{(N)}(\mathbf{R}_1,...,\mathbf{R}_N))$ is not positive definite, meaning that $\mathcal{K}_F^{(N)}(\mathbf{R}_1,...,\mathbf{R}_N)$ is a complex potential and cannot be evaluated using standard simulation techniques. There are complex overdamped Langevin equation techniques (Fredrickson, 2006) that can be used for complex potential functions, but these have not been applied to the many fermion problem. (The Langevin and generalized Langevin equations are discussed in Chapter 15.) Because bosonic systems can be evaluated, an alternative approach is to find a related bosonic system and reweight averages of observables with the factor $\exp(-\beta(\mathcal{K}_F^{(N)} - \mathcal{K}_B^{(N)})$ according to procedures discussed in Chapter 8. This fact allows systems containing small numbers ($N < 10$) to be simulated straightforwardly. For larger systems of interacting fermions, the Gibbs-Bogliubov inequality (see Problem 10.9) can be exploited to simulate a simpler system, *e.g.*, a system of strongly interacting fermions versus a system of weakly interacting fermions, in order to obtain an upper bound on the free energy of an N-fermion system (Hirshberg *et al.*, 2020).

When evaluating estimators of N-body quantum systems, whether Boltzmann, fermion, or boson statistics are used, the quantum (spring) kinetic energy terms grow linearly with P. From a numerical viewpoint, this is problematic, as these harmonic terms become quite stiff for systems with strong quantum effects and exhibit large, rapid fluctuations, making them difficult to converge. In the remainder of this chapter, we will discuss numerical techniques for the evaluation of path integrals that explicitly

address how to handle these stiff harmonic interactions.

12.7 Quantum free-energy profiles

In Chapter 8, we discussed the calculation of classical free energies. In this section, we will discuss quantum free energies. For simplicity, we restrict the discussion to one-dimensional free-energy profiles whose features are used to calculate quantum rates using the approximate quantum dynamical techniques discussed in Chapter 14. Extension to multidimensional quantum free-energy surfaces is straightforward.

Suppose we have a quantum N-particle system obeying Boltzmann statistics. Let $\hat{\mathbf{r}}_1, ..., \hat{\mathbf{r}}_N$ be the quantum position operators for the N particles. Given a collective variable operator $\hat{q} = \mathcal{F}(\hat{\mathbf{r}}_1, ..., \hat{\mathbf{r}}_N)$, the analog of eqn. (8.7.1) for a quantum system is

$$P(s) = \frac{1}{Q(N,V,T)} \mathrm{Tr}\left[\mathrm{e}^{-\beta\hat{\mathcal{H}}} \delta\left(\mathcal{F}(\hat{\mathbf{r}}_1, ..., \hat{\mathbf{r}}_N) - s\right)\right] \tag{12.7.1}$$

which yields the marginal distribution $P(s)$. Equation (12.7.1) is an expectation value for a position-dependent operator expressed in terms of a δ-function. Because of eqns. (12.3.5) and (12.3.8), we can express the marginal as a path integral average using two possible estimators:

$$\pi_1\left(\left\{\mathbf{r}^{(1)}\right\}; s\right) = \delta\left(\mathcal{F}(\mathbf{r}_1^{(1)}, ..., \mathbf{r}_N^{(1)}) - s\right) \tag{12.7.2}$$

$$\pi_P\left(\left\{\mathbf{r}^{(1)}, ..., \mathbf{r}^{(P)}\right\}; s\right) = \frac{1}{P}\sum_{k=1}^{P} \delta\left(\mathcal{F}(\mathbf{r}_1^{(k)}, ..., \mathbf{r}_N^{(k)}) - s\right). \tag{12.7.3}$$

If a path integral simulation (which will be described in Section 12.8) is able to sample the entire domain of $P(s)$, then the optimal estimator is that in eqn. (12.7.3) since the statistics of P beads leads to more rapid convergence than the single-bead estimator of eqn. (12.7.2). If the corresponding free-energy $A(s) = -kT \ln P(s)$ has one or more high barriers leading to rare events such that the enhanced sampling approaches in Chapter 8 are needed, then eqn. (12.7.3) would be of little utility. Suppose, for example, we were to employ the bluemoon method of Section 8.7. Recalling that the bluemoon method imposes a constraint on the system, if the constraint implied by the estimator in eqn. (12.7.2) were employed, the constraint would be imposed only among beads of index 1 on each particle, *i.e.*, the constraint would be $\mathcal{F}(\mathbf{r}_1^{(1)}, ..., \mathbf{r}_N^{(1)}) = s$. On the other hand, if we attempted to use the estimator in eqn. (12.7.3), then we would need to run P bluemoon simulations with the constraint imposed on each bead index separately and compute the average. However, given the cyclic invariance of the ring polymers, these P simulations would be expected to give exactly the same result within the statistical sampling error, and hence, the computational time needed to run the P simulations would be wasted. Yet since the convergence of a single-bead estimator would be expected to be quite slow, a common approximation made in the calculation of free energies consists in replacing the single-bead estimator in eqn. (12.7.2) with an

estimator based on the N particle *path centroids*, defined as the average position of the P beads in a ring polymer:

$$\mathbf{r}_i^{(c)} = \frac{1}{P}\sum_{k=1}^{P}\mathbf{r}_i^{(k)}. \tag{12.7.4}$$

The centroid estimator then takes the form

$$\pi_c\left(\left\{\mathbf{r}^{(c)}\right\};s\right) = \delta\left(\mathcal{F}(\mathbf{r}_1^{(c)},...,\mathbf{r}_N^{(c)}) - s\right). \tag{12.7.5}$$

The estimator in eqn. (12.7.5) might be expected to be a good approximation for the estimators in eqns. (12.7.2) and (12.7.3) if the ring polymers are localized, so that the centroid accurately captures, in an average sense, the locations of the beads. However, if a ring polymer is highly delocalized, with beads divided between two sides of a potential energy barrier, then the centroid will be located in a central location near the top of the barrier, which would not accurately capture the fact that very few beads are located there. In this case, one might expect the free energy derived from the centroid

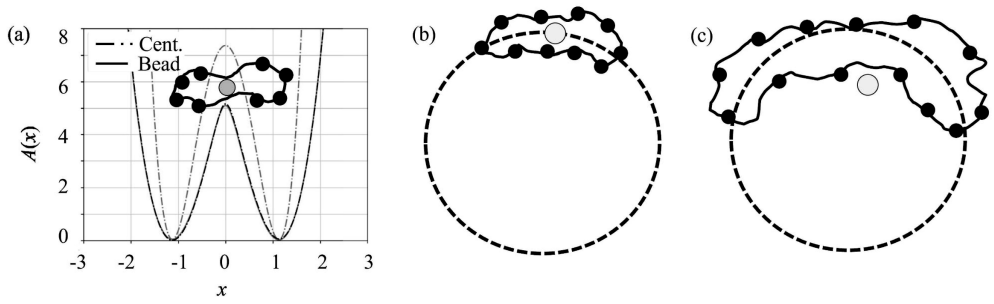

Fig. 12.11 (a) Free-energy profiles $A(x)$ at temperature $kT = 1$ for the potential $U(x,y) = 5\left(x^2-1\right)^2 + y^2/2 + 2.878xy$ using the centroid estimator in eqn. (12.7.5) and the all-bead estimator in eqn. (12.7.3). The division of beads among the two minima is illustrated, with the centroid shown as the grey sphere. (b) Snapshot of beads in a localized ring polymer on a spherical surface (shown in cross section), as would occur, for example, for a harmonic bond potential at high temperature. The centroid position is again shown as the grey sphere. (c) Same for a delocalized ring polymer on the spherical surface, as would occur, for example, for a harmonic bond potential at low temperature. The centroid is shown as the grey sphere and is located inside the sphere.

estimator to be a poor representation of the actual bead locations, as illustrated on the left in Fig. 12.11(a). Alternatively, the ring polymer could be delocalized over the surface of a sphere, as occurs, for example, in a radial potential such as a bond potential. In this situation, the centroid would likely be located *inside* the sphere, also providing a poor representation of the bead locations (Witt *et al.*, 2009), as illustrated in panels (b) and (c) of the figure. Nevertheless, imposing a constraint on the centroids is as straightforward as imposing a constraint on a single bead, and eqn. (12.7.5) has

the advantage of rapid convergence. The corresponding approximate quantum free-energy profile $A_c(s) = -kT\ln\langle\pi_c(\{\mathbf{r}^{(c)}\})\rangle_f$ is an essential component in path integral based quantum rate theories (Geva *et al.*, 2001; Craig and Manolopoulos, 2005).

It is important to note that dynamical enhanced sampling methods such as the metadynamics and d-AFED/TAMD methods described in Chapter 8 allow us to use the all-bead estimator in eqn. (12.7.3) to compute the quantum free energy (Cendagorta *et al.*, 2021). To see how this can be done, we write the average of the estimator in eqn. (12.7.3) as

$$\langle\pi_P\left(\left\{\mathbf{r}^{(1)},...,\mathbf{r}^{(P)}\right\};s\right)\rangle_f = \frac{\int \mathrm{d}\sigma\ \langle\pi_P\left(\left\{\mathbf{r}^{(1)},...,\mathbf{r}^{(P)}\right\};s\right)\rangle_f(\sigma)\mathrm{e}^{-\beta A_c(\sigma)}}{\int \mathrm{d}\sigma\ \mathrm{e}^{-\beta A_c(\sigma)}} = \mathrm{e}^{-\beta A(s)}, \tag{12.7.6}$$

where

$$\langle\pi_P\left(\left\{\mathbf{r}^{(1)},...,\mathbf{r}^{(P)}\right\};s\right)\rangle_f(\sigma) = \frac{\langle\pi_c\left(\left\{\mathbf{r}^{(c)}\right\};\sigma\right)\pi_P\left(\left\{\mathbf{r}^{(1)},...,\mathbf{r}^{(P)}\right\};s\right)\rangle_f}{\langle\pi_c\left(\left\{\mathbf{r}^{(c)}\right\};\sigma\right)\rangle_f}$$

$$= \frac{\left\langle\delta\left(\mathcal{F}(\mathbf{r}_1^{(c)},...,\mathbf{r}_N^{(c)})-\sigma\right)\pi_P\left(\left\{\mathbf{r}^{(1)},...,\mathbf{r}^{(P)}\right\};s\right)\right\rangle_f}{\left\langle\delta\left(\mathcal{F}(\mathbf{r}_1^{(c)},...,\mathbf{r}_N^{(c)})-\sigma\right)\right\rangle_f}. \tag{12.7.7}$$

According to eqns. (12.7.6) and (12.7.7), we only need to perform an enhanced sampling simulation targeting $\mathcal{F}(\mathbf{r}_1^{(c)},...,\mathbf{r}_N^{(c)})$ and save the result as a function of σ and the corresponding probability distribution in the denominator of eqn. (12.7.7), *i.e.*, $P_c(\sigma) = \langle\delta\left(\mathcal{F}(\mathbf{r}_1^{(c)},...,\mathbf{r}_N^{(c)})-\sigma\right)\rangle_f$ and associated free energy. The average of the all-bead free-energy estimator is then computed from eqn. (12.7.6) with these saved quantities.

12.8 Numerical evaluation of path integrals

Early numerical studies using path integrals to study condensed-phase problems focused on one or a few quantum particles in simple liquids (Sprik *et al.*, 1985; Sprik *et al.*, 1986; Coker *et al.*, 1987; Wallqvist *et al.*, 1987; Martyna *et al.*, 1993; Liu and Berne, 1993). Somewhat later, path integrals were applied to study quantum effects in bulk fluids such as water (Delbuono *et al.*, 1991; Chen *et al.*, 2003; Fanourgakis *et al.*, 2006; Paesani *et al.*, 2007; Paesani and Voth, 2009; Morrone and Car, 2008) and aqueous solutions (Marx *et al.*, 1999*a*; Tuckerman *et al.*, 2002), and in biological processes such as enzyme catalysis (Hwang *et al.*, 1991; Hwang and Warshel, 1996). Numerical path integration is also central to studies of lattice gauge theories (Weingarten and Petcher, 1981; Weingarten, 1982; Brown and Christ, 1988; Brown *et al.*, 1991). The application of path integrals to many types problems using increasingly sophisticated models and computational algorithms is now becoming routine. In this section, we will discuss the use of molecular dynamics and Monte Carlo techniques to evaluate path integrals numerically, identifying several technical challenges that affect

the construction of the numerical algorithms and the formulation of the thermodynamic estimators. While our focus here will be on the quantum canonical ensemble, it is possible to perform isothermal-isobaric and grand canonical path integral simulations, the latter using the adaptive resolution approach outlined in Section 6.9. These will be discussed further in Section 12.8.7.

12.8.1 Path integral molecular dynamics

We begin our discussion with the molecular dynamics approach. It must be mentioned at the outset that molecular dynamics is used here *only* as a means of sampling the quantum canonical distribution. No quantum dynamical properties can be generated using the techniques in this subsection. In Chapter 14, we will revisit the quantum dynamics problem and see how *approximate* dynamical quantities can be generated within a path integral molecular dynamics framework.

Let us start by considering, once again, a single particle moving in a one-dimensional potential $U(\hat{x})$. In eqn. (12.3.9), we introduced the notion of the discrete partition function $Q_P(L,T)$, which is explicitly defined to be

$$Q_P(L,T) = \left(\frac{mP}{2\pi\beta\hbar^2}\right)^{P/2} \int_{D(L)} \mathrm{d}x_1 \cdots \mathrm{d}x_P \times \exp\left\{-\frac{1}{\hbar}\sum_{k=1}^{P}\left[\frac{mP}{2\beta\hbar}(x_{k+1}-x_k)^2 + \frac{\beta\hbar}{P}U(x_k)\right]\right\}\Bigg|_{x_{P+1}=x_1} . \tag{12.8.1}$$

Equation (12.8.1) can be manipulated to resemble the classical canonical partition function of a cyclic ring polymer moving in a classical potential $U(x)/P$ by recasting the prefactor as a set of Gaussian integrals over variables we will call $p_1, ..., p_P$ so that they resemble momenta conjugate to $x_1, ..., x_P$:

$$Q_P(L,T) = \int \mathrm{d}p_1 \cdots \mathrm{d}p_P \int_{D(L)} \mathrm{d}x_1 \cdots \mathrm{d}x_P \times \exp\left\{-\beta\sum_{k=1}^{P}\left[\frac{p_k^2}{2m'} + \frac{1}{2}m\omega_P^2(x_{k+1}-x_k)^2 + \frac{1}{P}U(x_k)\right]\right\}\Bigg|_{x_{P+1}=x_1} . \tag{12.8.2}$$

The partition function represented in eqn. (12.8.2) resembles a classical phase-space integral of a system of P pseudoparticles with momenta $p_1, ..., p_P$ in an effective potential

$$\phi(x_1, ..., x_P) = \frac{1}{2}m\omega_P^2(x_{k+1}-x_k)^2 + \frac{1}{P}U(x_k). \tag{12.8.3}$$

In the exponential of eqn. (12.8.2), we have replaced the prefactor of $1/\hbar$ with a β prefactor. We have also introduced a frequency $\omega_P = \sqrt{P}/(\beta\hbar)$, which we call the *chain frequency*, since it is the frequency of the harmonic nearest-neighbor coupling of our cyclic chain. Finally, the parameter m' appearing in the Gaussian integrals is formally given by $m' = mP/(2\pi\hbar)^2$. However, since the prefactor does not affect any equilibrium averages, including those used to calculate thermodynamic estimators, we are

free to choose m' as we like. The resemblance of the partition function in eqn. (12.8.2) to that of a classical cyclic ring polymer of P points led Chandler and Wolynes (1981) to coin the term "classical isomorphism" and to exploit the isomorphism between the classical and approximate (since P is finite) quantum partition functions. The classical isomorphism is illustrated in Fig. 12.12. The figure depicts a cyclic ring polymer

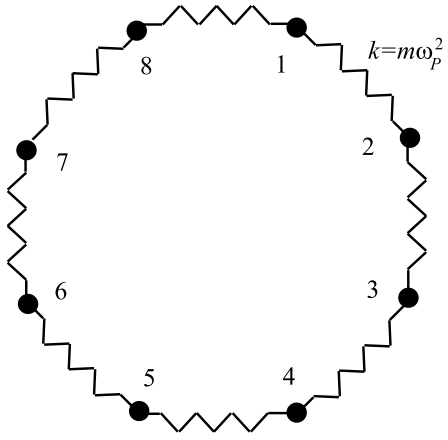

Fig. 12.12 Classical isomorphism: The figure shows a cyclic ring polymer having $P = 8$ described by the partition function in eqn. (12.8.2).

having $P = 8$ with a harmonic nearest-neighbor coupling constant $k = m\omega_P^2$. Because the ring polymer resembles a necklace, its P points are often referred to as "beads." According to the classical isomorphism, we can treat the cyclic ring polymer using all the techniques we have developed thus far for classical systems to obtain approximate quantum properties, and the latter can be systematically improved simply by increasing P.

The classical isomorphism allows us, in principle, to introduce a molecular dynamics scheme for eqn. (12.8.2), starting with the classical Hamiltonian

$$\mathcal{H}_{\rm cl}(x,p) = \sum_{k=1}^{P} \left[\frac{p_k^2}{2m'} + \frac{1}{2} m\omega_P^2 (x_{k+1} - x_k)^2 + \frac{1}{P} U(x_k) \right] \Bigg|_{x_{P+1}=x_1}, \tag{12.8.4}$$

which yields the following equations of motion:

$$\dot{x}_k = \frac{p_k}{m'}, \qquad \dot{p}_k = -m\omega_p^2 \left(2x_k - x_{k+1} - x_{k-1}\right) - \frac{1}{P}\frac{\partial U}{\partial x_k}. \tag{12.8.5}$$

If eqns. (12.8.5) are coupled to a thermostat, as discussed in Section 4.11, then the dynamics will sample the canonical distribution in eqn. (12.8.2). Although one of the first path integral molecular dynamics calculations by Parrinello and Rahman (1984) employed a scheme of this type, it was simultaneously recognized by Hall and Berne (1984) that path integral molecular dynamics based on eqns. (12.8.5) can suffer from very slow

convergence problems due to the wide range of time scales present in the dynamics. If one applies a normal mode transformation (see Section 1.7) to the harmonic coupling term in eqn. (12.8.4), the normal-mode frequencies range densely from 0 to $4P/(\beta\hbar)$. Thus, even for moderately large P, this constitutes a broad frequency spectrum. The time step that can be employed in a molecular dynamics algorithm is limited by the highest frequency, which means that the low-frequency modes, which are associated with large-scale changes in the shape of the cyclic chain, will be inadequately sampled unless very long runs are performed.

Because the normal-mode frequencies are closely spaced (approaching a continuum as $P \to \infty$), multiple time-scale integration algorithms such as RESPA (see Section 3.11) are insufficient to solve the problem. However, if we can devise a suitable coordinate transformation capable of uncoupling the harmonic term in eqn. (12.8.4), then we can replace the single fictitious mass m' in the classical Hamiltonian with a set of masses $m'_1, ..., m'_P$ such that only one harmonic frequency remains. Finally, we can then adjust the time step for stable integration of motion having that characteristic frequency and/or employ RESPA to the problem. This will ensure adequate sampling of all modes of the cyclic chain. In fact, we have already seen an example of such a transformation in Section 4.6. Equations (4.6.38) and (4.6.39) illustrate how a simple transformation uncouples the harmonic term for a model polymer that, when made cyclic, is identical to the discrete path integral. The one-dimensional analog of this transformation appropriate for eqn. (12.8.2) is

$$\begin{aligned} u_1 &= x_1 \\ u_k &= x_k - \frac{(k-1)x_{k+1} + x_1}{k}, \qquad k = 2, ..., P, \end{aligned} \tag{12.8.6}$$

the inverse of which is

$$\begin{aligned} x_1 &= u_1 \\ x_k &= u_k + \frac{k-1}{k} x_{k+1} + \frac{1}{k} u_1, \qquad k = 2, ..., P. \end{aligned} \tag{12.8.7}$$

Note that, as in eqn. (4.6.39), eqn. (12.8.7) is defined recursively. Because $x_1 = u_1$, the recursion can be seeded by starting with the $k = P$ term and working backwards to $k = 2$. The inverse can also be expressed in closed form as

$$\begin{aligned} x_1 &= u_1 \\ x_k &= u_1 + \sum_{l=k}^{P} \frac{k-1}{l-1} u_l, \qquad k = 2, ..., P. \end{aligned} \tag{12.8.8}$$

The transformation defined in eqns. (12.8.6), (12.8.7), and (12.8.8) is known as a *staging transformation* because of its connection to a particular path integral Monte Carlo algorithm (Ceperley and Pollock, 1984), which we will discuss in the next section. The staging transformation was first introduced for path integral molecular dynamics by Tuckerman *et al.* (1993). The variables $u_1, ..., u_P$ are known as *staging variables*, as distinguished from the original variables, which are referred to as *primitive variables*.

We now proceed to develop a molecular dynamics scheme in terms of the staging variables. When the harmonic coupling term is evaluated using these variables, the result is

$$\sum_{k=1}^{P}(x_k - x_{k+1})^2 = \sum_{k=2}^{P}\frac{k}{k-1}u_k^2, \tag{12.8.9}$$

which is completely separable. Since the Jacobian of the transformation is 1, as we showed in eqn. (4.6.45), the discrete partition function becomes

$$Q_P(L,T) = \int \mathrm{d}p_1 \cdots \mathrm{d}p_P \int \mathrm{d}u_1 \cdots \mathrm{d}u_P \times \exp\left\{-\beta \sum_{k=1}^{P}\left[\frac{p_k^2}{2m_k'} + \frac{1}{2}m_k\omega_P^2 u_k^2 + \frac{1}{P}U(x_k(u))\right]\right\}. \tag{12.8.10}$$

In eqn. (12.8.10), the parameters m_k are defined to be

$$m_1 = 0, \qquad m_k = \frac{k}{k-1}m, \qquad k = 2, ..., P, \tag{12.8.11}$$

and $m_1' = m$, $m_k' = m_k$. The notation $x_k(u)$ indicates the inverse transformation in eqn. (12.8.7) or (12.8.8). In order to evaluate eqn. (12.8.10), we can employ a classical Hamiltonian of the form

$$\tilde{\mathcal{H}}_{\mathrm{cl}}(u,p) = \sum_{k=1}^{P}\left[\frac{p_k^2}{2m_k'} + \frac{1}{2}m_k\omega_P^2 u_k^2 + \frac{1}{P}U(x_k(u))\right], \tag{12.8.12}$$

which leads to the equations of motion

$$\begin{aligned}\dot{u}_k &= \frac{p_k}{m_k'} \\ \dot{p}_k &= -m_k\omega_P^2 u_k - \frac{1}{P}\frac{\partial U}{\partial u_k}.\end{aligned} \tag{12.8.13}$$

From the chain rule, the forces on the staging variables can be expressed recursively as

$$\begin{aligned}\frac{1}{P}\frac{\partial U}{\partial u_1} &= \frac{1}{P}\sum_{l=1}^{P}\frac{\partial U}{\partial x_l} \\ \frac{1}{P}\frac{\partial U}{\partial u_k} &= \frac{1}{P}\left[\frac{\partial U}{\partial x_k} + \frac{k-2}{k-1}\frac{\partial U}{\partial u_{k-1}}\right].\end{aligned} \tag{12.8.14}$$

The recursive staging force calculation is performed starting with $k = 2$ and using the first expression for $\partial U/\partial u_1$. Equations (12.8.13) need to be thermostatted to ensure that the canonical distribution is generated. The presence of the high-frequency force on each staging variable combined with the $1/P$ factor that attenuates the potential-energy derivatives leads to a weak coupling between these two forces. Therefore, it is

important to have as much thermalization as possible in order to achieve equipartitioning of the energy. It is, therefore, strongly recommended (Tuckerman *et al.*, 1993) that path integral molecular dynamics calculations be carried out using the "massive" thermostatting mechanism described in Section 4.11. This protocol requires that a separate thermostat be attached to each Cartesian component of every staging variable. Thus, for the single-particle one-dimensional system described by eqns. (12.8.13), if Nosé-Hoover chain thermostats of length M are employed, the actual equations of motion would be

$$\begin{aligned}
\dot{u}_k &= \frac{p_k}{m'_k} \\
\dot{p}_k &= -m_k\omega_P^2 u_k - \frac{1}{P}\frac{\partial U}{\partial u_k} - \frac{p_{\eta_{k,1}}}{Q_1}p_k \\
\dot{\eta}_{k,\gamma} &= \frac{p_{\eta_{k,\gamma}}}{Q_k} \\
\dot{p}_{\eta_{k,1}} &= \frac{p_k^2}{m'_k} - kT - \frac{p_{\eta_{k,2}}}{Q_k}p_{\eta_{k,1}} \\
\dot{p}_{\eta_{k,\gamma}} &= \left[\frac{p_{\eta_{k,\gamma-1}}^2}{Q_k} - kT\right] - \frac{p_{\eta_{k,\gamma+1}}}{Q_k}p_{\eta_{k,\gamma}} \qquad \gamma = 2, ..., M-1 \\
\dot{p}_{\eta_{k,M}} &= \left[\frac{p_{\eta_{k,M-1}}^2}{Q_k} - kT\right],
\end{aligned} \tag{12.8.15}$$

where γ indexes the thermostat chain elements. When ω_P is the highest frequency in the system, the optimal choice for the parameters $Q_1, ..., Q_P$ are $Q_1 = kT\tau^2$ and $Q_k = kT/\omega_P^2$ for $k = 2, ..., P$. Here τ is a characteristic time scale of the corresponding classical system. Since each staging variable has its own thermostat of length M, the dimensionality of the thermostat phase space is $2MP$, which is considerably larger than the physical phase space! Luckily, with the exception of simple "toy" problems, the computational overhead of "massive" thermostatting is low relative to that of a force calculation in a complex system. Moreover, the massive thermostatting method is rapidly convergent, particularly when integrated using a multiple time scale algorithm such as the RESPA method of Section 3.11. Alternatively, Cayley matrix methods (see Problem 3.7) also allow increased efficiency by improving numerical stability and allowing large time steps to be employed (Korol *et al.*, 2019; Korol *et al.*, 2020; Rosa-Raíces *et al.*, 2021). The staging transformation is simple to implement and because of the recursive relations in eqns. (12.8.7) and (12.8.14), it scales linearly with P.

As an interesting alternative to the staging transformation, it is also possible to use the normal modes of the cyclic chain (Tuckerman *et al.*, 1993; Cao and Voth, 1994*b*). The normal mode transformation can be derived straightforwardly from a Fourier expansion of the periodic path

$$x_k = \sum_{l=1}^{P} a_l \mathrm{e}^{2\pi i(k-1)(l-1)/P}. \tag{12.8.16}$$

The complex expansion coefficients a_l are then used to construct a transformation to a set of normal mode variables $u_1, ..., u_P$ via

$$u_1 = a_1, \qquad u_P = a_{(P+2)/2}$$

$$u_{2k-2} = \mathrm{Re}(a_k), \qquad u_{2k-1} = \mathrm{Im}(a_k). \tag{12.8.17}$$

The normal-mode transformation can also be constructed as follows: 1) Generate the matrix $A_{ij} = 2\delta_{ij} - \delta_{i,j-1} - \delta_{i,j+1}$, $i, j = 1, ..., P$, with the path periodicity conditions $A_{i0} = A_{iP}$, $A_{i,P+1} = A_{i1}$; 2) Diagonalize the matrix and save the eigenvalues and eigenvectors; 3) From the eigenvectors, construct the orthogonal matrix O_{ij} that diagonalizes A. The forward and inverse transformations are then given by

$$u_k = \frac{1}{\sqrt{P}} \sum_{l=1}^{P} O_{kl} x_l$$

$$x_k = \sqrt{P} \sum_{l=1}^{P} O^{\mathsf{T}}_{kl} u_l. \tag{12.8.18}$$

Although the eigenvalues emerge directly from the diagonalization procedure, they can also be constructed by hand according to

$$\lambda_{2k-1} = \lambda_{2k-2} = 2\left[1 - \cos\left(\frac{2\pi(k-1)}{P}\right)\right] = 4\sin^2\left(\frac{\pi(k-1)}{P}\right). \tag{12.8.19}$$

Note the twofold degeneracy. When evaluated in terms of the normal mode variables, the harmonic coupling term becomes

$$\sum_{k=1}^{P} (x_k - x_{k+1})^2 = \sum_{k=2}^{P} \lambda_k u_k^2. \tag{12.8.20}$$

As with the staging transformation, the harmonic term is now separable. The transformation also has unit Jacobian. Thus, the transformed partition function is identical to eqn. (12.8.10) if the masses m_k are defined as $m_k = m\lambda_k$, $m'_1 = m$, and $m'_k = m_k$. With this identification, eqns. (12.8.12), (12.8.13), and (12.8.15) are applicable to the normal-mode case exactly as written. The only difference occurs when the chain rule is used to obtain the forces on the normal mode variables, whence we obtain

$$\frac{1}{P}\frac{\partial U}{\partial u_1} = \frac{1}{P} \sum_{l=1}^{P} \frac{\partial U}{\partial x_l}$$

$$\frac{1}{P}\frac{\partial U}{\partial u_k} = \frac{1}{\sqrt{P}} \sum_{l=1}^{P} \frac{\partial U}{\partial x_l} O^{\mathsf{T}}_{lk}. \tag{12.8.21}$$

In addition to its utility as a computational scheme, the normal-mode formulation of the path integral has several other interesting features. First, the variable u_1 can be shown to be equal to

$$u_1 = \frac{1}{P}\sum_{k=1}^{P} x_k \quad \underset{P\to\infty}{\longrightarrow} \quad \frac{1}{\beta\hbar}\int_0^{\beta\hbar} \mathrm{d}\tau\; x(\tau). \tag{12.8.22}$$

That is, the sum on the left becomes the continuous integral on the right when $P \to \infty$. The variable u_1 is an average over all of the path variables and, therefore, corresponds, for finite P, to the center of mass of the ring polymer. This point is also path centroid defined previously. Note that the force on this mode is also just the average force $(1/P)\sum_{k=1}^{P} \partial U/\partial x_k$. It can be shown that, for the staging transformation, the force on the mode u_1 is also the average force; however this mode is not physically the same as the centroid.

In a seminal paper by Feynman and Kleinert (1986), it was shown that the path centroid could be used to capture approximate quantum effects in a system. Consider eqn. (12.8.10) with the variables $u_1, ..., u_P$ representing the normal modes. If we integrate over the variables $u_2, ..., u_P$ and the corresponding momenta $p_1, ..., p_P$, then the result can, in the spirit of Section 8.10, be written as

$$Q_P(L,T) \propto \int \mathrm{d}p_1\; \mathrm{d}u_1 \exp\left\{-\beta\left[\frac{p_1^2}{2m_1} + W(u_1)\right]\right\}, \tag{12.8.23}$$

where $W(u_1)$ is the potential of mean force on the centroid given by

$$W(u_1) = -kT \ln\left\{\int \mathrm{d}u_2 \cdots \mathrm{d}u_P \right.$$
$$\left. \times\; \exp\left[-\beta\sum_{k=1}^{P}\left(\frac{1}{2}m_k\omega_P^2 u_k^2 + \frac{1}{P}U(x_k(u))\right)\right]\right\} \tag{12.8.24}$$

up to an additive constant. Although we cannot determine $W(u_1)$ for an arbitrary potential $U(x)$, Feynman and Kleinert were able to derive an analytical expression for $W(u_1)$ for a harmonic oscillator using the functional integral techniques discussed in Section 12.4. In particular, they showed how to derive the parameters of a harmonic oscillator potential $U_{\mathrm{ho}}(x; u_1)$ that minimize the expectation value $\langle U(x) - U_{\mathrm{ho}}(x; u_1)\rangle$. The parameters of the potential depend on the position of the centroid so that the harmonic potential takes the general form $U_{\mathrm{ho}}(x; u_1) = (1/2)\Omega^2(u_1)(x - u_1)^2 + L(u_1)$. That is, the frequency and vertical shift depend on the centroid u_1. The optimization procedure leads to a simple potential function $\tilde{W}(u_1)$ of the centroid that can then be used in eqn. (12.8.23) to obtain approximate quantum equilibrium and thermodynamic properties.

We close this section by showing how the path integral molecular dynamics protocol extends to N Boltzmann particles in d dimensions. Since most path integral calculations fall into this category, we will limit our discussion to these. Excellent descriptions of path integral algorithms for bosons and fermions can be found in the literature (Ceperley, 1995; Miura and Okazaki, 2000). The discrete N-particle partition function for Boltzmann particles follows directly from eqn. (12.6.11). After introducing dNP momentum integrations as in eqn. (12.8.2), the discrete partition function becomes

$$Q_P(N,V,T) = \prod_{i=1}^{N} \int \prod_{i=1}^{N} \mathrm{d}\mathbf{r}_i^{(1)} \cdots \mathrm{d}\mathbf{r}_i^{(P)} \mathrm{d}\mathbf{p}_i^{(1)} \cdots \mathrm{d}\mathbf{p}_i^{(P)} \tag{12.8.25}$$

$$\times \exp\left\{ -\beta \sum_{k=1}^{P} \left[\sum_{i=1}^{N} \frac{\mathbf{p}_i^{(k)^2}}{2m_i'} + \sum_{i=1}^{N} \frac{1}{2} m_i \omega_P^2 \left(\mathbf{r}_i^{(k+1)} - \mathbf{r}_i^{(k)} \right)^2 + \frac{1}{P} U\left(\mathbf{r}_1^{(k)}, ..., \mathbf{r}_N^{(k)} \right) \right] \right\}$$

with the condition $\mathbf{r}_i^{(P+1)} = \mathbf{r}_i^{(1)}$. An important point to make about eqn. (12.8.25) is that the potential $U(\mathbf{r}_1^{(k)}, ..., \mathbf{r}_N^{(k)})$ only acts between beads with the same imaginary-time index k. This means that all beads with imaginary-time index 1 interact with each other, but these do not interact with beads having imaginary-time indices 2,3,....,P and so forth. This is illustrated for the case of two particles in Fig. 12.13.

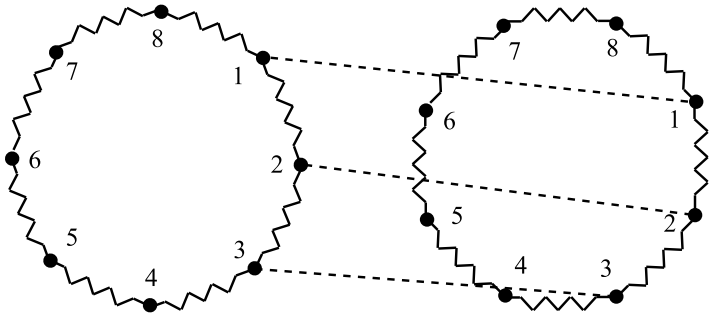

Fig. 12.13 Interaction pattern between two quantum particles represented as ring polymers within the discrete path integral framework. The cyclic chains obey the rule that only "beads" with the same imaginary-time index on different chains interact with each other.

The construction of a path integral molecular dynamics algorithm for N Boltzmann particles in d dimensions proceeds in the same manner as for a single particle in one dimension. First, a transformation from primitive to staging or normal-mode variables is performed for each quantum particle's cyclic path. In staging or normal-mode variables, the classical Hamiltonian from which the equations of motion are derived is

$$\mathcal{H} = \sum_{k=1}^{P} \left[\sum_{i=1}^{N} \frac{\mathbf{p}_i^{(k)^2}}{2m_i^{(k)'}} + \sum_{i=1}^{N} \frac{1}{2} m_i^{(k)} \omega_P^2 \mathbf{u}_i^{(k)^2} + \frac{1}{P} U\left(\mathbf{r}_1^{(k)}(\mathbf{u}_1), ..., \mathbf{r}_N^{(k)}(\mathbf{u}_N) \right) \right]. \tag{12.8.26}$$

Here, each primitive variable $\mathbf{r}_i^{(k)}$ depends on the staging or normal-mode variables with the same particle index i. In deriving the equations of motion from eqn. (12.8.26), the forces on the mode variables are obtained using eqns. (12.8.14) or (12.8.21). Importantly, if the equations of motion are coupled to Nosé-Hoover chains, it is critical to follow the protocol of coupling each component of each staging or normal-mode variable to its own thermostat, for a total of dNP thermostats. At first sight, this might seem like overkill because it adds $dNMP$ additional degrees of freedom to a

system, where M is the length of each Nosé-Hoover chains. However, if we think back to Fig. 4.12 and note that a path integral, according to eqn. (12.8.26), is a collection of weakly coupled harmonic oscillators, then this protocol makes sense. Generally, the computational overhead of $dNMP$ thermostats is small compared to that associated with the calculation of the forces.

12.8.2 Path integral Monte Carlo

We saw in Chapter 7 that Monte Carlo methods are very effective for sampling an equilibrium distribution such as the canonical ensemble. Therefore, it is worth using a little space to discuss the calculation of path integrals using a Monte Carlo approach. The algorithm we will describe here uses many of the same ideas discussed in the previous subsection. In particular, for a quantum free particle in one dimension ($U(\hat{x}) = 0$), the discretized action expressed in terms of staging or normal-mode variables is just a sum of uncoupled harmonic oscillators, and as we saw in Section 3.8.3, these can be easily sampled using the Box-Muller method. The idea of path integral Monte Carlo, then, is to construct an M(RT)^2 algorithm (see Section 7.3.3), in which we sample the free particle distribution directly and use the change in the potential energy to build an acceptance probability. However, unlike path integral molecular dynamics, where a staging or normal-mode transformation can be applied to the entire ring polymer, the same cannot always be done in path integral Monte Carlo. The reason for this is that if P is sufficiently large, the complete set of staging or normal modes is simply too large to be sampled in its entirety in one Monte Carlo move: the average acceptance probability would, for most problems, simply be too low. Thus, in path integral Monte Carlo, staging or normal-mode transformations are applied to segments of the ring polymer of a certain length j that must be optimized to give a desired average acceptance probability.

In fact, we have already seen how to perform both normal-mode and staging transformations to a set of j particles with a harmonic nearest-neighbor coupling anchored to fixed endpoints in Sections 1.7 and 4.6, respectively. We first describe the staging transformation. The idea of staging was originally introduced by Ceperley and Pollock (1984) as a means of constructing an efficient Monte Carlo scheme. However, explicit variable transformations were not employed in the original work. Here we modify the original staging algorithm to incorporate explicit transformations. In order to sample a segment of length j of the free particle distribution for the ring polymer, we start by randomly choosing a starting bead. Suppose that the chosen bead has an imaginary-time index l. This bead forms one of the fixed endpoints of the segment and the other is $l+j+1$ beads away from this one. This leaves us with j intermediate beads having primitive coordinates $x_{l+1}, ..., x_{l+j}$. We now transform these primitive variables to staging variables using eqn. (4.6.38), which, for this case, appears as follows:

$$u_{l+k} = x_{l+k} - \frac{k x_{l+k+1} - x_l}{(k+1)} \qquad k = 1, ..., j. \tag{12.8.27}$$

Equation (4.6.39) also allows a recursive inverse to be defined as

$$x_{l+k} = u_{l+k} + \frac{k}{k+1} x_{l+k+1} + \frac{1}{k+1} x_l. \tag{12.8.28}$$

Applying the transformation to the following portion of the quantum kinetic energy

$$\frac{1}{2}m\omega_P^2\sum_{k=0}^{j}\left(x_{l+k}-x_{l+k+1}\right)^2,$$

we obtain

$$\sum_{k=0}^{j}\left(x_{l+k}-x_{l+k+1}\right)^2=\sum_{k=1}^{j}\frac{k+1}{k}u_{l+k}^2+\frac{1}{j+1}\left(x_{l+j+1}-x_l\right)^2 \tag{12.8.29}$$

(see, also, eqn. (4.6.44)). Since the j staging variables have a distribution proportional to $\exp(-\beta m_k\omega_P^2u_{l+k}^2/2)$, where $m_k=(k+1)m/k$, we sample each u_{l+k} randomly from its corresponding Gaussian distribution and then use eqn. (12.8.28) to generate the proposed move to new primitive variables x'_{l+k}, $k=1,...,j$. Let x denote the original coordinates x_{l+k}, with $k=1,...,j$, and let x′ denote the coordinates x'_{l+k} of the proposed move. The change in potential energy will be

$$\Delta U(\mathrm{x},\mathrm{x}')=\frac{1}{P}\sum_{k=1}^{j}\left[U(x'_{l+k})-U(x_{l+k})\right], \tag{12.8.30}$$

and the acceptance probability is then

$$A(\mathrm{x}'|\mathrm{x})=\min\left[1,\mathrm{e}^{-\beta\Delta U(\mathrm{x},\mathrm{x}')}\right]. \tag{12.8.31}$$

Thus, if the move lowers the potential energy, it will be accepted with probability 1; otherwise, it is accepted with probability $\exp[-\beta\Delta U(\mathrm{x},\mathrm{x}')]$. On the average, P/j such moves will displace all the beads of the ring polymer, and hence the set of P/j staging moves is called a *Monte Carlo pass*.

The algorithm works equally well with a normal-mode transformation between fixed endpoints x_l and x_{l+j+1}, as in eqn. (1.7.12). In this case, the normal-mode variables are sampled from independent Gaussian distributions, and eqn. (12.8.31) is used to determine whether the move is accepted or rejected.

The staging and normal-mode schemes described above move only the internal modes of the cyclic chain. Therefore, in both algorithms, one additional move is needed, which is a displacement of the chain as a whole. This can be achieved by an attempted displacement of the uncoupled mode variable u_1 (recall that u_1 is the centroid variable in the normal-mode scheme) according to

$$u'_{1,\alpha}=u_{1,\alpha}+\frac{1}{\sqrt{d}}\left(\zeta_\alpha-0.5\right)\Delta. \tag{12.8.32}$$

Here, α runs over the spatial dimensions and Δ is a displacement length (see, also, eqn. (7.3.33)). Since the positions of all the beads change under such a trial move, the potential energy changes as

$$\Delta U(\mathrm{x},\mathrm{x}')=\frac{1}{P}\sum_{k=1}^{P}\left[U(x'_k)-U(x_k)\right]. \tag{12.8.33}$$

Again, eqn. (12.8.31) determines whether the move is accepted or rejected. A complete Monte Carlo pass, therefore, requires P/j staging or normal-mode moves plus one

move of the centroid. Typically, the parameter j is chosen such that the average acceptance probability is 40%. For a system of N particles, the algorithm extends straightforwardly. First a ring polymer is chosen at random, and a Monte Carlo pass is performed on that chain. On average, N such passes will move the entire system.

We conclude this subsection by noting an important difference between path integral Monte Carlo and path integral molecular dynamics. In molecular dynamics, a single time step generates a move of the entire system, while in Monte Carlo, each individual attempted move only changes a part of the system. This difference becomes important when implementing path integrals on parallel computing platforms. path integral molecular dynamics parallelizes much more readily than staging or normal-mode path integral Monte Carlo. Thus, if a molecular dynamics algorithm could be constructed with a convergence efficiency that rivals Monte Carlo, then the former becomes a competitive method. As part of our discussion of thermodynamic estimators in the next subsection, we will also present a comparison of the molecular dynamics and Monte Carlo approaches for a simple system.

12.8.3 Numerical aspects of thermodynamic estimators

As noted in Section 12.3, the estimators in eqns. (12.3.20), (12.3.24), and (12.6.13) suffer from large fluctuations in the kinetic energy due to their linear dependence on P. The consequence of this dependence is that in highly quantum systems, which require a large number of discretizations, it becomes increasingly difficult to converge such estimators. A solution to this dilemma was presented by Herman, Bruskin, and Berne (1982), who employed a path integral version of the virial theorem. For a single particle in one dimension, the theorem states

$$\frac{P}{2\beta} - \left\langle \frac{1}{2} m\omega_P^2 \sum_{k=1}^{P} (x_k - x_{k+1})^2 \right\rangle_f = \left\langle \frac{1}{2P} \sum_{k=1}^{P} x_k \frac{\partial U}{\partial x_k} \right\rangle_f . \tag{12.8.34}$$

Before we prove this theorem, we demonstrate its advantage in a simple application. First, note that when eqn. (12.8.34) is substituted into eqn. (12.3.19), a new energy estimator known as the *virial energy estimator* results:

$$\varepsilon_{\rm vir}(x_1, ..., x_P) = \frac{1}{P} \sum_{k=1}^{P} \left[\frac{1}{2} x_k \frac{\partial U}{\partial x_k} + U(x_k) \right] . \tag{12.8.35}$$

The elimination of the kinetic energy yields an energy estimator with a much lower variance and, therefore, better convergence behavior than the primitive estimator of eqn. (12.3.20). In Fig. 12.14, we show a comparison between the instantaneous fluctuations and cumulative averages of the primitive and virial estimators for a harmonic oscillator with $m = 1$ and $\omega = 10$ computed using staging molecular dynamics with $P = 32$, $P = 64$, and $P = 128$ beads. The figure shows how the fluctuations, shown in grey, grow with P while the fluctuations in the virial estimator are insensitive to P. Despite the fact that the fluctuations of the primitive estimator grow with P, the cumulative averages between the two estimators agree for all P. This illustrates the idea that in any path integral simulation, one should monitor both estimators and

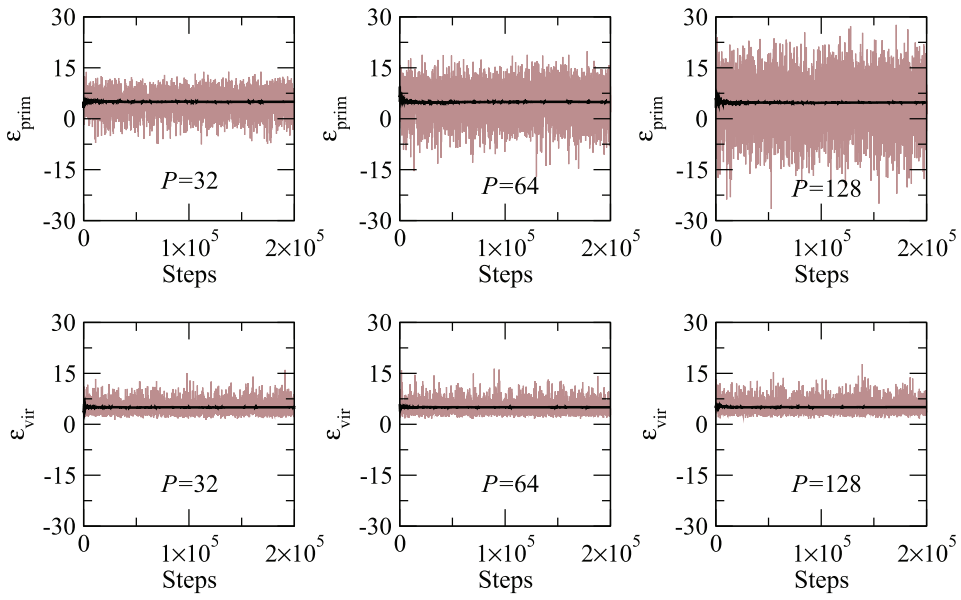

Fig. 12.14 Instantaneous fluctuations (grey) and cumulative averages (black) of the primitive (top row) and virial (bottom row) energy estimators for a harmonic oscillator simulated with staging path integral molecular dynamics using $P = 32$ (left column), $P = 64$ (middle column), and $P = 128$ (right column) beads.

ensure that they agree. If they do not, this should be taken as a sign of a problem in the simulation.

We now proceed to prove the theorem. First, we define a function $\alpha(x_1, ..., x_P)$ as

$$\alpha(x_1, ..., x_P) = \frac{1}{2} m\omega_P^2 \sum_{k=1}^{P} (x_k - x_{k+1})^2 . \tag{12.8.36}$$

Note that the effective potential in eqn. (12.2.28) can now be written as

$$\begin{aligned} \phi(x_1, ..., x_P) &= \alpha(x_1, ..., x_P) + \frac{1}{P} \sum_{k=1}^{P} U(x_k) \\ &\equiv \alpha(x_1, ..., x_P) + \gamma(x_1, ..., x_P). \end{aligned} \tag{12.8.37}$$

Recalling the discussion of Euler's theorem in Section 6.2, the function $\alpha(x_1, ..., x_P)$ is a homogeneous function of degree 2. Hence, applying Euler's theorem, we can write $\alpha(x_1, ..., x_P)$ as

$$\alpha(x_1, ..., x_P) = \frac{1}{2} \sum_{k=1}^{P} x_k \frac{\partial \alpha}{\partial x_k}. \tag{12.8.38}$$

Now consider the average $\langle\alpha\rangle_f$ over the finite-P path integral distribution f of eqn. (12.3.9), which we can write as

$$\begin{aligned}\langle\alpha\rangle_f &= \frac{C_P}{2Q_P}\int \mathrm{d}x_1\cdots\mathrm{d}x_P \sum_{k=1}^{P} x_k\frac{\partial\alpha}{\partial x_k}\mathrm{e}^{-\beta\alpha(x_1,\ldots,x_P)}\mathrm{e}^{-\beta\gamma(x_1,\ldots,x_P)} \\ &= -\frac{C_P}{2\beta Q_P}\int \mathrm{d}x_1\cdots\mathrm{d}x_P \sum_{k=1}^{P}\left(x_k\frac{\partial}{\partial x_k}\mathrm{e}^{-\beta\alpha(x_1,\ldots,x_P)}\right)\mathrm{e}^{-\beta\gamma(x_1,\ldots,x_P)}. \qquad (12.8.39)\end{aligned}$$

where $C_P = (mP/2\pi\beta\hbar^2)^{1/2}$. Integrating eqn. (12.8.39) by parts yields

$$\begin{aligned}\langle\alpha\rangle_f &= \frac{C_P}{2\beta Q_P}\int \mathrm{d}x_1\cdots\mathrm{d}x_P\ \mathrm{e}^{-\beta\alpha(x_1,\ldots,x_P)}\sum_{k=1}^{P}\frac{\partial}{\partial x_k}\left[x_k\mathrm{e}^{-\beta\gamma(x_1,\ldots,x_P)}\right] \\ &= \frac{C_P}{2\beta Q_P}\int \mathrm{d}x_1\cdots\mathrm{d}x_P\left[P-\frac{\beta}{P}\sum_{k=1}^{P}x_k\frac{\partial U}{\partial x_k}\right]\mathrm{e}^{-\beta\gamma(x_1,\ldots,x_P)}\mathrm{e}^{-\beta\alpha(x_1,\ldots,x_P)} \\ &= \frac{P}{2\beta}-\left\langle\frac{1}{2P}\sum_{k=1}^{P}x_k\frac{\partial U}{\partial x_k}\right\rangle_f, \qquad (12.8.40)\end{aligned}$$

from which eqn. (12.8.34) follows.

Using the virial estimator, we now present a comparison (Fig. 12.15) of path integral molecular dynamics with no variable transformations (top row), path integral molecular dynamics with a staging transformation (middle row), and staging path integral Monte Carlo (bottom row). The system is a one-dimensional harmonic oscillator with $\beta\hbar\omega = 15.8$, $m\omega/\hbar = 0.03$, and $P = 400$. With these parameters, the thermodynamic energy is dominated by the ground-state value $\hbar\omega/2$. The figure shows the instantaneous value of the virial estimator (left column), the cumulative average of the virial estimator (middle column), and the error bar in the value of the estimator. The error bar is calculated by grouping individual samplings from molecular dynamics or Monte Carlo into blocks of size n, computing the average over each block, and then computing the error bar from these block averages with respect to the global average (Cao and Berne, 1989). The purpose of this type of "block averaging" is to remove unwanted correlations between successive samplings. As the right column indicates, the error bar starts off small and then reaches a plateau when the blocks are large enough that correlations are no longer present. This example demonstrates that without variable transformations, path integral molecular dynamics performs rather poorly, but when a staging transformation is employed, molecular dynamics and staging Monte Carlo are equally efficient, as evidenced by the fact that they converge to the same error bar after the same number of steps.

As written, the virial estimator in eqn. (12.8.35) is only valid for bound systems because the term $x_k(\partial U/\partial x_k)$ is not translationally invariant. This problem can be circumvented by defining the virial part of the estimator in terms of the path centroid. The generalization of eqn. (12.8.34) for N particles in d dimensions is

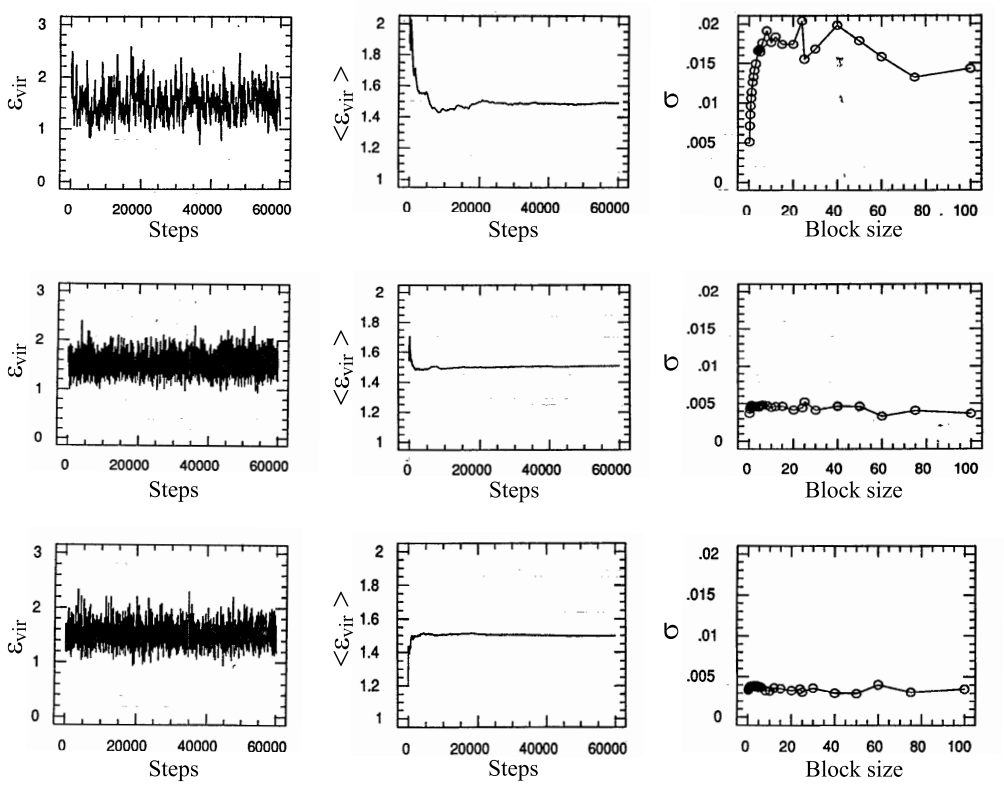

Fig. 12.15 (*Left column*) Instantaneous virial estimator. (*Middle column*) Cumulative average of virial estimator. (*Right column*) Error bar as a function of block size. (*Top row*) Path integral molecular dynamics with no variable transformations. (*Middle row*) path integral molecular dynamics with staging transformation. (*Bottom row*) Staging path integral Monte Carlo with $j = 80$. All energies are in units of $\hbar\omega$ (reprinted with permission from Tuckerman *et al.*, *J. Chem. Phys.* **99**, 2796 (1993), copyright, American Institute of Physics).

$$\frac{dNP}{2\beta} - \left\langle \sum_{i=1}^{N}\sum_{k=1}^{P} \frac{m_i\omega_P^2}{2}\left(\mathbf{r}_i^{(k)} - \mathbf{r}_i^{(k+1)}\right)^2 \right\rangle_f = \left\langle \frac{1}{2P}\sum_{i=1}^{N}\sum_{k=1}^{P} \mathbf{r}_i^{(k)} \cdot \frac{\partial U}{\partial \mathbf{r}_i^{(k)}} \right\rangle_f , \quad (12.8.41)$$

and for N particles in d dimensions, the generalization of the virial estimator is

$$\varepsilon_{\rm vir}(\{\mathbf{r}^{(1)},...,\mathbf{r}^{(P)}\}) = \frac{dN}{2\beta} + \sum_{k=1}^{P}\sum_{i=1}^{N} \frac{1}{2P}\left(\mathbf{r}_i^{(k)} - \mathbf{r}_i^{(c)}\right)\cdot\frac{\partial U}{\partial \mathbf{r}_i^{(k)}} + \frac{1}{P}\sum_{k=1}^{P} U\left(\mathbf{r}_1^{(k)},...,\mathbf{r}_N^{(k)}\right), \quad (12.8.42)$$

where $\mathbf{r}_i^{(c)}$ is the centroid of particle i. Similarly, by applying the path integral virial

theorem to the pressure estimator in eqn. (12.6.13), one can derive a virial pressure estimator

$$\mathcal{P}_{\rm vir}(\{\mathbf{r}^{(1)},...,\mathbf{r}^{(P)}\}) = \frac{dNkT}{V} - \frac{1}{V}\sum_{i=1}^{N}\frac{1}{P}\mathbf{r}_i^{(c)}\cdot\sum_{k=1}^{P}\frac{\partial}{\partial\mathbf{r}_i^{(c)}}U(\mathbf{r}_1^{(k)},...,\mathbf{r}_N^{(k)},V)$$

$$-\frac{1}{P}\sum_{k=1}^{P}\frac{\partial}{\partial V}U(\mathbf{r}_1^{(k)},...,\mathbf{r}_N^{(k)},V), \qquad (12.8.43)$$

which includes the possibility that the potential depends explicitly on the volume.

Path integral simulations should be applied whenever nuclear quantum effects are expected to be important, for example, when light nuclei such as hydrogen are present. Proton transfer reactions will often exhibit nontrivial quantum effects such as tunneling and zero-point motion. In malonaldehyde ($C_3H_4O_2$), a small, cyclic organic molecule with an internal O−H···O hydrogen bond, the hydrogen bond can reverse its polarity and become O···H−O via a proton transfer reaction (see Fig. 12.16, top). A free-energy profile for this reaction can be computed using the blue moon ensemble approach of Section 8.7 with a reaction coordinate $\delta = d_{O_1H} - d_{O_2H}$, where d_{O_1H} and d_{O_2H} are the distances between the two oxygens and the transferring proton. The free-energy profile in this reaction coordinate exhibits a typical double-well shaped. Interestingly, even at 300 K, there is a pronounced quantum effect on this free energy. The quantum free-energy profiles can be computed using the centroid of the reaction coordinate denoted δ^c (see eqn. (12.7.5)) in the figure (Voth *et al.*, 1989; Voth, 1993). Figure 12.16 shows that, at the level of theory utilized in the simulation (Tuckerman and Marx, 2001), the quantum free-energy barrier to the reaction decreases by approximately 2 kcal/mol from 3.6 kcal/mol to 1.6 kcal/mol due to the inclusion of nuclear quantum effects, which include both zero-point energy and tunneling contributions. Since enzymatic reaction barriers are in this energetic neighborhood, this simple example illustrates the important role that nuclear quantum effects, particularly quantum tunneling, can play in real biological proton transfer reaction. Another interesting point is that if only the transferring H is treated quantum mechanically, the reduction in the free energy is underestimated by roughly 0.4 kcal/mol, which shows that secondary nuclear quantum effects of the molecular skeleton are also important. These free-energy profiles are generated using *ab initio* molecular dynamics (Car and Parrinello, 1985; Marx and Hutter, 2009) and *ab initio* path integral techniques, in which a dynamical or path integral simulation is driven by forces generated from electronic structure calculations performed "on the fly" as the simulation is carried out (Marx and Parrinello, 1994; Marx and Parrinello, 1996; Tuckerman *et al.*, 1996; Marx and Hutter, 2009; Tuckerman, 2002).

In the malonaldehyde example of Fig. 12.16, nuclear quantum effects reduced the classical barrier by approximately 2 kcal/mol. Let us consider another example, in which nuclear quantum effects can actually lead to an increase of a barrier relative to the classical result. The example is a bulk host-guest system, structure-II hydrogen clathrate, which consists of cages of hydrogen-bonded water molecules that hold hydrogen molecules within the cages. More specifically, this material is composed of small cages made up of twelve pentagonal rings and large cages made up of twelve pentagonal

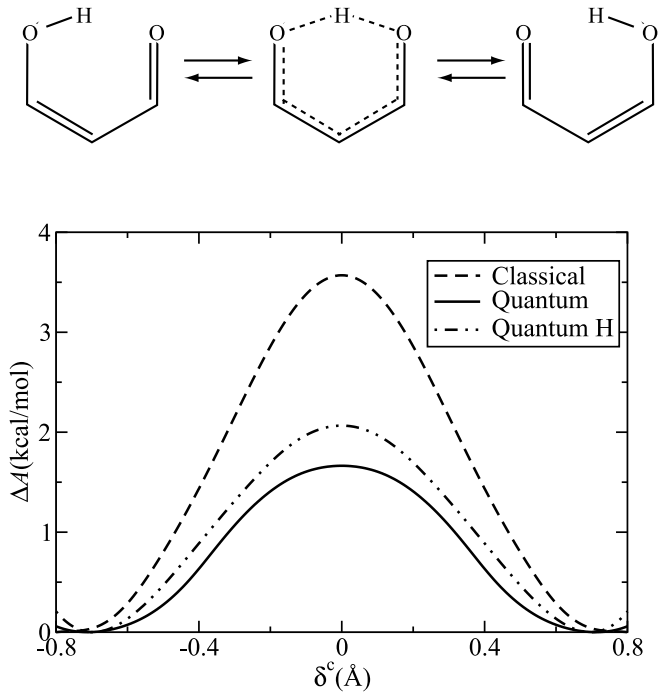

Fig. 12.16 (*Top*) Sketch of the internal proton transfer reaction in malonaldehyde. (*Bottom*) Classical, quantum, and quantum-H free-energy profiles at 300 K.

and four hexagonal rings. Hydrogen molecules can diffuse among the cages, typically moving from large cage to large cage through the hexagonal faces. The rate of diffusion is predominantly determined by the free-energy barrier for a hydrogen molecule to pass through a hexagonal face, a barrier that is strongly influenced by nuclear quantum effects at different temperatures. These barriers were computed by Cendagorta *et al.* (2016) using path integral based enhanced sampling, specifically a quantum version of d-AFED/TAMD (Cendagorta *et al.*, 2021). In their study, Cendagorta *et al.* employed a flexible quantum TIP4P potential (q-TIP4P/F) (Habershon *et al.*, 2009) to model water-water interactions, while H_2-H_2O interactions consisted of Coulomb and Lennard-Jones contributions. The point charges for the water molecules were taken from the q-TIP4P/F model, and charges on the H_2 atoms were set at $0.4238e$ on each H atom and $-0.9864e$ on the molecular center of mass. Lennard-Jones interactions were taken between the H_2 mass centers and between the H_2 mass center and the water oxygens. The parameters were $\sigma = 3.038$ Å and $\epsilon = 0.06816$ kcal/mol on the H_2 mass center and $\sigma = 3.166$ Å and $\epsilon = 0.1554$ kcal/mol on the water oxygen (Alavi *et al.*, 2005). Progress of the transfer process was measured by the reaction coordinate

$$q(\mathbf{r}) = \left[\frac{1}{2}\left(\mathbf{r}_{\mathrm{H}_1} + \mathbf{r}_{\mathrm{H}_2}\right) - \mathbf{R}_{\mathrm{A}}\right] \cdot \mathbf{u}_{\mathrm{AB}} - \frac{|\mathbf{R}_{\mathrm{B}} - \mathbf{R}_{\mathrm{A}}|}{2}. \tag{12.8.44}$$

Here, $\mathbf{r}_{\mathrm{H}_1}$ and $\mathbf{r}_{\mathrm{H}_2}$ are the coordinates of the two H atoms in the H_2 molecule, $\mathbf{R}_{\mathrm{A}}$ and $\mathbf{R}_{\mathrm{B}}$ are the centers of the left and right cages, respectively, and $\mathbf{u}_{\mathrm{AB}}$ is the unit vector along the direction between these two centers. Free-energy profiles using the centroid-based free-energy estimator of eqn. (12.7.5) for a single H_2 molecule transferring from one cage to another (all other cages are taken to be unoccupied) at temperatures of 50 K, 17 K, and 8 K are shown in Fig. 12.17 together with snapshots showing the path integral beads of the H_2 molecule during a transfer event. As with malonaldehyde, the free-energy profiles are constructed using the centroid estimator in eqn. (12.7.5). The figure shows that at 50 K, the quantum barrier is actually higher than the classical barrier. This is due to the delocalization of the H_2 ring polymer along the direction orthogonal to the line that joins the two cage centers. The increased barrier reflects the fact that it is more difficult for a delocalized object to pass through the hexagonal ring than it is for a classical point particle to do so. As the temperature is decreased to 17 K and 8 K, we see from the snapshots that the H_2 ring polymer spreads and is simultaneously located in both cages; this spreading is accompanied by a decrease in the bead density close to the plane of the hexagonal ring. This phenomenon is particularly pronounced at 17 K and 8 K: the quantum free-energy profiles at these temperatures flatten, and the quantum barrier is now below the classical barrier, which is a signature of deep tunneling of the H_2 molecule through the free-energy barrier.

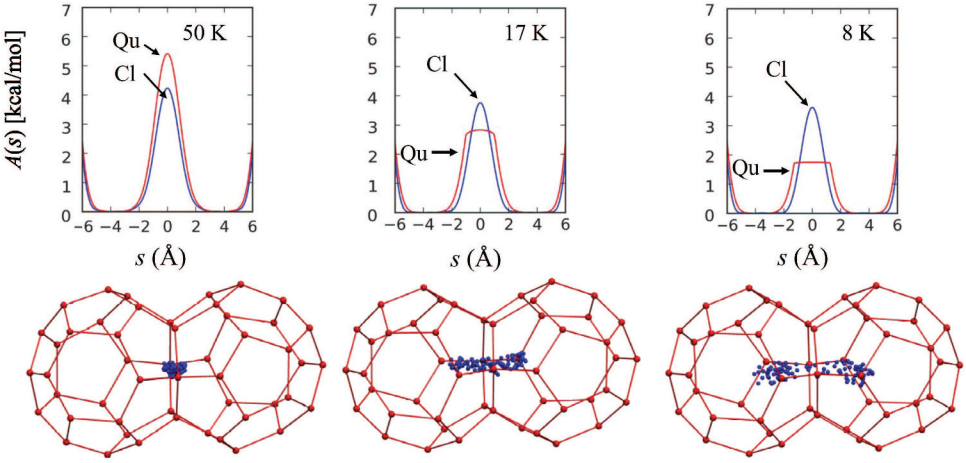

Fig. 12.17 Classical (Cl) and quantum (Qu) free-energy profiles for H_2 transfer between two large cages in structure-II hydrogen clathrate through a hexagonal face at temperatures 50 K, 17 K, and 8 K with snapshots of a path configuration of H_2 during transfer shown below the profiles (reprinted with permission from Cendagorta *et al.*, *Phys. Chem. Chem. Phys.* **18**, 32169 (2016), copyright Royal Society of Chemistry).

Before leaving this section, we note that care is needed when deciding whether to apply path integrals to a given problem. One must consider both the physical nature of the problem and the source of the potential-energy model used in each application before deciding to embark on a path integral investigation. Consider, for example, an empirical potential-energy function $U(\mathbf{r}_1, ..., \mathbf{r}_N)$ whose parameters are obtained by careful fits to experimental data. Since experiments are inherently quantum mechanical, the potential model U contains nuclear quantum effects by construction. Therefore, if such a model were used in conjunction with path integrals, quantum effects would be "double counted." By contrast, simulations performed with potential models whose parameters are fit to *ab initio* calculations do not contain quantum effects implicitly, and therefore, these models are strictly correct *only* when used in conjunction with path integral methods. Examples include the water model of Fanourgakis *et al.* (2006, 2006), Paesani *et al.* (2007), the many-body polarizable (MB-Pol) water model of Medders *et al.* (2014), and machine learning potentials for water and ice (Kapil *et al.*, 2016); these generally yield accurate results when simulated via path integrals. When nuclear quantum effects can be safely neglected, then simulations using classical molecular dynamics or Monte Carlo algorithms can be performed. Similarly, when potential energies and forces in a simulation are computed "on the fly" from the electronic structure via the *ab initio* molecular dynamics technique (Car and Parrinello, 1985; Marx and Hutter, 2009), these simulations should, strictly speaking, be performed within the path integral framework since nuclear quantum effects are not implicitly included in this approach. Simulations using this technique have yielded important insights, for example, into the solvation and transport of charge defects (in the form of hydronium and hydroxide ions) in aqueous solution (Marx *et al.*, 1999*a*; Tuckerman *et al.*, 2002; Marx *et al.*, 2010) and in acid crystal hydrates (Hayes *et al.*, 2009; Hayes *et al.*, 2011).

12.8.4 Open-chain path integral molecular dynamics

We saw in Section 12.3 that the calculation of momentum-dependent observables requires sampling off-diagonal elements of the density matrix, which can only be achieved by sampling thermal paths with different endpoints. For a single particle in one dimension, the integral that must be performed is given by eqn. (12.3.15). Molecular dynamics or Monte Carlo can also be used to sample configurations of an open-chain path integral, and, as was the case with cyclic or ring polymers, transforming to mode variables ensures efficient sampling. An open chain path integral is equivalent to the bead-spring model of Section 1.7 and Section 4.6.3, in which, respectively, normal mode and staging transformations were introduced. Here, let us consider the complete staging transformation for an open chain with beads at positions $\mathbf{r}_1, ..., \mathbf{r}_{P+1}$ for a single particle in three dimensions. The transformation takes the form

$$\begin{aligned}
\mathbf{u}_1 &= \frac{1}{2}(\mathbf{r}_1 + \mathbf{r}_{P+1}) \\
\mathbf{u}_k &= \mathbf{r}_k - \frac{1}{k}\left[(k-1)\mathbf{r}_{k+1} + \mathbf{r}_1\right], \qquad k = 2, ..., P \\
\mathbf{u}_{P+1} &= (\mathbf{r}_1 - \mathbf{r}_{P+1})
\end{aligned} \tag{12.8.45}$$

(Morrone *et al.*, 2007; Pérez and Tuckerman, 2011). Note that $\mathbf{u}_1$ and $\mathbf{u}_{P+1}$ are the average and relative positions of the two endpoint beads, respectively. In open-chain staging variables, the potential $\phi(\mathbf{r}_1, ..., \mathbf{r}_{P+1})$, analogous to that in eqn. (12.2.28) but corresponding to the open-chain distribution in eqn. (12.3.15), becomes

$$\begin{aligned}\phi(\mathbf{r}_1, ..., \mathbf{r}_{P+1}) &= \sum_{k=1}^{P}\left[\frac{1}{2}m\omega_P^2(\mathbf{r}_{k+1}-\mathbf{r}_k)^2 + \frac{1}{2P}\left(U(\mathbf{r}_{k+1})+U(\mathbf{r}_k)\right)\right] \\ \phi(\mathbf{u}_1, ..., \mathbf{u}_{P+1}) &= \frac{1}{2P}m\omega_P^2\mathbf{u}_{P+1}^2 + \sum_{k=2}^{P}\frac{1}{2}m_k\omega_P^2\mathbf{u}_k^2 + \frac{1}{P}\sum_{k=2}^{P}U(\mathbf{r}_k(\mathbf{u}_1, ..., \mathbf{u}_{P+1})) \\ &\quad + \frac{1}{2P}\left[U(\mathbf{r}_1(\mathbf{u}_1, \mathbf{u}_{P+1}) + U(\mathbf{r}_{P+1}(\mathbf{u}_1, \mathbf{u}_{P+1})\right] \qquad (12.8.46)\end{aligned}$$

where

$$\mathbf{r}_k(\mathbf{u}_1, ..., \mathbf{u}_{P+1}) = \mathbf{u}_1 + \frac{(P/2-k+1)}{P}\mathbf{u}_{P+1} + \sum_{l=k}^{P}\frac{k-1}{l-1}\mathbf{u}_l, \qquad (12.8.47)$$

$\mathbf{r}_1(\mathbf{u}_1, \mathbf{u}_{P+1}) = \mathbf{u}_1 + \mathbf{u}_{P+1}/2$, $\mathbf{r}_{P+1}(\mathbf{u}_1, \mathbf{u}_{P+1}) = \mathbf{u}_1 - \mathbf{u}_{P+1}/2$, and $m_k = [k/(k-1)]m$. In a normal mode transformation, the same assignment would be made to $\mathbf{u}_1$ and $\mathbf{u}_{P+1}$, and $\mathbf{u}_k$, $k = 2, ..., P$ would be obtained by a normal mode transformation. It is also straightforward to generalize these expressions for N particles in d dimensions obeying Boltzmann statistics. As an example application, Morrone *et al.* (2007) studied the momentum distribution of a proton distribution in bulk water, and in this study, the ring polymer of a single proton was opened for the calculation of the distribution, while the paths of the remaining particles were kept closed. We note, for completeness, that it is also possible to use closed paths within a perturbative approach to obtain a momentum distribution (Lin *et al.*, 2011).

In general, because they are less constrained by the cyclic wrapping condition of ring polymers, convergence of the distribution of open chains is slower than that of cyclic chains, which makes open path integral simulations more time consuming. In the last subsections of this chapter, we will discuss schemes for reducing the cost of both closed and open chain path integral calculations.

12.8.5 Reducing the number of beads for improved efficiency

Path integral Monte Carlo calculations and path integral molecular dynamics calculations require P evaluations of potential energies and forces for molecular dynamics. This means that such calculations are P times more costly in computational time than corresponding classical Monte Carlo and molecular dynamics calculations, for which $P = 1$. However, the index-wise interaction pattern between beads on different ring polymers (or between different sub-chains of joined ring polymers in systems of identical bosons or fermions) mean that path integral calculations exhibit nearly perfect parallel scaling with P and one can simply spread a path integral calculation out over P nodes on a parallel computer. As it happens, however, a variety of techniques exists for reducing the number of beads needed to converge properties of interest from a path

integral calculation, and these can be leveraged to reduce the computational time. We will discuss two such strategies in this section.

The first approach harkens back to a concept introduced in Section 3.13 for the classical propagator. In that section, we introduced the Baker-Campbell-Hausdorff formula (cf. eqn. (3.13.4)) for expressing a low-order factorization of an operator of the form $\exp(\lambda(\hat{\mathrm{A}}+\hat{\mathrm{B}}))$ when $[\hat{\mathrm{A}},\hat{\mathrm{B}}]\neq 0$. When we apply eqn. (3.13.4) to the high-temperature Boltzmann operator $\exp[-\beta\hat{\mathcal{H}}/P]$, we obtain

$$\mathrm{e}^{-\beta\hat{U}/2P}\mathrm{e}^{-\beta\hat{K}/P}\mathrm{e}^{-\beta\hat{U}/2P}=\exp\left[-\frac{\beta}{P}\left(\hat{\mathcal{H}}+\sum_{k=1}^{\infty}\left(\frac{\beta}{P}\right)^{2k}\hat{C}_k\right)\right], \tag{12.8.48}$$

where $\hat{\mathcal{H}}=\hat{K}+\hat{U}$. As noted in Section 3.13, the operators $\hat{C}_k$ are multiply nested commutators of $\hat{K}$ and $\hat{U}$, *e.g.*,

$$\hat{C}_1=-\frac{1}{24}[\hat{U}+2\hat{K},[\hat{U},\hat{K}]]. \tag{12.8.49}$$

If the sum over k in eqn. (12.8.48) is truncated after the $k=1$ term, and a trace is taken of both sides, it can be shown that

$$\mathrm{Tr}\left[\mathrm{e}^{-\beta\hat{\mathcal{H}}}\right]\approx\mathrm{Tr}\left(\left[\mathrm{e}^{-\beta\hat{K}/P}\mathrm{e}^{-\beta\hat{C}/P}\right]^{P}\right)+\mathcal{O}\left(\beta^5P^{-4}\right), \tag{12.8.50}$$

where $\hat{C}$ is the operator

$$\hat{C}=\hat{U}+\frac{1}{24}\left(\frac{\beta}{P}\right)^2\left[\hat{U},\left[\hat{K},\hat{U}\right]\right] \tag{12.8.51}$$

(Takahashi and Imada, 1984). The double commutator can be evaluated using the fact that $[\hat{\mathbf{p}},f(\mathbf{r})]=-i\hbar(\partial f/\partial\mathbf{r})$, so that when eqn. (12.8.50) is used to evaluate the partition function for N Boltzmann particles, the result is (see Problem 12.9)

$$Q_P^{(4)}(N,V,T)=\prod_{i=1}^{N}\left(\frac{m_iP}{2\pi\beta\hbar^2}\right)^{dP/2}\int\prod_{i=1}^{N}\mathrm{d}\mathbf{r}_i^{(1)}\cdots\mathrm{d}\mathbf{r}_i^{(P)} \tag{12.8.52}$$

$$\times\exp\left\{-\beta\sum_{k=1}^{P}\left[\sum_{i=1}^{N}\frac{1}{2}m_i\omega_P^2\left(\mathbf{r}_i^{(k+1)}-\mathbf{r}_i^{(k)}\right)^2+U^{(4)}\left(\mathbf{r}_1^{(k)},...,\mathbf{r}_N^{(k)}\right)\right]\right\},$$

where

$$\begin{aligned}U^{(4)}(\mathbf{r}_1,...,\mathbf{r}_N)&=\frac{1}{P}U(\mathbf{r}_1,...,\mathbf{r}_N)+\sum_{i=1}^{N}\frac{1}{24m_iP^2\omega_P^2}\left[\frac{\partial U}{\partial\mathbf{r}_i}\right]^2\\&\equiv\frac{1}{P}U(\mathbf{r}_1,...,\mathbf{r}_N)+U_{\mathrm{TI}}(\mathbf{r}_1,...,\mathbf{r}_N).\end{aligned} \tag{12.8.53}$$

Here, $U_{\mathrm{TI}}(\mathbf{r}_1,...,\mathbf{r}_N)$ is referred to as the *Takahashi-Imada* (TI) potential. It is evident from the form of eqn. (12.8.53) that use of the TI potential $U^{(4)}(\mathbf{r}_1,...,\mathbf{r}_N)$ in path

integral molecular dynamics would require calculation of second derivatives of the potential. We will shortly describe some ways in which this can be handled efficiently within path integral molecular dynamics; use of path integral Monte Carlo would clearly avoid the need for second derivatives. However, there is a more immediate technical issue concerning the calculation of observables within the TI framework. Because eqn. (12.8.52) can only be derived for the trace of an exponential operator, an expression for $\langle \hat{A} \rangle$ requires recasting the expectation value as

$$\langle \hat{A} \rangle = -\frac{1}{\beta Q(N,V,T)} \frac{\mathrm{d}}{\mathrm{d}\lambda} \mathrm{Tr} \left[e^{-\beta(\hat{\mathcal{H}} + \lambda \hat{A})} \right]_{\lambda=0} \tag{12.8.54}$$

so that the quantity $\hat{U} + \lambda \hat{A}$ can be treated as an effective "potential" for the purposes of applying the TI factorization. When this is done for a position-dependent operator, the resulting estimator for $\langle \hat{A} \rangle$ becomes

$$a_P^{(4)}(\mathbf{R}) = \frac{1}{P} \sum_{k=1}^{P} \left[a\left(\mathbf{r}_1^{(k)}, ..., \mathbf{r}_N^{(k)}\right) + \sum_{i=1}^{N} \frac{1}{12 m_i P \omega_P^2} \left(\frac{\partial U}{\partial \mathbf{r}_i^{(k)}} \right) \cdot \left(\frac{\partial a}{\partial \mathbf{r}_i^{(k)}} \right) \right], \tag{12.8.55}$$

where, for simplicity, we have introduced the notation $\mathbf{R}$ to denote the full set of N ring-polymer bead coordinates. A primitive energy estimator can also be derived using the standard relation $E = -(\partial/\partial\beta) \ln Q^{(4)}(N,V,T)$ following the procedure in Section 12.3. This yields

$$\begin{aligned} \varepsilon^{(4)}(\mathbf{R}) = \frac{3NP}{2\beta} - \frac{\omega_P^2}{2} \sum_{i=1}^{N} \sum_{k=1}^{P} m_i \left(\mathbf{r}_i^{(k)} - \mathbf{r}_i^{(k+1)} \right)^2 + \frac{1}{P} \sum_{k=1}^{P} U(\mathbf{r}_1^{(k)}, ..., \mathbf{r}_N^{(k)}) \\ + 3U_{\mathrm{TI}}(\mathbf{r}_1^{(k)}, ..., \mathbf{r}_N^{(k)}). \end{aligned} \tag{12.8.56}$$

If we follow the procedure for deriving a virial estimator, the result is an expression that involves the second derivative of the potential. We will return to this issue later in the present section.

The most straightforward way to compute an average at fourth order within the TI scheme that also avoids the need to compute second derivatives of the potential is simply to reweight an average of $a_P^{(4)}$ using standard (second-order) path integral molecular dynamics. If done this way, a fourth-order average would be computed using

$$\langle \hat{A} \rangle^{(4)} = \frac{\langle a_P^{(4)}(\mathbf{R}) \mathrm{e}^{-\beta U_{\mathrm{TI}}(\mathbf{R})} \rangle^{(2)}}{\langle \mathrm{e}^{-\beta U_{\mathrm{TI}}(\mathbf{R})} \rangle^{(2)}} \tag{12.8.57}$$

(Jang *et al.*, 2001; Pérez and Tuckerman, 2011), where $\langle \cdots \rangle^{(2)}$ indicates an average over a standard (second-order) path integral sampling. The advantage of reweighting at fourth order is that it can be done *a posteriori*, with no changes to a path integral code, simply by saving all of the quantities needed to construct the average. However, in systems with many degrees of freedom, extensivity of $U_{\mathrm{TI}}(\mathbf{R})$ will cause slow convergence of reweighted averages as a function of simulation time if the system visits many configurations at second order for which $U_{\mathrm{TI}}(\mathbf{R})$ is large. Another

technical difficulty with the TI scheme concerns the need to compute the derivative of the function $a_P(\mathbf{r}_1^{(k)}, ..., \mathbf{r}_N^{(k)})$ with respect to $\mathbf{r}_i^{(k)}$ in order to evaluate the second term in eqn. (12.8.55). For certain observables, the derivative can be performed straightforwardly; however, should we wish to compute, for example, a radial distribution function (not an uncommon task), the observable would involve δ-functions of the form $\delta(|\mathbf{r}_i^{(k)} - \mathbf{r}_j^{(k)}| - r)$ and its derivatives with respect to $\mathbf{r}_i^{(k)}$ and $\mathbf{r}_j^{(k)}$. Similar derivatives would be needed for other types of distributions. The presence of derivatives of a δ-function is troublesome at best (see Appendix A); if we attempt to integrate the second term in the average by parts, we again obtain terms involving second derivatives of the potential.

An approach that simplifies the calculation of higher-order path integrals is that of Suzuki and Chin (Suzuki, 1995; Chin, 1997) and is similar in spirit to the approach of Suzuki and Yoshida discussed in Section 4.12. Here, imaginary-time steps of different lengths are used to cancel error terms in an exponential operator factorization scheme. Unlike the Suzuki-Yoshida approach, which has positive and negative step lengths, for the Boltzmann operator it is critical that all steps have the same sign. The Suzuki-Chin (SC) factorization takes the form

$$\mathrm{e}^{-\beta(\hat{K}+\hat{U})/P} = \mathrm{e}^{-\beta\hat{U}_e/6P}\mathrm{e}^{-\beta\hat{K}/2P}\mathrm{e}^{-2\beta\hat{U}_m/3P}\mathrm{e}^{-\beta\hat{K}/2P}\mathrm{e}^{-\beta\hat{U}_e/6P} + \mathcal{O}\left(\frac{\beta}{P}\right)^5, \quad (12.8.58)$$

where the operators $\hat{U}_e$ and $\hat{U}_m$ are defined as

$$\hat{U}_e(\mathbf{r}_1, ..., \mathbf{r}_N) = \hat{U}(\mathbf{r}_1, ..., \mathbf{r}_N) + \sum_{i=1}^{N} \frac{\alpha}{6m_i}\left(\frac{\beta\hbar}{P}\frac{\partial\hat{U}}{\partial\mathbf{r}_i}\right)^2$$

$$\hat{U}_m(\mathbf{r}_1, ..., \mathbf{r}_N) = \hat{U}(\mathbf{r}_1, ..., \mathbf{r}_N) + \sum_{i=1}^{N} \frac{1-\alpha}{12m_i}\left(\frac{\beta\hbar}{P}\frac{\partial\hat{U}}{\partial\mathbf{r}_i}\right)^2, \quad (12.8.59)$$

with $\alpha \in [0, 1]$ being an adjustable parameter. Within the SC scheme, the canonical partition function is given by

$$Q_P^{(4)}(N, V, T) = \prod_{i=1}^{N}\left(\frac{m_i P}{2\pi\beta\hbar^2}\right)^{dP/2} \int \prod_{i=1}^{N} \mathrm{d}\mathbf{r}_i^{(1)} \cdots \mathrm{d}\mathbf{r}_i^{(P)}\; w_{\mathrm{SC}}(\mathbf{R}) \quad (12.8.60)$$

$$\times \exp\left\{-\beta\sum_{k=1}^{P}\left[\sum_{i=1}^{N}\frac{1}{2}m_i\omega_P^2\left(\mathbf{r}_i^{(k+1)} - \mathbf{r}_i^{(k)}\right)^2 + U\left(\mathbf{r}_1^{(k)}, ..., \mathbf{r}_N^{(k)}\right),\right]\right\}$$

where

$$w_{\mathrm{SC}}(\mathbf{R}) = w_{\mathrm{JJ}}(\mathbf{R}) \exp\left\{-\frac{\beta}{3P}\sum_{k=1}^{P/2}\left[U(\mathbf{r}_1^{(2k)}, ..., \mathbf{r}_N^{(2k)}) - U(\mathbf{r}_1^{(2k-1)}, ..., \mathbf{r}_N^{(2k-1)})\right]\right\} \quad (12.8.61)$$

and

$$w_{\rm JJ}(\mathbf{R}) = \exp\left\{-\beta\sum_{i=1}^{N}\sum_{k=1}^{P/2}\frac{1}{9m_i\omega_P^2}\left[\frac{\alpha}{P^2}\left(\frac{\partial U(\mathbf{r}_1^{(2k-1)},...,\mathbf{r}_N^{(2k-1)})}{\partial \mathbf{r}_i^{(2k-1)}}\right)^2\right.\right.$$

$$\left.\left. + \frac{1-\alpha}{P^2}\left(\frac{\partial U(\mathbf{r}_1^{(2k)},...,\mathbf{r}_N^{(2k)})}{\partial \mathbf{r}_i^{(2k)}}\right)^2\right]\right\}. \tag{12.8.62}$$

The advantage of the SC factorization is that it applies directly to the Boltzmann operator, as eqn. (12.8.58) makes clear, rather than to traces involving the Boltzmann operator. For this reason, the traces needed to compute observables take a more familiar form. For example, if we wish to compute the ensemble average of an operator $\hat{A}$ at fourth order within the SC approach, we could start with a weighted version of eqn. (12.3.5),

$$\langle \hat{A}\rangle^{(4)} = \frac{\langle a(\mathbf{r}_1^{(1)},...,\mathbf{r}_N^{(1)})w_{\rm SC}(\mathbf{R})\rangle^{(2)}}{\langle w_{\rm SC}(\mathbf{R})\rangle^{(2)}}. \tag{12.8.63}$$

Ultimately, we would like to apply the cyclic invariance of the ring polymer to recast eqn. (12.8.63) in the form of eqn. (12.3.7), which has better convergence properties. However, in the SC formulation, even beads and odd beads have different effective potentials and are, thus, not equivalent. Consequently, cyclic invariance of the ring polymer in the SC framework only applies to cyclic relabelings of the form $k \to k+2$, rather than $k \to k+1$, as could be used to derive eqn. (12.3.7). Performing the cyclic relabeling $k \to k+2$, we obtain $P/2$ equivalent expressions and can, therefore, express eqn. (12.8.63) as

$$\langle \hat{A}\rangle^{(4)} = \frac{2}{P}\sum_{k=1}^{P/2}\frac{\langle a(\mathbf{r}_1^{(2k-1)},....,\mathbf{r}_N^{(2k-1)})w_{\rm SC}(\mathbf{R})\rangle^{(2)}}{\langle w_{\rm SC}(\mathbf{R})\rangle^{(2)}}, \tag{12.8.64}$$

which allows us to compute ensemble averages within the SC formalism using the reweighting approach. (Problem 12.16 asks for a derivation of primitive and virial energy estimators within the SC scheme.) Another important point is that the SC approach can be easily extended to open chains (Pérez and Tuckerman, 2011; Cendagorta *et al.*, 2018) (see Section 12.8.4), which is not possible within the TI framework.

Let us now return to the question of how to avoid reweighting the averages within a fourth-order approximation. If we wished to generate the path integral molecular dynamics trajectories directly within either the TI or SC framework, we would need forces from $U_{\rm TI}(\mathbf{r}_1,...,\mathbf{r}_N)$ or from terms in the exponential of $w_{\rm JJ}(\mathbf{R})$. Consider, for example, the derivative of $U_{\rm TI}(\mathbf{r}_1,...,\mathbf{r}_N)$, given analytically by

$$\frac{\partial U_{\rm TI}}{\partial \mathbf{r}_j} = C\sum_{i=1}^{N}\frac{1}{m_i}\frac{\partial^2 U}{\partial \mathbf{r}_j\partial \mathbf{r}_i}\cdot\frac{\partial U}{\partial \mathbf{r}_i} = -C\sum_{i=1}^{N}\frac{\partial^2 U}{\partial \mathbf{r}_j\partial \mathbf{r}_i}\cdot\frac{\mathbf{f}_i}{m_i}, \tag{12.8.65}$$

where $C = 1/(12P^2\omega_P^2)$ and $\mathbf{f}_i = -\partial U/\partial \mathbf{r}_i$. Rather than calculate the second deriva-

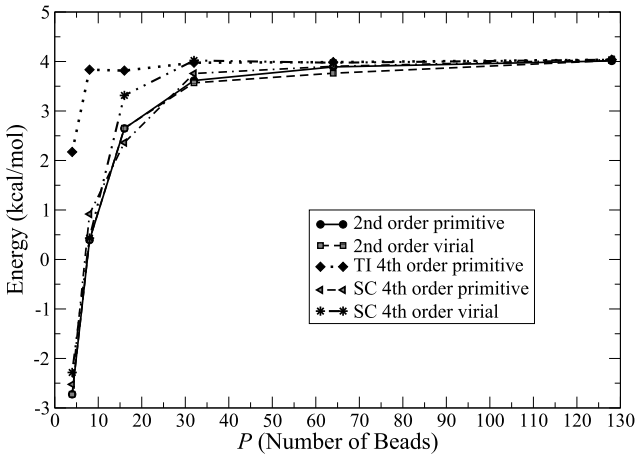

Fig. 12.18 Convergence as a function of P of second-order primitive and virial estimators, the TI primitive estimator, and the SC primitive and virial estimators for a system of 64 q-SPC/Fw water molecules.

tive matrix of the potential, we can use a finite-difference formula (Kapil *et al.*, 2016)

$$\frac{\partial U_{\mathrm{TI}}}{\partial \mathbf{r}_j} = C \lim_{\epsilon \to 0} \frac{1}{2\epsilon\delta} \left[\mathbf{f}_i(\mathbf{r} - \epsilon\delta\mathbf{u}) - \mathbf{f}_i(\mathbf{r} + \epsilon\delta\mathbf{u}) \right], \tag{12.8.66}$$

where $\mathbf{r} \equiv \mathbf{r}_1, ..., \mathbf{r}_N$, $\mathbf{u} \equiv \mathbf{u}_1, ..., \mathbf{u}_N$, with

$$\mathbf{u}_i = \frac{\mathbf{f}_i}{m_i}$$

$$\delta = \left[\frac{1}{NP} \sum_{k=1}^{P} \mathbf{f}_k \cdot \mathbf{f}_k \right]^{-1/2}. \tag{12.8.67}$$

(Problem 12.17 asks for a derivation of eqn. (12.8.66), which can be adapted for the SC approach as well.) Because the fourth-order corrections are small, the finite-difference approximation, although inexact, nevertheless yields stable path integral molecular dynamics trajectories (Kapil *et al.*, 2016).

A simple application to liquid water serves to demonstrate the convergence of the energy estimators for the different second-order and fourth-order methods as a function of P. In this example, the q-SPC/Fw model (Paesani *et al.*, 2006) is employed. Path integral molecular dynamics simulations of a system of 64 water molecules in a periodic box of length 12.416 Å are carried out at 300 K with $P = 2, 4, 8, 16, 32, 64$, and 128 beads. Figure 12.18 compares second-order primitive and virial estimators, the TI

fourth-order estimator, and primitive and virial fourth-order estimators (see Problem 12.16) for the SC scheme with $\alpha = 0$. All averages are computed using the reweighting scheme. The figure clearly shows the improvements in convergence with P for the fourth-order methods. Interestingly, the TI method, despite its technical difficulties, exhibits the best convergence of the different methods (although the convergence of the SC virial estimator is only slightly less efficient). From this example, it is clear that fourth-order methods offer an advantage. In the next section, we explore methods for reducing the computational overhead of path integral molecular dynamics within the second-order approach.

12.8.6 Ring polymer contraction

In Section 3.11, we introduced the idea of multiple time-stepping in classical molecular dynamics to avoid having to evaluate expensive and slowly varying forces at every time point in a simulation, thus increasing the efficiency of the simulation. Path integration in statistical mechanics involves stepping through imaginary time at intervals of $\epsilon = \beta\hbar/P$. As is clear from eqn. (12.8.25), the full potential $U(\mathbf{r}_1, ..., \mathbf{r}_N)$ must be evaluated at each step in imaginary time. It is possible to develop an analogous scheme in imaginary time for potentials that can be decomposed into a relatively cheap and rapidly varying term $U_\mathrm{f}(\mathbf{r}_1, ..., \mathbf{r}_N)$, which is evaluated at every imaginary-time slice, and an expensive but slowly varying term $U_\mathrm{s}(\mathbf{r}_1, ..., \mathbf{r}_N)$, which only needs to be evaluated at a small fraction of the imaginary-time slices. In this way, we could reduce the computational time needed to evaluate path integrals by reducing the number of expensive potential and force evaluations around the ring polymer. However, because of the strong coupling of the ring-polymer modes, rather than subdividing beads, it

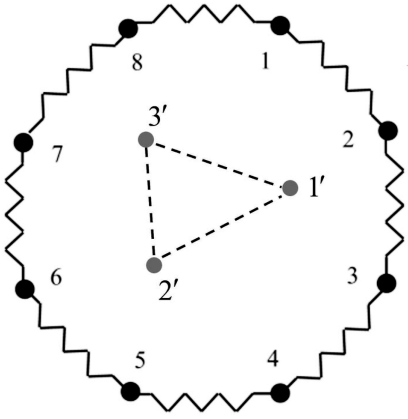

Fig. 12.19 Illustration of imaginary-time multiple time-stepping, in which expensive and slowly varying potential and force evaluations are performed on a smaller ring polymer with $n < P$ beads (here, $P = 8$, $n = 3$), connected by dashed lines.

proves more optimal to subdivide modes and evaluate the slow potential on a ring polymer generated from low-frequency modes only. Such a ring polymer is "contracted" down to one having fewer beads, which achieves the goal of reducing the number of evaluations of the slow potential. This idea is illustrated in Fig. 12.19. The notion of a contracted ring polymer was first introduced by Markland and Manolopoulos (2008*a*, 2008*b*), who formulated a contraction scheme in normal-mode variables.

In order to construct the contracted ring polymer in Fig. 12.19 using normal modes, we start with the P modes with frequencies given in eqn. (12.8.19) and we discard $P-n$ of these modes, where $n < P$. We thus retain the n lowest-frequency modes, and we use these n modes to construct the contracted ring polymer. To this end, we simply need an orthogonal transformation $\tilde{O}_{kl}$ for transforming the n lowest-frequency mode variables $\mathbf{u}_i^{(k)}$ for particle i to n primitive variables $\mathbf{s}_i^{(k)}$ of the contracted ring polymer. The transformation matrix $\tilde{O}_{kl}$ is constructed in the same way as the original matrix O_{kl} of eqn. (12.8.18) except that we start with a matrix $\tilde{A}_{ij} = 2\delta_{ij} - \delta_{i,j-1} - \delta_{i,j+1}$, where $i, j = 1, ..., n$ with the condition $\tilde{A}_{i0} = \tilde{A}_{in}$, $\tilde{A}_{i,n+1} = \tilde{A}_{i1}$. This smaller $n \times n$ matrix is then diagonalized, and the resulting orthogonal matrix that diagonalizes $\tilde{\mathrm{A}}$ is used to construct the coordinates $\mathbf{s}_i^{(k)}$ of the contracted ring polymer via

$$\mathbf{s}_i^{(k)} = \sqrt{n} \sum_{l=1}^{n} \tilde{O}_{kl}^{\mathsf{T}} \mathbf{u}_i^{(l)}. \tag{12.8.68}$$

However, eqn. (12.8.18) allows us to express the coordinates of the contracted ring polymer in terms of the coordinates of the full P-bead ring polymer as

$$\begin{aligned} \mathbf{s}_i^{(k)} &= \sqrt{\frac{n}{P}} \sum_{l=1}^{n} \sum_{m=1}^{P} \tilde{O}_{kl}^{\mathsf{T}} O_{lm} \mathbf{r}_i^{(m)} \\ &\equiv \sum_{m=1}^{P} T_{km} \mathbf{r}_i^{(m)}, \end{aligned} \tag{12.8.69}$$

where the matrix T is given by

$$T_{km} = \sqrt{\frac{n}{P}} \sum_{l=1}^{n} \tilde{O}_{kl}^{\mathsf{T}} O_{lm}. \tag{12.8.70}$$

Note that T is not a square matrix but is, rather, $n \times P$. Moreover, note that if $n = 1$, then the $1 \times P$ T would simply generate the centroid of the original P-bead ring polymer, *i.e.*,

$$\mathbf{s}_i^{(1)} = \mathbf{r}_i^{(c)} = \frac{1}{P} \sum_{m=1}^{P} \mathbf{r}_i^{(m)}, \tag{12.8.71}$$

indicating that the original ring polymer had contracted down to a single point. Equation (12.8.71) also makes clear that the original and contracted ring polymers always

have the same centroid position, even if $n > 1$. The computational efficiency of ring polymer contraction results from approximating $U_{\rm s}$ as

$$\frac{1}{P}\sum_{k=1}^{P} U_{\rm s}(\mathbf{r}_1^{(k)}, ..., \mathbf{r}_N^{(k)}) \approx \frac{1}{n}\sum_{k=1}^{n} U_{\rm s}(\mathbf{s}_1^{(k)}, ..., \mathbf{s}_N^{(k)}). \tag{12.8.72}$$

Finally, the chain rule allows us to relate the forces on the contracted ring polymer from the slow potential $U_{\rm s}$ to those needed to evolve the full P-bead ring polymer. The relation connecting these forces is

$$\frac{1}{P}\frac{\partial U_{\rm s}}{\partial \mathbf{r}_i^{(m)}} = \frac{1}{n}\sum_{k=1}^{n} \frac{\partial U_{\rm s}}{\partial \mathbf{s}_i^{(k)}} T_{km}. \tag{12.8.73}$$

Equation (12.8.73) allows us to evaluate the forces from the slow potential only on the n beads of the contracted ring polymer and then to distribute those forces throughout the full P-bead ring polymer. The generality of formulating the ring polymer contraction scheme in terms of transformation matrices allows the approach to be extended to staging modes with relative ease (see Problem 12.19).

As a simple example of the ring polymer contraction scheme, we consider the quantum analog of the problem laid out in eqn. (3.14.2). That is, we take a harmonic oscillator potential $U(\hat{x}) = m\omega^2\hat{x}^2/2$ and break it up into two contributions of different frequencies

$$U(\hat{x}) = \frac{1}{2}\lambda m\omega^2\hat{x}^2 + \frac{1}{2}(1-\lambda)m\omega^2\hat{x}^2, \tag{12.8.74}$$

where $\lambda \in [0, 1]$. If λ is close to 1, then the first term represents a high-frequency oscillator, which we denote $U_{\rm fast}(\hat{x})$, and the second term represents a low-frequency oscillator, which we denote $U_{\rm slow}(\hat{x})$. In Fig. 12.20, we show the instantaneous and cumulative average of the virial energy estimator for the harmonic oscillator potential, subdivided as in eqn. (12.8.74), with $\lambda = 0.93$ and the same parameters used to generate Fig. 12.15. The analytical result is $\varepsilon_{\rm vir} = 1.5$ in the units of the problem. The three panels show different choices of j and n: Larger values of n indicate more evaluations of the slow potential in the ring polymer contraction scheme. We see from the figure that there is very little difference in the behavior of the cumulative average and instantaneous fluctuations in the virial when 100 evaluations of the slow potential per time step are compared with only $n = 1$ evaluation per time step. In simulations for which the slow potential carries a high computational overhead, the gains in efficiency when using ring polymer contraction can be substantial. As an example, the reader is referred to the work of Marsalek and Markland (2016), who studied several small protonated or deprotonated water clusters and liquid water at an *ab initio* level. In their work, these authors found that a crude, semi-empirical potential could be used as $U_{\rm fast}$, while the difference between the desired *ab initio* and semi-empirical potentials could serve as $U_{\rm slow}$ and could be evaluated on a few beads, or even just one bead, without compromising the accuracy of the results. In this way, full *ab initio* accuracy of path integral calculations could be achieved at a computational overhead similar to that of an *ab initio* calculation with classical nuclei, but using a crude, inexpensive

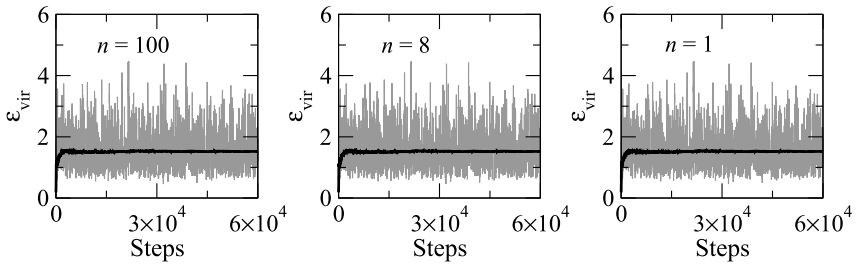

Fig. 12.20 Instantaneous and cumulative average of the virial energy estimator for the harmonic oscillator with potential divided into high- and low-frequency terms as given in eqn. (12.8.74). The parameters of the simulation are the same as those used to generate Fig. 12.15.

electronic structure level of theory as the "fast" potential and the difference between an accurate and the cruder level of theory as the "slow" potential, showing substantial gains in efficiency.

12.8.7 Path integrals in other ensembles

Throughout this chapter, we have focused on the representation of the quantum canonical partition function and associated equilibrium observables in terms of the Feynman path integral. However, other quantum ensembles can also be formulated in terms of a path integral. Before closing out this chapter, we will comment briefly on these formulations and point to specific references where details can be found. In a quantum isothermal-isobaric ensemble, one starts with the trace formula for the partition function $\Delta(N,P,T) = \mathrm{Tr}\{\exp[-\beta(\hat{\mathcal{H}} + PV)]\}$, and in a quantum grand canonical ensemble, one would start with $\mathcal{Z}(\mu,V,T) = \mathrm{Tr}\{\exp[-\beta(\hat{\mathcal{H}} - \mu N)]\}$. Recall, however, that these partition functions can be expressed in terms of the quantum canonical partition function with an additional volume integration (see Section 5.3) or particle sum (see Section 6.4). Consequently, performing path integral molecular dynamics or Monte Carlo calculations in these ensembles requires specifying how the volume fluctuations or particle number fluctuations can be sampled.

The literature on the quantum isothermal-isobaric ensemble contains descriptions of both Monte Carlo and molecular dynamics algorithms for path integral calculations (Marchi *et al.*, 1990; Scharf *et al.*, 1993; Martyna *et al.*, 1999). The procedure for deriving the path integral is exactly the same as described in this chapter; specifically, the trace is performed in the coordinate basis using a Trotter decomposition of the quantum canonical density matrix. Generating the associated volume fluctuations can be achieved using a virial estimator for the pressure involving all of the path integral ring-polymer modes; however, this tends to lead to large pressure fluctuations. If, instead, the path integral virial theorem is used, a centroid-based pressure estimator can be derived (Martyna *et al.*, 1999) (cf. eqn. (12.8.43)), which reduces the pressure fluctuations considerably and leads to more efficient path integral Monte Carlo and path integral algorithms. Although pressure is an intensive thermodynamic quantity,

it is also macroscopic, and one would not expect quantum fluctuations within the ring polymers to play a significant role in determining the magnitude of the volume fluctuations, suggesting that the rapidly varying terms from the high-frequency ring-polymer modes largely cancel out over long simulation times but lead to large errors due to imperfect cancellation. Once it is determined that a centroid-based pressure estimator can be employed, the formulation of an isothermal-isobaric path integral molecular dynamics algorithm in terms of normal modes or staging variables becomes straightforward.

In a grand canonical ensemble, the challenge to varying the number of quantum particles is the insertion and deletion of entire ring polymers, and once again, both Monte Carlo (Wang *et al.*, 1997) and molecular dynamics algorithms (Kreis *et al.*, 2016; Agarwal and Delle Site, 2016; Kreis *et al.*, 2017) have been developed for this purpose. Because direct insertion of a ring polymer would generally be expected to be a low-probability operation due to their extended nature, an efficient grand canonical path integral Monte Carlo algorithm would require a database of pre-equilibrated configurations. These could be drawn from an ideal-gas distribution or from a previously equilibrated canonical path integral calculation on the exact same system for which one seeks to perform the grand canonical ensemble calculation. However, even the availability of such a database leads only to modest increases in the acceptance probability. The technical problems associated with the insertion of ring polymers in path integral grand canonical Monte Carlo simulations can be elegantly addressed within molecular dynamics using a quantum analog of the adaptive resolution approach of Section 6.9. The key to this type of algorithm is to "collapse" the ring polymers to roughly the size of point particles as they move from the fine-grained region, where observables are computed, to the coarse-grained or "classical" reservoir region, as illustrated in Fig. 12.21. The figure shows how ring polymers in the fine-grained quantum region have physical mass and are fully expanded at the desired temperature. As they pass through the hybrid region, the mass increases such that when they enter the coarse-grained or classical region, they collapse roughly to point particles. Such a procedure allows for seamless flow of particles between the two regions. Collapse of the ring polymers can be achieved by assigning a position-dependent mass to each quantum particle, the position dependence of which is controlled by the λ parameter discussed in Section 6.9.

Let us now analyze how a position-dependent mass in a quantum Hamiltonian influences the derivation of the path integral. Consider a single quantum particle in one dimension with position operator $\hat{x}$ and momentum operator $\hat{p}$; the Hamiltonian takes the form

$$\hat{\mathcal{H}} = \frac{1}{2}\hat{p}\mu^{-1}(\hat{x})\hat{p} + U(\hat{x}), \tag{12.8.75}$$

where $\mu(\hat{x})$ is an operator corresponding to the position-dependent mass and $\mu^{-1}(\hat{x})$ is its inverse. Kreis *et al.* (2016) discuss the path integral quantization of such a Hamiltonian, which involves modifying some of the coordinate-space matrix elements needed for the path integral. In particular, it can be shown that for the kinetic energy operator, the coordinate-space matrix elements become

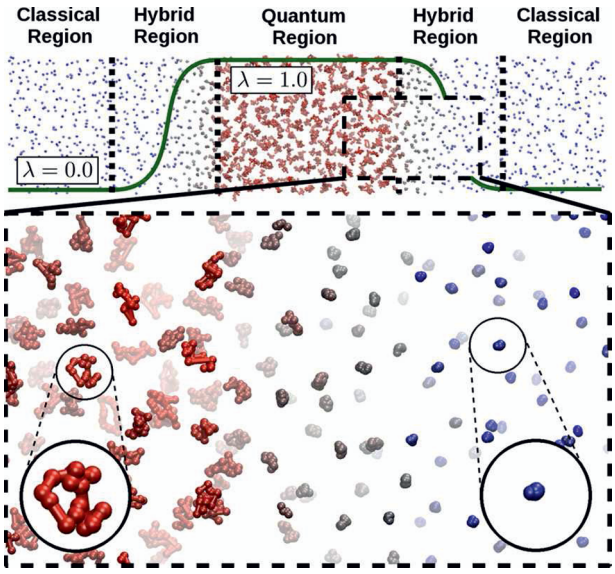

Fig. 12.21 Illustration of the quantum adaptive resolution scheme (reproduced with permission from Kreis *et al.*, *J. Chem. Theor. Comput.* **12**, 3030 (2016), copyright American Chemical Society).

$$\langle x_{k+1}|\mathrm{e}^{-\beta\hat{p}\mu^{-1}(\hat{x})\hat{p}/2P}|x_k\rangle = \left(\frac{\mu(x_{k+1})P}{2\pi\beta\hbar^2}\right)^{1/2} \times \exp\left\{-\frac{\beta\mu(x_{k+1})P}{2(\beta\hbar)^2}\left[(x_{k+1}-x_k) - \frac{\beta\hbar^2}{2P}\frac{\mathrm{d}\mu^{-1}}{\mathrm{d}x}\bigg|_{x_{k+1}}\right]^2\right\}. \quad (12.8.76)$$

The additional mass-derivative term can be neglected assuming that the average nearest-neighbor bead coupling is comparatively large, and this fact provides some guidance on the choice of the mass function $\mu(\hat{x})$: we should choose this mass function such that $\mu(\hat{x})$ has the value of the physical mass in the fine-grained region and is sufficiently large in the coarse-grained region so as to cause the desired collapse of the ring polymers (see Fig. 12.21). With this condition, particle number fluctuations consistent with a grand canonical ensemble can be generated.

12.9 Problems

12.1. Recall the definitions of the quantum propagator $U(t)$ and the canonical density matrix $\rho(\beta)$:

$$U(t) = e^{-i\hat{H}t/\hbar}, \qquad \rho(\beta) = e^{-\beta\hat{H}}.$$

Prove the following relations:

$$\rho(\beta) = C_1 \int_{-\infty}^{\infty} \mathrm{d}s \; e^{-i\beta\hbar s} \int_0^{\infty} \mathrm{d}t \; e^{-st} U(t)$$

$$U(t) = C_2 \int_{-\infty}^{\infty} \mathrm{d}\omega \; e^{\omega t/\hbar} \int_0^{\infty} \mathrm{d}\beta \; e^{i\omega\beta} \rho(\beta)$$

In the course of your proofs, find the (constant and possibly complex) coefficients C_1 and C_2 that make the relations true.

12.2. Derive primitive and virial estimators for the full pressure tensor $P_{\alpha\beta}$ defined by

$$P_{\alpha\beta} = \frac{kT}{\det(\mathbf{h})} \sum_{\gamma} \frac{\partial \ln Q}{\partial h_{\alpha\gamma}} h_{\beta\gamma},$$

where $h_{\mu\nu}$ is the cell matrix.

*12.3. Derive a virial form for the heat capacity at constant volume using the thermodynamic relation

$$C_V = k\beta^2 \frac{\partial^2 \ln Q}{\partial \beta^2}.$$

12.4. Derive eqns. (12.6.7) and (12.6.8) and generalize these equations to the case of N particles in three dimensions.

12.5. Derive eqn. (12.4.22).

12.6. The following problem considers the path integral theory for the tunneling of a particle through a barrier.

a. Show that the path integral expression for the density matrix can be written as:

$$\rho(x, x'; \beta) = \int_{x(-\beta\hbar/2)=x}^{x(\beta\hbar/2)=x'} \mathcal{D}[x] \exp\left[-\frac{1}{\hbar} \int_{-\beta\hbar/2}^{\beta\hbar/2} \mathrm{d}\tau \left(\frac{1}{2} m\dot{x}^2(\tau) + U(x(\tau)) \right) \right].$$

b. Consider a double-well potential of the form

$$U(x) = \frac{\omega^2}{8a^2}(x^2 - a^2)^2.$$

Show that, for a particle of unit mass, the dominant path for the density matrix $\rho(-a, a; \beta)$ is given by

$$x(\tau) = a\tanh[(\tau - \tau_0)\omega/2]$$

in the low-temperature limit with negligible error in the endpoint conditions. This path is called an *instanton* or *kink* solution. Discuss the behavior of this trajectory in imaginary time τ.

c. Calculate the classical imaginary-time action for the kink solution.

*12.7. Consider two distinguishable particles in one dimension with respective coordinates x and y and conjugate momenta p_x and p_y with a Hamiltonian

$$\hat{\mathcal{H}} = \frac{\hat{p}_x^2}{2m} + \frac{\hat{p}_y^2}{2M} + U(\hat{x}) + \frac{1}{2}M\omega^2\hat{y}^2 - \lambda\hat{x}\hat{y}.$$

a. Show that the density matrix $\rho(x, y, x', y'; \beta)$ can be written in the form

$$\rho(x, y, x', y'; \beta)$$

$$= \int_{x(0)=x}^{x(\beta\hbar)=x'} \mathcal{D}x(\tau) \exp\left[-\frac{1}{\hbar}\int_0^{\beta\hbar} \mathrm{d}\tau \left(\frac{1}{2}m\dot{x}^2(\tau) + U(x(\tau))\right)\right] T[x; y, y'],$$

where $T[x; y, y']$ is known as the *influence functional*. What is the functional integral expression for $T[x; y, y']$, and of what function is $T[x; y, y']$ a functional?

b. Using the method of expansion about the classical path, derive a closed form expression for $T(x(\tau), y, y')$ by evaluating the functional integral.

12.8. In Section 12.6, we discussed a recursion relation for the path integral formulation of N-particle bosonic and fermionic systems. Consider a system of $N = 4$ bosons or fermions. Generate a set of ring-polymer configurations analogous to Fig. 12.10 for this four-particle system, and determine the number of topologically distinct configurations. Finally, use the recursion relations in eqns. (12.6.21) and (12.6.24) to generate $\exp(-\beta\mathcal{K}_{B/F}^{(4)})$ and show these relations reproduce the correct exchange terms with the corresponding topological weighting factors.

12.9. A fourth-order Trotter formula valid for traces is

$$\mathrm{Tr}\left[\mathrm{e}^{-\lambda(\hat{A}+\hat{B})}\right] \approx \mathrm{Tr}\left\{\left[\mathrm{e}^{-\lambda\hat{A}/P}\mathrm{e}^{-\lambda\hat{C}/P}\right]^P\right\} + \mathcal{O}\left(\lambda^5 P^{-4}\right),$$

when $[\hat{A}, \hat{B}] \neq 0$.

$$\hat{C} = \hat{B} + \frac{1}{24}\left(\frac{\lambda}{P}\right)^2\left[\hat{B}, \left[\hat{A}, \hat{B}\right]\right].$$

Derive the discrete path integral expression for the canonical partition function $Q(N, V, T)$ for N Boltzmann particles in three dimensions that results

from applying this approximation. In particular, show that the N-particle potential $U(\mathbf{r}_1, ..., \mathbf{r}_N)$ is replaced by a new effective potential $\tilde{U}(\mathbf{r}_1, ..., \mathbf{r}_N)$ and derive the expression for this new potential.

12.10. In path integral molecular dynamics, convergence to the true quantum limit as a function of P can be slow, requiring large values of P. It is claimed that this problem can be circumvented by *starting* from the continuous form of the path integral (in which the limit $P \to \infty$ is already taken) and deriving an algorithm based on it. In order to explore this claim, the goal of this problem is to derive a path integral molecular dynamics algorithm for sampling continuous paths and consider its convergence behavior.
Recall that the continuous form of the path integral for the canonical partition function of a single quantum particle of mass m subject to a one-dimensional potential $U(x)$ is

$$Q(\beta) = \oint \mathcal{D}x(\tau) \ \exp\left\{-\frac{1}{\hbar}\int_0^{\beta\hbar} d\tau \ \left[\frac{1}{2}m\dot{x}^2(\tau) + U(x(\tau))\right]\right\},$$

where $\dot{x} = dx/d\tau$. Consider representing the paths $x(\tau)$ in a basis of sine and cosine functions as

$$x(\tau) = x_c + \sum_{k=1}^{\infty}\left[a_k \sin\left(\frac{2\pi k\tau}{\beta\hbar}\right) + b_k \cos\left(\frac{2\pi k\tau}{\beta\hbar}\right)\right],$$

where x_c is the path centroid

$$x_c = \frac{1}{\beta\hbar}\int_0^{\beta\hbar} x(\tau)d\tau.$$

Starting from this continuous (not discrete) path integral representation of the partition function and the above expansion of the paths, design a path integral molecular dynamics algorithm that propagates, and therefore samples the distribution of, the path centroid x_c as well as the expansion coefficients a_k and b_k. In the design of your algorithm, you should provide clear answers to the following questions:

a. What is the most simplified representation of the imaginary-time action in terms of x_c and the expansion coefficients a_k and b_k? This means explicitly performing as many integrals analytically as possible.

b. What is the classical Hamiltonian from which your algorithm is derived, and how did you derive it?

c. What are the equations of motion for your algorithm? In deriving these equations, be sure to obtain explicit expressions for the forces on the centroid and expansion coefficients.

d. How will you ensure that the correct ensemble distribution is generated by your equations of motion? Give an example of how you would address this question.

e. Since, on a computer, the number of sine and cosine basis functions must be finite, what parameter determines the convergence of the algorithm to the true quantum limit?

12.11. Consider a system of two distinguishable degrees of freedom with position operators $\hat{x}$ and $\hat{X}$ and corresponding momenta $\hat{p}$ and $\hat{P}$, respectively, with Hamiltonian

$$\hat{\mathcal{H}} = \frac{\hat{p}^2}{2m} + \frac{\hat{P}^2}{2M} + U(\hat{x}, \hat{X}).$$

Assume that the masses M and m are such that $M \gg m$, meaning that the two degrees of freedom are adiabatically decoupled.

a. Show that the partition function of the system can be approximated as

$$Q(\beta) = \sum_n \oint \mathcal{D}X(\tau) \exp\left\{ -\frac{1}{\hbar} \int_0^{\beta\hbar} \mathrm{d}\tau \left[\frac{1}{2} M \dot{X}^2(\tau) + \varepsilon_n\left(X(\tau)\right) \right] \right\},$$

where $\varepsilon_n(X)$ are the eigenvalues that result from the solution of the Schrödinger equation

$$\left[-\frac{\hbar^2}{2m} \frac{\partial^2}{\partial x^2} + U(x, X) \right] \psi_n(x; X) = \varepsilon_n(X) \psi_n(x; X)$$

for the light degree of freedom at a fixed value X of the heavy degree of freedom. This approximation is known as the *path integral Born-Oppenheimer approximation* (Cao and Berne, 1993). The eigenvalues $\varepsilon_n(X)$ are the Born-Oppenheimer surfaces.

b. Under what conditions can the sum over n in the above expression be approximated by a single term involving only the ground-state surface $\varepsilon_0(X)$?

12.12. a. Consider making the following transformation in eqn. (12.3.14):

$$r = \frac{1}{2}(x + x'), \qquad s = x - x'.$$

Show that the ensemble average of $\hat{A}(\hat{p})$ can be written as

$$\langle \hat{A} \rangle = \frac{1}{Q(L,T)} \int \mathrm{d}p \, \mathrm{d}r \; a(p) \rho_W(r, p),$$

where $\rho_W(r, p)$, known as the *Wigner distribution function* after Eugene P. Wigner (1902–1995), is defined by

$$\rho_W(r, p) = \int \mathrm{d}s \; \mathrm{e}^{ips/\hbar} \left\langle r - \frac{s}{2} \left| e^{-\beta \hat{\mathcal{H}}} \right| r + \frac{s}{2} \right\rangle.$$

b. Calculate $\rho_W(r,p)$ for a harmonic oscillator of mass m and frequency ω and show that in the classical limit, $\rho_W(r,p)$ becomes the classical canonical distribution.

12.13. Path integrals can be used to calculate isotope fractionation of an element X between two phases. If X has two isotopes I and I′ with masses m_{I} and $m_{\mathrm{I}\prime}$, then the required factor we need in each phase is denoted $\ln \beta^{\mathrm{I}\prime}$, given by

$$\ln \beta^{\mathrm{I}'} = \frac{\Delta A_{\mathrm{I}-\mathrm{I}'}}{kT} - \frac{3}{2} \ln \frac{m_{\mathrm{I}'}}{m_{\mathrm{I}}},$$

where $\Delta A_{\mathrm{I}-\mathrm{I}'}$ is the free-energy difference associated with a change from isotope I to isotope I′. This free-energy difference can be determined via thermodynamic integration by letting the mass of X vary from m_{I} to $m_{\mathrm{I}\prime}$ using a λ-path for the mass $m(\lambda)$, where $m(0) = m_{\mathrm{I}}$ and $m(1) = m_{\mathrm{I}'}$. Suppose there is only one atom of X in a system of N quantum particles obeying Boltzmann statistics. Derive a thermodynamic integration scheme for the free-energy difference $\Delta A_{\mathrm{I}-\mathrm{I}'}$ by determining an estimator for the free-energy derivative $\mathrm{d}A/\mathrm{d}\lambda$.

12.14. Show that the transition path ensemble of Section 7.7 can be formulated as a kind of path integral when the limit $n \to \infty$ and $\Delta t \to 0$ is taken. Give an explicit functional integral expression for partition function in eqn. (7.7.5).

12.15. Write down a complete set of path integral molecular dynamics equations of motion (using Nosé-Hoover chain thermostats of length M) for the numerical evaluation of an imaginary-time path integral for a system of N quantum particles in d dimensions obeying Boltzmann statistics at temperature T.

12.16. Using the partition function in eqn. (12.8.60), derive primitive and virial estimators for the energy within the Suzuki-Chin fourth-order scheme.

12.17. Derive eqn. (12.8.66).

12.18. Using the commutation relation

$$f(\hat{x})\hat{p} = \hat{p}f(\hat{x}) + [f(\hat{x}), \hat{p}] = \hat{p}f(\hat{x}) + i\hbar \frac{\mathrm{d}f}{\mathrm{d}x}$$

for an arbitrary differentiable function $f(\hat{x})$ of the coordinate operator, derive eqn. (12.8.76).

12.19. Reformulate the ring polymer contraction scheme in Section 12.8.6 in terms of staging modes. In staging variables, do the original P-bead ring polymer and contracted ring polymer have any beads in common?